Stratospheric dynamics of slowly rotating terrestrial planets

Martin Okánik

Supervisors: Dr. Hella Garny
Dr. Aarnout van Delden
Dr. Michiel Baatsen

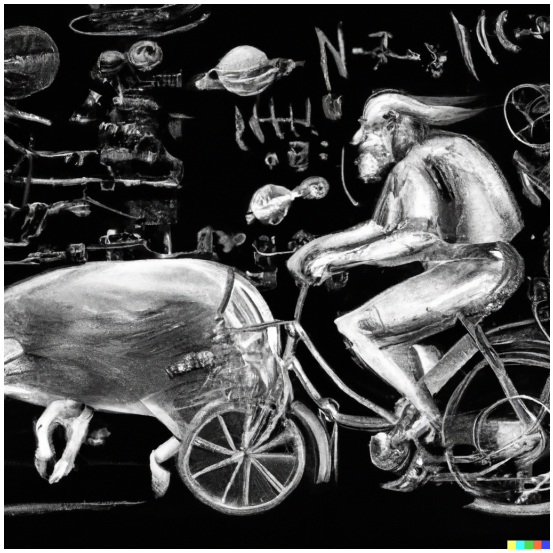

A thesis presented for Master's degree in Climate Physics at Utrecht University

August 7, 2023

Project

Title: Stratospheric dynamics of slowly rotating terrestrial planets
Project timeline: 13/02/2023 - 07/08/2023
Host institute: Deutsches Zentrum für Luft- und Raumfahrt (DLR), Oberpfaffenhofen, Germany

Student

Name: Martin Okánik
Student number: REMOVED FROM THE VERSION FOR PUBLICATION
Affiliation: Institute for Marine and Atmospheric research Utrecht (IMAU), Department of Physics, Faculty of Science, Utrecht University (UU)

Supervisors

Dr. Hella Garny: Host supervisor. Researcher at DLR and Junior Professor at LMU.
Dr. Aarnout van Delden: First supervisor at UU. Associate Professor at IMAU.
Dr. Michiel Baatsen: Second supervisor at UU. Junior Assistant Professor at IMAU.

Deutsches Zentrum
für Luft- und Raumfahrt
German Aerospace Center

Declaration

I hereby confirm that this thesis was written independently by myself without the use of any sources beyond those cited, and all passages and ideas taken from other sources are cited accordingly.

Martin Okánik

07/08/2023
In Banská Bystrica, Slovakia.

Acknowledgements

First of all, I would like to thank my main supervisor **Dr. Hella Garny** for being, put simply, such a good supervisor. Thank you for supporting me with all that was necessary, for giving me so much freedom to explore my own ideas, for providing the indispensable scrutiny of my explanations, for all the "aha" moments that occurred during our discussions, which sometimes significantly exceeded the expected time.

I can not imagine how much longer my settling-in in the group would take were it not for **Anna Goetz** (by now MSc.), who introduced me to her research and showed me how to work with the cluster. I kept looking up your summary email from my first day in Munich for the entire five months of my stay, among other things for the permanent link to the Zoom meetings. My thanks go also to **Prof. Thomas Birner**, for all the useful feedback on my research and often important dynamical insights casually mentioned during lunch discussions. Similar applies to his entire group, and to my colleagues at DLR, who created such a pleasant working atmosphere.

On the Dutch side of things, I thank **Dr. Aarnout van Delden** for being such an inspiring and kind teacher for both Dynamical Meteorology and Transport & Mixing. I also thank **Dr. Michiel Baatsen** for his infectious enthusiasm for Earth System Modelling and important discussions they both led, and constructive criticism they both delivered, which significantly helped raise the quality of my work.

Naturally, I would not get very far without the support of **my family and friends**. In particular my two wonderful **parents** and my one and only "little" **sister** provided crucial support to navigate the ups and downs of the past few years, which there were more than in the preceding two decades. I would also like to specifically mention my late grandfather, who used to listen with such enthusiasm whenever I talked about physics and astronomy as a teenager, and who by this point would certainly demand a complete translation of this work to Slovak language.

Honourable mention goes to the huge angry **wild boar** I ran into a few weeks ago in a pristine German forest, for allowing me to escape on my own terms - despite his very clear annoyance at my sight. If I am to believe the (dubious?) online statistics, his decision to not attack gives him claim to 15-30% of this thesis, and almost 10-20 years of my remaining statistical life expectancy. To do him some justice, I dedicated the first and last pages of this scholarly work to celebrate these magnificent native inhabitants of European forests[1]

[1]Images were created using DALL.E online generative AI model by Open AI (`https://openai.com/dall-e-2`). The model was asked to paint a picture of Navier-Stokes equations floating in space between planets, on one of which there is a wild boar charging into a cyclist. Apparently, generative AI has not yet grasped the equations of fluid dynamics very well, and just how fragile is the distinction between a planet and a pig in the very last picture, is indeed somewhat unsettling...

Abstract

With the advent of space travel in 20th century, and discoveries of thousands of exoplanets in the 21st, the field of atmospheric dynamics faces new challenges and opportunities. Of particular interest is qualitative understanding of how the astronomical, physical and chemical parameters of terrestrial planets influence their general circulation, whose nature can bridge the gap between a *potentially* habitable planet and a habitable one. Previous research used idealized GCMs to study the tropospheres of planets with smooth surface and an Earth-like set of bulk properties, one of which was varied at a time. Dependent on the rotation rate, meridional radiative forcing gradient, and the dampling timescale, they identified several qualitatively distinct tropospheric circulation regimes.

This work aims to be a step towards building similar understanding for layers above the troposphere. The research question is what happens to a stratosphere with a constant radiative forcing similar to a solstice on Earth, when the relative planetary rotation rate $\Omega^* = \Omega/\Omega_E$ is lowered. The results indicate a regime transition from a wave-driven circulation for the Earth-like $\Omega^* \sim 1$ to a non-linear regime at $\Omega^* \leq 10^{-1}$, with a stronger, radiatively driven Hadley-like cell in the stratosphere. This overturning is an inherently seasonal effect developping because of the downwelling present over the winter pole, and likely enhanced to some extent because of the warmth of the ozone layer in lower latitudes. It is centered around 30 hPa in winter mid-latitudes, and extends all the way to mid-latitudes of the summer hemisphere. A somewhat surprising result is the emergence of superrotation in the stratosphere, separate from the better-known superrotation region near tropopause. This result is less understood, it is hypothesised to be a result of gravity-wave breaking in the upper summer stratosphere, with angular momentum potentially advected across the equator by the Hadley-like cell. More research is needed to properly understand this phenomenon.

This work also tentatively proposes a suitable parameter space for a more detailed future study. Compared to the troposphere, frictional Taylor number should be replaced with radiative Taylor number, and a further parameter shown to be related to Burger number might be considered.

List of symbols

Latin alphabet

a radius of the Earth, $a = 6.37 \times 10^6$ m
c_p specific heat at constant pressure for a diatomic gas, $c_p = \frac{7}{2}R = 1005$ J/kg/K
f Coriolis parameter, $f = 2\Omega \sin\theta$ (/s)
$\vec{F}$ Eliassen-Palm flux vector (m^2/s^2)
g gravitational acceleration, $g = 9.8$ m/s
G net eddy forcing of $\frac{\partial[u]}{\partial t}$, $G = \nabla \cdot \vec{F}$ (m/s^2)
H atmospheric scale height, $H = \frac{RT_s}{g} = 8400$ m
J diabatic heating rate per unit mass (W/kg)
k zonal component of wavevector (k, l, m) (/m)
k_{damp} linear (Rayleigh) horizontal wind damping coefficient (/s)
l meridional component of wavevector (k, l, m) (/m)
K a common thermodynamic constant, $K = \frac{R}{c_p} = \frac{2}{7}$
L generic horizontal length scale (m)
m vertical component of wavevector (k, l, m) (/m)
M specific angular momentum $M = a\cos\theta(\Omega a \cos\theta + u)$ (m^2/s)
N Brunt-Väisälä frequency of buoyancy oscillations (s)
p pressure (Pa)
p_s pressure at the surface (Pa)
q quasi-geostrophic potential vorticity (/s)
r radial coordinate from the centre of the Earth (m)
R molar gas constant per unit mass of air, $R = 287$ J/kg/K
s superrotation index $s = \frac{M}{\Omega a^2} - 1$
S_p static stability parameter, $S_p = \frac{KT}{p} - \frac{\partial T}{\partial p}$ (K/Pa)
t time (s)
T temperature (K)
T_{eq} restoration temperature in the Newtonian radiative parametrization (K)
T_s temperature at the surface (K)
u zonal velocity component (m/s)
v meridional velocity component (m/s)
w vertical velocity component (m/s)
x coordinate parallel to longitude, $x = a\lambda$ (m)
y coordinate parallel to latitude, $y = a\theta$ (m)
z height coordinate, later in the workthe log-pressure coordinate $z = z^* = -H\ln(p/p_s)$ (m)

Other

Q generic quantity
Q_r residual generic quantity Q (i.e. in TEM picture)
$\langle Q \rangle_x$ mean of Q w.r.t. a generic variable x
$[Q]$ zonal mean, i.e. $\langle\rangle_\lambda$
$\frac{\partial Q}{\partial x}$ partial derivative of Q when all other variables except x are held constant, depends on context
$\frac{\mathrm{D}Q}{\mathrm{D}t}$ material derivative of Q in the coordinates of interest, e.g. $\frac{\mathrm{D}}{\mathrm{D}t} = \frac{\partial}{\partial t} + u\frac{\partial}{\partial x} + v\frac{\partial}{\partial y} + \omega\frac{\partial}{\partial p}$

Greek alphabet

β first derivative of the Coriolis parameter, $\beta = \frac{\mathrm{d}f}{\mathrm{d}y}$ (/m/s)

ϵ_Q usually reserved to error in quantity Q

ζ relative vorticity

θ latitude (rad)

Θ potential temperature (K)

κ diffusive coefficient (SI units dependent on quantity)

λ longitude (rad)

μ inverse relaxation timescale, $\mu = \frac{1}{\tau}$ (/s)

ν angular frequency of an oscillation or a wave (rad/s)

π 3.14159265...

ρ density (kg/m^3)

τ relaxation timescale (radiative: τ_r, frictional: τ_f, no index: in the main body of work, it means radiative) (s)

ϕ cyclostrophic frequency, $\phi = \frac{u \tan\theta}{a}$ (/s)

Φ geopotential (m^2/s^2)

ψ quasi-geostrophic streamfunction, $\psi = \frac{\Phi}{f}$

Ψ streamfunction, $\Psi = \frac{2\pi a \cos\theta}{g} \int_0^p [v] dp$

ω pressure velocity (Pa/s)

Ω general rotation rate (rad/s)

Ω_E Earth rotation rate (rad/s)

Ω^* relative rotation rate, $\Omega^* = \frac{\Omega}{\Omega_E}$

List of abbreviations

Miscallaneous
eqn. equation
$[u]$-eqn. zonal mean zonal momentum equation
$[v]$-eqn. zonal mean meridional momentum equation
$[T]$-eqn. zonal mean temperature (heat, energy) equation
t.m. temporal mean
z.m. zonal mean
t.m.z.m. temporal mean and zonal mean
w.r.t. with respect to

Acronyms
ECHAM (the dynamical core)
EMIL ECHAM-MESSy Idealized (the idealized model used)
EPF Eliassen-Palm flux
FFT Fast Fourier Transform
GCM general circulation model
GW gravity wave
HS Held-Suarez (restoration temperature profile)
MESSy Modular Earth Submodel System (the simulation model framework)
PK Polvani-Kushner (restoration temperature profile)
PV potential vorticity
QG guasi-geostrophic
TEM transformed Eulerian mean
WSJ winter stratospheric jet

Contents

1 Introduction

In this section, I lay out the background, motivation and aims of this thesis. In the next section, which complements this one, more background is provided to specific topics of interest for this work - in terms of fundamental principles, previous studies, and assumptions in this research.

1.1 Context

In their essence, planetary atmospheres can be abstracted as rotating stratified fluids undergoing differential diabatic heating because of the spherical shape of the planet intercepting stellar radiation, and sometimes also through local physical and chemical sources of heat (e.g. water cycle). As recognized more than half a century ago by Lorenz (1967), "a general theory of planetary atmospheric circulations is as suitable a subject for theoretical study as the specialized theory of the circulation of the Earth's atmosphere". Since roughly that time, human made spacecraft are bringing data about Solar System objects, several of which have shallow but substantial atmospheres comparable to Earth. Among the objects with a solid surface, these are primarily Venus, Mars and Titan. Earth and Mars have similar rotation rates and relatively similar distance from Sun. Both atmospheres are roughly in geostrophic balance and exhibit Rossby waves and multiple circulation cells per hemisphere. There are still significant quantitative differences with regards to structure of winds and the extent of circulation cells, because of a factor of two difference in planetary radius, an order of two difference in atmospheric mass, and the fact that Earth has continent and oceans. On top of that - more precisely in the stratosphere - there is no ozone layer on Mars, so temperature monotonously decreases with height, which also has a dynamical effect. In contrast, Venus and Titan exhibit circulation regime not at all similar to Earth. This is mainly because of the dramatically lower rotation rate, which makes Coriolis force too weak to play a major dynamical role side by side to thermally-induced pressure gradients. Such atmospheres exhibit strong hemispheres-spanning Hadley cells, and strong westerlies above the equator - which, from the terrestrial point of view, can be called "anomalous". See Read et al. (2018) for a detailed review of planetary atmospheres in the Solar System.

As interesting as the Solar system is, it pales in comparison with the diversity of already known planets beyond the Solar system ("exoplanets"). First exoplanet detected around a main-sequence star was 51 Pegasi b back in 1995 (Mayor and Queloz, 1995). Since then the field of exoplanetary research became a firm part of mainstream astronomy, with upwards of 5000 confirmed detections at the time of writing in summer 2023. With so many parameters to vary necessarily comes the dynamical diversity of planetary atmospheres. Despite the large quantity of known exoplanets, many of them are poorly constrained - in many cases only one number from the pair (mass, radius) is known. Atmospheric composition is known in relatively few cases, which typically correspond to gas planets much larger and hotter than the Earth. For now, theoreticians seem to have the most to say about the possible conditions on such planets, and they need to resort to general physical principles rather than observational data.

The examples from planetary science quoted in previous paragraphs served mainly to motivate and illustrate the usefulness of thinking about planets as points in a many-dimensional parameter space, comprised by dimensions related to their astronomical context (related to star, orbit, natural satellites etc.), their bulk physical properties (gravity, size, rotation rate, atmospheric mass, presence of oceans) and to presence of key trace chemical species (CO_2, H_2O, ozone...). Note that the third category that I mentioned is the most problematic in this thinking, since these species often need to be present under specific conditions to accomplish a particular task, e.g. latent heat release in the Hadley cell is only possible if planet has appropriate temperature. Had the surface temperature at equator been 500 K rather than 300 K, the presence of given amount of water vapour would not have the same effect, although a "background" dry circulation would be rather independent of temperature (the latter claim features in Vallis (2012)). Such complication is still not incompatible with the general parametric approach, since 500 K and 300 K correspond to different locations along at least one axis. In

an ideal case, properly understanding the parametric dependence of circulation regimes would give researchers the ability to predict climate on any planet. Such "theory of everything" in planetary science would also have to explain the Earth, and its various paleoclimates (Caballero et al. (2008)).

First parametric studies emerged in 1980's: (Williams and Holloway, 1982),(Geisler et al., 1983), (Del Genio and Suozzo, 1987),(Williams, 1988a), (Williams, 1988b). A common feature that links these older studies with more modern ones is the use of fairly simple numerical models. This is to some extent because many specifics of modern Earth System Models are in fact unwanted in such a general study - after all we have no particular planet in mind, and even if we had, we would not know such details about it. More importantly, a simple model that is easier to interpret and link to the fundamental physics is a more suitable choice for this, still very theoretical, line of research. On a practical level, a computationally cheaper model allows to cover greater parameter space. The more modern work on this subject differs in motivations and the philosophy of treatment of the abstract space of planetary parameters. Kaspi and Showman (2015) seem to study partial variations of as many parameters as possible, to reason about tropospheric heat and moisture fluxes, with the motivation of assessing habitability of generic Earth-like exoplanets. Other studies are attacking the issue from a more theoretical perspective, trying to find dynamical similarities that would reduce this parameter space. (Wang et al., 2019) is such an example, where a classification of tropospheric regimes is made in a plane spanned by two dimensionless numbers - see section 2.9 for details.

1.2 Aims and assumptions

The aim of this work is to describe stratospheric features that emerge in an idealized GCM under a permanent solstice-like radiative forcing on *slowly rotating planets*, to study the quantitative budgets of the zonal mean equations, and to understand the underlying causal mechanisms. The single parameter which changes is the relative rotation rate $\Omega^* \equiv \frac{\Omega}{\Omega_E}$, and it takes values from 1 (Earth-like) down to 1/64, even though 1/16 and 1/32 are given more emphasis because of issues that 1/64 has, among other things with the diurnal cycle (see later). For the purposes of this work "fast rotator" means $\Omega^* = 1$ (sometimes 1/2), a "slow rotator" usually means $\Omega^* \leq 1/16$, and "intermediate rotator" is sometimes used for what is in between. It will later be shown that this terminology roughly corresponds to three distinct tropospheric circulation regimes. It will also be shown why rotation rate is the most useful single parameter to vary.

Assumptions, approximations and at times inadequacies are discussed in also in the next chapter and in the main body of work, where appropriate, and many of them are summarized in the final discussion section. Here I lay out the most important ones, so that reader is aware of them from the beginning. This Master thesis is in a way a sequel to the work Goetz (2023a), which explored many different aspects of tropospheric regimes, and among other things arrived to a similar classification to Wang et al. (2019) using K-means clustering. Unlike the previous studies, this thesis has the stratosphere as its main focus. Studying the stratosphere in a general parametric approach of the previous studies is somewhat more complex and problematic in terms of assumptions. The main reasons are:

1. Stratosphere is inherently seasonal. While the tropospheric features like the strength and position of the Hadley cell change *somewhat* with seasons, the fundamental nature of the circulation and the zonal wind pattern remains the same. This is what allowed studies like Wang et al. (2019) to use a simple, hemispherically symmetric and time-independent restoration temperature profile for their radiative parametrization - and still obtain very generally applicable instights into tropospheric dynamics. In contrast, behaviour of the stratosphere, in particular its radiatively determined state, fundamentally changes through the seasonal cycle, especially between near-equinox conditions and near-solstice conditions.

2. Large part of stratospheric dynamics is driven by trace species, in particular the ozone layer. Another influence is the rate of radiative cooling in the polar night region, set

mainly by the greenhouse gases. While the main parameters for the troposphere are the relatively immutable bulk physical parameters like the rotation rate, atmospheric mass, planetary radius, or the total amount of greenhouse gas (e.g. in CO_2 equivalent), stratosphere is also sensitive to relative details like the (photo)chemical equilibria that produce a given amount of ozone at a given altitude. This might be dependent also on how much UV is absorbed above the ozone layer by the bulk atmosphere, or what is the share of a particular sub-region of UV light on the stellar energy spectrum. Note that a planet with similar net insolation to Earth, revolving around a hotter star on a more distant orbit, could receive significantly more photochemically active UV than Earth, and vice versa.

The second issue stated is largerly philosophical, it can be avoided by proper framing of the research task. In this case, I am interested in planets that have Earth-like amounts of radiative forcing in places corresponding to the ozone layer on Earth, which quite likely means an Earth-like ozone layer. The subspace covering parameters that allow all the different mechanisms how this was achieved is in a way "collapsed" on this outcome. However, note that the ingredients for an ozone layer (i.e. O_2 and UV radiation) are likely not very rare in the Universe. In a similar fashion, it is assumed that the radiative relaxation timescale is similar to Earth, both in magnitude and in spatial distribution, in stratosphere and troposphere. This likely means similar total amount of greenhouse gases (in CO_2 equivalent). Net insolation is also assumed to be constant and roughly equal to Earth's through all simulations. How exactly these thermodynamic conditions are implemented will be addressed in the next two sections.

The first issue is fundamentally more problematic, since the model I had available for this work had a radiative parametrization in terms of a restoration temperature field independent of time and longitude, and similar in the meridional profile to the radiatively determined state of the Earth's atmosphere in January. This creates potential problems both with the seasonal cycle and the day-night cycle. For the seasonal cycle, the problems arise if the time scale that it takes for the simulation to converge is longer than the seasonal cycle. The seasonal cycle for Earth can be thought of as a timescale of a few months - at most 6, more reasonably 3. Planets on longer orbits should in principle be possible, but for the purposes of this study, a 3 months seasonal cycle will be used as a reference. It is not trivial to decide which circulation features that take more than 3-6 months to emerge would be present in a real time-dependent case. Further, the emergence of phenomena in the spin-up phase, when radiative forcing is suddenly applied to an initial state is not the same as the emergence of stratospheric solstice-time phenomena when going from an equinoctal "initial" state. For the problem with the daily cycle, the issue cannot be solved just by adding a temporal variation of the background profile, also a longitudinal dependence would be necessary, to account for the temperature gradient developing between the day and night sides. To which extent this gradient can develop depends on how the half-time of planetary rotation compares to the radiative relaxation timescale (40 days in the stratosphere). Rotation rates were chosen so that the former timescale is always smaller than the latter, although this is an exceedingly optimistic approach.

1.3 Structure

Next section defines and summarizes the essential theoretical concepts used in this work, and introduces the previous work on those topics that is relevant in our context. Section 3 describes the model setup and experiment planning. Section 4 is a quick overview of relevant simulation results, which also serves to define the particular questions that should be answered. Section 5 illustrates and justifies the mathematical framework used in the analysis, and applies it on the troposphere. Section 6 extends this to the stratosphere, and starts asking questions about causality. Section 7 studies the spin-up phase to answer on which timescales various features set in from a homogeneous motionless initial state. Section 8 takes a brief look at the zonal asymmetries that drive some of the zonal mean features described in preceding sections. Finally section 9 wraps up the discussion, once again critically assesses which parts of this idealized setup are likely generalizable, and how could further research on this topic look like.

2 Geophysical fluid dynamics on and beyond Earth

This section, which is a natural continuation of the introductory section, has several aims. The first aim is to introduce the notation, coordinate systems, constants, conversions and underlying equations that will be drawn upon in the main body of text. This is mainly accomplished through sections 2.1-2.2.

The second aim is to introduce or recapitulate those concepts in geophysical fluid dynamics that are either fundamental, or will be extensively used in this work. This will be typically done with the least possible mathematical complexity that still allows to qualitatively illustrate the main mechanisms. Complexity and precision of these will often be refined in the main body of the work, either because a more quantitative treatment is desired, or the approximations (like quasi-geostrophy) no longer hold outside of a certain range of length/time scales or Ω^* values. This aim is mainly accomplished through sections 2.3-2.8.

The third aim is to put this work in the context of previous research in a more methodic and detailed way, one that did not fit well in the introductory part. This will be the subject of section 2.9

2.1 Equations of geophysical fluid dynamics

The basic point of departure for any theoretical analysis is the full set of geophysical fluid equations on a spherical planet, see Vallis (2017), Chapter 1 for background and more comprehensive treatment. Let us first state the equations valid for an adiabatic and inviscid flow, and these two restrictions will be addressed shortly:

$$\frac{\mathrm{D}u}{\mathrm{D}t} - \left(2\Omega + \frac{u}{r\cos\theta}\right)(v\sin\theta - w\cos\theta) = -\frac{1}{\rho r\cos\theta}\frac{\partial p}{\partial\lambda} \tag{1}$$

$$\frac{\mathrm{D}v}{\mathrm{D}t} + \frac{wv}{r} + \left(2\Omega + \frac{u}{r\cos\theta}\right)u\sin\theta = -\frac{1}{\rho r}\frac{\partial p}{\partial\theta} \tag{2}$$

$$\frac{\mathrm{D}w}{\mathrm{D}t} - \frac{u^2+v^2}{r} - 2\Omega u\cos\theta = -\frac{1}{\rho}\frac{\partial p}{\partial r} - g \tag{3}$$

$$\frac{\partial\rho}{\partial t} + \frac{1}{r\cos\theta}\frac{\partial(u\rho)}{\partial\lambda} + \frac{1}{r\cos\theta}\frac{\partial}{\partial\theta} + \frac{1}{r^2}\frac{\partial}{\partial r} = 0 \tag{4}$$

$$\frac{\mathrm{D}}{\mathrm{D}t}\left[T\left(\frac{p_0}{p}\right)^{\frac{R}{c_p}}\right] = 0 \tag{5}$$

$$p = R\rho T \tag{6}$$

In addition, full spherical form of material derivative reads:

$$\frac{\mathrm{D}}{\mathrm{D}t} \equiv \frac{\partial}{\partial t} + \frac{u}{r\cos\theta}\frac{\partial}{\partial\lambda} + \frac{v}{r}\frac{\partial}{\partial\theta} + w\frac{\partial}{\partial r} \tag{7}$$

Where (r, θ, λ) denote radius from the center of the Earth, latitude and longitude measured in radians. The system above consists of six equations. Five are prognostic: three components of momentum, continuity and thermodynamics. One is diagnostic: equation of state for an ideal gas. In the equation of state $R = \frac{R_m}{\bar{M}_{m,air}} = 287$ J/K/kg, where $R_m = 8.31$ J/K/mol is the general molar gas constant and $\bar{M}_{m,air} = 28.97$ g/mol is the mean molar mass of air, which does not change from simulation to simulation. For a diatomic gas, $\frac{R}{c_p} = \frac{R}{7/2R} = \frac{2}{7}$, so this is also a constant across different simulations. There are six variables to be determined: u, v, w, p, ρ, T, so in its current form, the system is closed with no need of further equations to be provided.

A common baseline for analysis, are the *primitive equations*, these include three basic assumptions:

(i) *The shallow fluid approximation*:
Fluid depth (i.e. the range of vertical coordinate measured from the surface) is much

smaller than the radius of the Earth: $z \ll a$. This means that the spherical coordinate r, which expresses the distance from the centre of the Earth: $r = a + z \approx a$.

(ii) *The hydrostatic approximation*:
vertical momentum equation is reduced to $\frac{\partial p}{\partial z} = -\rho g$

(iii) *The traditional approximation*:
Coriolis terms involving the vertical velocity and the metric terms $\frac{uw}{r}$ and $\frac{vw}{r}$ are neglected.

With these 3 assumptions, the system of primitive equations becomes:

$$\frac{\mathrm{D}u}{\mathrm{D}t} - 2\Omega \sin\theta v - \frac{uv\tan\theta}{a} = -\frac{1}{\rho a \cos\theta}\frac{\partial p}{\partial \lambda} \tag{8}$$

$$\frac{\mathrm{D}v}{\mathrm{D}t} + 2\Omega \sin\theta u + \frac{u^2\tan\theta}{a} = -\frac{1}{\rho a}\frac{\partial p}{\partial \theta} \tag{9}$$

$$-\frac{1}{\rho}\frac{\partial p}{\partial z} - g = 0 \tag{10}$$

$$\frac{\partial \rho}{\partial t} + \frac{1}{r\cos\theta}\frac{\partial(u\rho)}{\partial \lambda} + \frac{1}{a\cos\theta}\frac{\partial}{\partial \theta} + \frac{\partial(w\rho)}{\partial z} = 0 \tag{11}$$

with last two equations remaining the same as in full equations. Material derivative only changes as a result of (i), by replacing r with a. It will be mentioned in section 3.2 that the dynamical core used in this study uses primitive equations, in somewhat different form, but similar underlying assumptions. Going from full to primitive equations is a simplification that has been proven to work well enough by decades of practice of modelling terrestrial atmospheric dynamics, and can be shown theoretically by scale analysis using values typical for terrestrial flows. In section 2.2, it will be motivated why it is reasonable to assume that this simplification can still be done for planets that rotate *more slowly* than the Earth.

So far, both systems above are insufficient, because they do not feature the non-conservative effects, i.e. diabatic and frictional processes. A term like $\frac{J}{c_p}$ needs to be added to the right hand side of the energy equation to represent diabatic heating, which can further be decomposed into latent and radiative heating. Frictional terms $\mathcal{F}_x$, $\mathcal{F}_y$, $\mathcal{F}_z$ are needed on the right hand sides of the three momentum equations to represent energy transfer to unresolved scales. Hence, four new equations for these new quantities in terms of existing quantities u, v, w, p, ρ, T are needed to close the system. How exactly this is accomplished in the model will be addressed later, in section 3.3.

2.2 Coordinate systems

The equations in 2.1 featured the ordinary height measured in meters as the vertical coordinate. This work mainly uses pressure as the vertical coordinate, and this coordinate system is always the basis for data analysis - unless otherwise stated. Derivations of transformations between coordinate systems are elementary and can be found in most classical textbooks on atmospheric dynamics. The role of pressure is replaced with the geopotential $\Phi \equiv gz$. Vertical velocity is now expressed not in m/s but Pa/s, as $\omega \equiv \frac{\mathrm{D}p}{\mathrm{D}t}$. The meaning of horizontal derivatives has

shifted to $\frac{\partial}{\partial\lambda} \equiv \left(\frac{\partial}{\partial\lambda}\right)_p$, and the same for $\frac{\partial}{\partial\theta}$. Primitive equations now take the following form:

$$\frac{\mathrm{D}u}{\mathrm{D}t} - 2\Omega\sin\theta v - \frac{uv\tan\theta}{a} = -\frac{1}{a\cos\theta}\frac{\partial\Phi}{\partial\lambda} \tag{12}$$

$$\frac{\mathrm{D}v}{\mathrm{D}t} + 2\Omega\sin\theta u + \frac{u^2\tan\theta}{a} = -\frac{1}{a}\frac{\partial\Phi}{\partial\theta} \tag{13}$$

$$\frac{\partial\Phi}{\partial p} = -\frac{RT}{p} \tag{14}$$

$$\frac{1}{a\cos\theta}\frac{\partial u}{\partial\lambda} + \frac{1}{a\cos\theta}\frac{\partial(v\cos\theta)}{\partial\theta} + \frac{\partial\omega}{\partial p} = 0 \tag{15}$$

$$\frac{\mathrm{D}T}{\mathrm{D}t} - \frac{RT}{c_p p}\omega = 0 \tag{16}$$

Material derivative now takes the following form:

$$\frac{\mathrm{D}}{\mathrm{D}t} \equiv \frac{\partial}{\partial t} + \frac{u}{a\cos\theta}\frac{\partial}{\partial\lambda} + \frac{v}{a}\frac{\partial}{\partial\theta} + \omega\frac{\partial}{\partial p} \tag{17}$$

An advantage of this system is that it makes the continuity equation divergence-free. A disadvantage is that pressure in the stratosphere varies by several orders of magnitude. This system is the effective point of departure for the zonal mean analysis done in section 5.2 and beyond. Other reasons why pressure coordinates are used in this study include (i) relative ease of intuitive interpretation, (ii) continuity and ease of intercomparison with the preceding work Goetz (2023a), Wang et al. (2019), Kaspi and Showman (2015) and (iii) the fact that simulation output is naturally provided in pressure coordinates, without a potential for introducing errors by coordinate conversion on a coarse grid.

Another system sometimes used in this study is the log-pressure coordinate system, where the vertical coordinate is defined as $z^* \equiv -H\ln(p/p_s)$. Here p_s is a standard reference pressure, taken as 1000 hPa and $H \equiv RT_s/g$ is a standard scale height, based on the global average surface temperature T_s. All simulations have the same radiative parametrization (section 3.3), which means that T_s is almost precisely the same across all simulations. For this reason, a constant value of $H = 8400$ m will be used for all cases. Another important concept that features in the equations is the reference density $\rho_0(z^*) = \rho_s e^{-z^*/H}$.

In this study, log-pressure coordinates replace the standard pressure coordinates when analysing wave motions that propagate vertically, or even have a vertical phase components. There it is much more convenient to work with a coordinate system roughly proportional to the physical height, since the vertical wave period in log-pressure coordinates of those waves is much more constant than the corresponding difference in pressure levels, and one can assume a harmonic structure like e^{imz^*}. Note that for an isothermal atmosphere, z^* and the physical height z coincide. For very qualitative interpretations, this might also be used generally, especially in large regions of the stratosphere, whis is approximately isothermal (albeit at a different temperature than T_s). None of these wave-related studies will be particularly quantitative.

Horizontal momentum equations are the same in pressure and log-pressure systems, vertical equation changes form but is in principle the same, continuity equation becomes:

$$\frac{\partial u}{\partial x} + \frac{\partial v}{\partial y} + \frac{1}{\rho_0}\frac{\partial(\rho_0 w^*)}{\partial z^*} = 0 \tag{18}$$

and the thermodynamic equation becomes:

$$\left(\frac{\partial}{\partial t} + u\frac{\partial}{\partial x} + v\frac{\partial}{\partial y}\right)\frac{\partial\Phi}{\partial z^*} + w^* N^2 = \frac{RJ}{c_p H} \tag{19}$$

Where N^2 is the Brunt–Väisälä frequency. To avoid any confusion in section 8 about interchanging N^2 and the static stability parameter $S_p \equiv \frac{RT}{c_p p} - \frac{\partial T}{\partial p}$, let me now explicitly show

their connection (recall that potential temperature $\Theta \equiv T\left(\frac{p_s}{p}\right)^{\frac{R}{c_p}}$):

$$N^2 \equiv g\frac{\partial \ln \Theta}{\partial z^*} \overbrace{=}^{\text{chain rule}} \frac{R}{H}\left(\frac{\partial T}{\partial z^*} + \frac{RT}{c_p H}\right) \overbrace{=}^{\text{defn.of } z^*} \frac{Rp}{H^2}\left(\frac{RT}{c_p p} - \frac{\partial T}{\partial p}\right) \tag{20}$$

$$= S_p p \frac{g^2}{RT_s^2} \tag{21}$$

Note: throughout this work, and in particular irrespective of the vertical coordinate system used, longitude λ and latitude θ (in radians) are used as horizontal coordinates. However, they are used *interchangeably* with the respective horizontal distances x and y (in meters). The two sets (λ, θ) and (x, y) have the same origin where the equator crosses the prime meridian, and are related through $x = a\lambda\cos\theta$ and $y = a\theta$. The reader should not be confused when these two notations alternate without further notice.

2.3 Balanced flow and scales

An insight into the nature of a geophysical flow can be gained through asking the question which dynamical balance in the equations presented above is the dominant one. Let us restrict ourselves to *balanced* flows, i.e. those that are time-independent, at least locally ($\frac{\partial}{\partial t} = 0$).

2.3.1 Earth: quasi-geostrophy

It can be shown via scale analysis of the two horizontal momentum equations that many large-scale flows in conditions typical for Earth are in approximate *geostrophic balance*:

$$fv \approx fv_g \equiv \frac{\partial \Phi}{\partial x} \qquad \text{and} \qquad fu \approx fu_g \equiv -\frac{\partial \Phi}{\partial y} \tag{22}$$

From now on, $f \equiv 2\Omega\sin\theta$, and the left and right hand sides of this definition will be used interchangeably. As a first-order (i.e. small departure) time-dependent theory derived from this steady state, the quasi-geostrophic theory is the basis of qualitative understanding of many weather phenomena on Earth (see e.g. chapter 6 of Holton and Hakim (2012)). When geostrophic balance is combined with hydrostaticity, thermal wind balance (TWB) emerges:

$$\frac{\partial v_g}{\partial \ln p} = -\frac{R}{f}\frac{\partial T}{\partial x} \qquad \text{and} \qquad \frac{\partial u_g}{\partial \ln p} = \frac{R}{f}\frac{\partial T}{\partial y} \tag{23}$$

In the numerical model used in this study, hydrostaticity is hardwired, so the validities of geostrophic and thermal wind balances are equivalent, and these two concepts can be used interchangeably.

2.3.2 Slow rotators: beyond quasi-geostrophy

The validity of geostrophic assumption is however limited, since the terms $\frac{\mathrm{D}u}{\mathrm{D}t}$ and $\frac{uv\tan\theta}{a}$ are also present in the zonal momentum equation, and their equivalents feature in the meridional momentum equation. For now let us neglect $\frac{uv\tan\theta}{a}$. Let L be the characteristic length scale of a phenomenon of interest and U its horizontal velocity scale. Then, the ratio of advective acceleration scales $\frac{U^2}{L}$ and Coriolis acceleration fU is the well-known Rossby number:

$$\mathcal{R}o \equiv \frac{U}{fL} \sim \frac{1}{\Omega} \tag{24}$$

For given U, L, it is apparent that Rossby number increases as the planet rotates more slowly. This means that acceleration, i.e. departure from geostrophic balance, is no longer very small, and quasigeostrophic dynamics cease to hold.

In the limit $\Omega \to 0$, Coriolis term fv becomes irrelevant, but its role can be in a way emulated by $\frac{uv\tan\theta}{a}$, which does not depend on Ω. For future purposes, let me define:

$$\phi = \frac{u\tan\theta}{a} \tag{25}$$

as the "cyclostrophic frequency" in an apparent attempt at analogy of terms fv and ϕv. Certain analogy truly exists, since ϕ is also monotonously rising with latitude, and is linear in v. Since $\lim_{\theta\to 0}\tan\theta = \lim_{\theta\to 0}\sin\theta = \theta$, it can even be used to define an equatorial beta-plane similar to the one derived from f. This is meaningful if $u(\theta)$ is reasonably constant around the equator. As just noticed, the main difference of ϕ from f is that it also depends on u itself, so its spatial pattern is more heterogenous, as will be seen in later chapters. Within this work, this lowercase ϕ should not be confused with the capital Φ, which is always geopotential (just like θ is latitude and Θ is potential temperature). Reader should be advised that ϕ is not a standard notation in the field - there is, to my knowledge, no established tradition of labelling this in any particular way. The entire term $\frac{uv\tan\theta}{a}$ is usually called just "metric term". In the meridional momentum equation, there is the term $\frac{u^2\tan\theta}{a}$. Naturally, it is not very useful to rewrite this term as "ϕu", but it still carries a limited analogy to fu because of its monotonously increasing dependence on u and θ. It also effectively replaces fu in the limit $\Omega \to 0$ in a similary way to fv and ϕv in the zonal equation. In this limit, the balanced state of the atmosphere is called the *cyclostrophic balance*:

$$\frac{uv\tan\theta}{a} \approx \frac{u_c v_c\tan\theta}{a} \equiv \frac{\partial\Phi}{\partial x} \qquad \text{and} \qquad \frac{u^2\tan\theta}{a} \approx \frac{u_c^2\tan\theta}{a} \equiv -\frac{\partial\Phi}{\partial y} \tag{26}$$

The term cyclostrophic refers to the centrifugal force, however it should not be confused with the terms cyclostrophic (or gradient) balance as used for weather patterns for Earth. There, the centrifugal effect is provided by the intrinsic curvature of the flow on Earth, e.g. in a cyclone. In the term $\frac{u^2\tan\theta}{a}$, it is easy to see that it is the curvature of the Earth itself which provides the centrifugal effect.

For a cyclostrophic atmosphere and using the hydrostatic assumption, one can derive a relationship analogous to thermal wind balance in the geostrophic case. In the case of meridional momentum equation:

$$\frac{\partial u_c^2}{\partial \ln p} = -\frac{a}{RT^2\tan\theta}\frac{\partial T}{\partial y} \tag{27}$$

There is to my knowledge no such easy expression for v_c because of the product $u_c v_c$ in the zonal momentum equation. After differentiating through the product, one gets:

$$\frac{\partial u_c}{\partial p}v_c + \frac{\partial v_c}{\partial p}u_c = \frac{a}{\tan\theta}\frac{\partial}{\partial x}\frac{\partial\Phi}{\partial p} \tag{28}$$

This can only lead as far as

$$\frac{\partial \ln v_c}{\partial p} = \frac{a^2}{\tan^2\theta}\frac{\partial\Phi}{\partial x}\frac{\partial}{\partial x}\frac{\partial\Phi}{\partial p} - \frac{\partial \ln u_c}{\partial p} \tag{29}$$

Whether equation 27 is the dominant balance is also contrained by $\frac{\mathrm{D}v}{\mathrm{D}t}$. For lack of any established notation, let me define the "cyclostrophic Rossby number" $\mathcal{R}o_c$ as:

$$\mathcal{R}o_c = \frac{V^2/L}{U^2/a} = \frac{a}{L}\frac{V^2}{U^2} \tag{30}$$

Here, it was necessary to explicitely distinguish the horizontal wind scales in the meridional and zonal direction, otherwise it would (wrongly) suggest that advective acceleration is always larger than cyclostrophic acceleration, for so long as the horizontal scale $L < a$. Also, I defined it using the meridional advective term, since for future analysis of the zonal mean state, the horizontal advection $\sim u\frac{\partial v}{\partial x}$ cancels out.

2.4 Zonally symmetric Hadley circulation

The meridional circulation in the troposphere at low latitudes on Earth is named after George Hadley, who correctly identified the trade winds as being connected to the large-scale tropical overturning (Hadley (1735)). His theory was still flawed, since he postulated that momentum is materially conserved rather than angular momentum (Ferrel (1858)). Zonal mean specific angular momentum $[M]$ is defined as:

$$[M] = a\cos\theta([u] + \Omega a\cos\theta) \tag{31}$$

Here $[u]a\cos\theta$ is the relative angular momentum, and $\Omega a^2\cos^2\theta$ is the planetary angular momentum, their interpretation following straightforwardly from the definition of $\vec{M} = \vec{r} \times \vec{v}_{absolute} = \vec{r} \times (\vec{v}_{relative} + \vec{\Omega} \times \vec{r})$. If inviscid and axisymmetric meridional flow is subjected to the Coriolis force, then $[M]$ is materially conserved, angular momentum being exchanged between planetary and relative components.

A very useful approximate zonally symmetric model was proposed by Held and Hou (1980). It is based upon the differences between the meridional potential temperature profiles $\Theta_E(y)$ and $\Theta(y)$ arising respectively from: (i) hypothetical radiative equilibrium and (ii) thermal wind balance (TWB). TWB Θ-distribution is dictated by vertical wind shear $\partial u/\partial z$ between the angular momentum-conserving poleward flow in the inviscid upper branch, and the viscous lower branch $u \sim 0$. Using the continuity of Θ at the terminating latitude $\theta = \theta_H$ and conservation of Θ over a branch, one can derive the linearized equation:

$$\theta_H \approx \sqrt{\frac{5}{3}\frac{R\Delta\Theta_h}{\Omega^2 a^2}} = \sqrt{\frac{5}{3}\mathcal{R}o_T} \sim \frac{1}{\Omega} \tag{32}$$

Here $\mathcal{R}o_T$ is the thermal Rossby number (given more attention in section 2.9), H is the vertical scale and $\Delta\Theta_h$ is the horizontal potential temperature difference between polar and equatorial regions. If we roughly estimate the jet speed by angular momentum conservation, we get:

$$[u](\theta = \theta_H) \approx \frac{\Omega a\sin^2\theta_H}{\cos\theta_H} \approx \Omega a\theta_H^2 \sim \frac{1}{\Omega} \tag{33}$$

This model has natural limitations, like the absence of latent heating, seasonality, dissipative processes in the uper layer, and the mathematical simplifications made. The version presented here is the most simplistic one. It is still a useful reference point for the potentially expected scaling of related phenomena in a sequence of simulations with varying rotation rate. The formulas above are somewhat reasonable on Earth ($\pm 30\%$), but they are essentially a small θ_H limit, and for $\Omega^* < 1$, they are no longer adequate even for rough scaling arguments. In a later paper (Hou (1984)) a theory applicable to the other limit: $\Omega^* \ll 1$, or more generally $\mathcal{R}o_T \gg 1$. The formula for the angular extent then reads:

$$\theta_H \approx \frac{\pi a}{2}\left(1 - \frac{3}{8\mathcal{R}o_T}\right) \tag{34}$$

2.5 Waves

Waves are important drivers of atmospheric dynamics, since they carry momentum and energy, which they can deposit far from their place of origin. There are several types of waves in Earth's atmosphere, which can broadly be divided into those whose restoring force is provided by buyoancy effects, and by rotation effects.

2.5.1 Gravity waves

In the atmosphere, the former category comprises internal gravity waves (GWs). GWs require *stable* stratification, which is given by a real Brunt-Väisälä frequency N defined in section 2.2. Motions of air parcels under GWs can have horizontal components, making their orbit

tilted ellipses, and prolonging their periods. The shortest period $\frac{2\pi}{N}$ is for purely vertical oscillations (the accoustic-gravity waves), the longest periods, associated with largest spatial wavelenghts, are close to the rotational period of the planet (the inertia-gravity waves). Most GCMs, including the one in this study, can only directly resolve the latter extreme. The usual approach is to parametrize the effect of GWs on the general circulation on Earth. This is not done in the model used here, because so little is known about the climate on the hypothetical planets in this study. Note that the effect of accoustic-gravity waves on the general circulation is negligible on Earth, but there are still the intermediate frequencies that are at the same time dynamically important, and still not resolved by GCMs (Medvedev and Yiğit (2019)). It will later be seen and discussed that this is a drawback of this work.

2.5.2 Rossby waves

In a baroclinic atmosphere, Rossby waves (also called *planetary waves*) owe their existence to the meridional potential vorticity (PV) gradient. Within the QG model, their dispersion relation reads:

$$\nu = [u]k - \frac{\beta k}{k^2 + l^2 + \frac{f_0^2}{N^2}m^2} \tag{35}$$

Since the zonal phase speed is $c_x = \frac{\nu}{k}$, it is apparent that they always propage to the west with regards to the mean flow $[u]$. Via momentum conservation, their effect in their place of formation is to accelerate the mean flow to the east. This is how *eddy driven jets* form in the troposphere on Earth. Apart from being a decisive element for tropospheric weather in mid-latitudes, which is not the aim of this study, they propagate to the stratosphere, where they break and deposit their momentum and energy, and affect the mean flow (see section 2.6). Their main stratospheric effect is a deceleration of the eastward mean flow. Note that unlike the Rossby waves, gravity waves do not have a similar constraint, and can both accelerate and decelerate an eastward flow in the stratosphere.

2.6 Eddy-induced circulation

It was noted that waves are important because they carry energy and momentum around the atmosphere, thus impacting the mean flow. In this work, the term *eddy* is used for any deviation Q^* of a generic quantity Q from the zonal mean state $[Q]$, according to the decomposition:

$$Q^* \equiv Q - [Q] \tag{36}$$

In many contexts, the terms *eddies* and *waves* are used interchangeably in this work. Compared to the original meaning of the word, this is a slight abuse of terminology, that is nevertheless very common in the field (look no further than Holton and Hakim (2012)). Wave usually refers to the specific motion, and *eddy* is used in an abstract sense, especially when analyzing its impact on the zonal mean flow.

Decomposition 36 can be used for a convenient analysis of the impacts of eddies on the mean flow. Let us take the quasi-geostrophic (QG) zonal momentum and temperature equations on a mid-latitude f-plane as an example:

$$\frac{\partial u}{\partial t} + u\frac{\partial u}{\partial x} + v\frac{\partial u}{\partial y} + \omega\frac{\partial u}{\partial p} - f_0 v = -\frac{\partial \Phi}{\partial x} + \mathcal{F}_x \tag{37}$$

$$\frac{\partial T}{\partial t} + u\frac{\partial T}{\partial x} + v\frac{\partial T}{\partial y} + \omega\frac{\partial T}{\partial p} - \frac{RT}{c_p p}\omega = \frac{J}{c_p} \tag{38}$$

After performing the decomposition $Q = [Q] + Q^*$, taking the zonal mean, using the defining features of the operator[]: (i) $[Q^*] \equiv 0$, (ii) $[[Q]] \equiv [Q]$, (iii) $[\frac{\partial}{\partial x}] \equiv 0$ and using the scales typical for Earth to eliminate terms order-of-magnitude smaller than the main balance (essentially a

QG scaling), one is left with:

$$\frac{\partial[u]}{\partial t} + \frac{\partial}{\partial y}[v^*u^*] - f_0[v] = [\mathcal{F}_x] \tag{39}$$

$$\frac{\partial[T]}{\partial t} + \frac{\partial}{\partial y}[v^*T^*] - S_p[\omega] = \frac{[J]}{c_p} \tag{40}$$

$[v^*u^*]$ and $[v^*T^*]$ are the meridional eddy fluxes of zonal momentum and heat. They are obtained through the fact that advective terms are non-linear, and even though they were neglected in their mean flow component, their eddy component was retained. Note that this system based on QG scaling is not adequate for the task of this work (or, for that matter, analysis of the Earth), and a more robust scheme based on (i) primitive equations, and (ii) scales from the simulation output, will be employed in the main body of work.

Let us illustrate the use of the zonal mean equations above. In the troposphere, the two eddy divergence terms are primarily associated with Rossby waves, and both have maxima in mid-latitudes. In the $[u]$-eqn., $\frac{\partial[v^*u^*]}{\partial y}$ acts as a zonal force, which corresponds to negative (westward) momentum being deposited *into* the Rossby waves, which form in this region. Separately, it would act to accelerate the mean flow away from geostrophic balance, which in QG picture creates a perpendicular (meridional) pressure gradient, which drives a meridional circulation. On Earth, this is called the Ferrel cell. Meridional circulation in turn produces a zonal Coriolis force $f_0[v]$ which opposes the initial tendency caused by eddies, and allows to preserve a long-term steady state $\frac{\partial[u]}{\partial t} = 0$. A similar argument exists for the $[T]$-equation, where the steady state is maintained by the fact that eddy heat divergence $\frac{\partial[v^*T^*]}{\partial y}$ and diabatic heating $\frac{[J]}{c_p}$ are compensated by the adiabatic heating $S_p[\omega]$ associated with the induced meridional circulation. See any dynamic meteorology textbook (e.g. Holton and Hakim (2012)) for more details.

So far, it was not mentioned that even the so called "ideal" (= linear, frictionless, isentropic, amplitude conserving) Rossby waves posses Stokes drifts, which means that the so called Eulerian-mean circulation ($[v], [\omega]$) they induce is not equal to the actual mean trajectories of air parcels. The so called residual velocities correct for the effect of Stokes drifts:

$$[v]_r = [v] + \frac{\partial}{\partial p}\left(\frac{[v^*T^*]}{S_p}\right) \tag{41}$$

$$[\omega]_r = [\omega] - \frac{\partial}{\partial y}\left(\frac{[v^*T^*]}{S_p}\right) \tag{42}$$

Note that these components are physically consistent, i.e. the meridional circulation ($[v]_r, [\omega]_r$) is still divergence-free. Substituting these components into the (Eulerian) zonal mean equations for $[u]$ and $[T]$, one gets the so called transformed Eulerian mean (TEM) equations:

$$\frac{\partial[u]}{\partial t} = f_0[v]_r \overbrace{- \frac{\partial}{\partial y}[v^*u^*] - f_0 \frac{\partial}{\partial p}\left(\frac{v^*T^*}{S_p}\right)}^{\nabla \cdot \vec{F}} + [\mathcal{F}_x] \tag{43}$$

$$\frac{\partial[T]}{\partial t} = S_p[\omega]_r + \frac{[J]}{c_p} \tag{44}$$

Where $\nabla \cdot \vec{F}$ is the divergence of the Eliassen-Palm flux (also called EPF, or EP flux). According to the standard view, $\nabla \cdot \vec{F}$ gives the net effect of eddies on the mean zonal flow. Note that the influence of eddies was eliminated from the $[T]$-equation. This version of this equation shows that any steady-state residual vertical motion must be counteracted by diabatic heating. Note that this does not mean that this motion is *caused* by diabatic heating. The $[T]$-equation says nothing about causality, a fact that I am going to use extensively in the main body of work. It can very easily be that $[J]$ is a *result* of adiabatic heating $S_p[\omega]_r$, where $[\omega]_r$ is forced by $[v]_r$ via the continuity equation, where $[v]_r$ is driven by eddies. In fact, this is the established interpretation of the causation chain in the stratosphere on Earth (Becker (2012)). However,

the freedom in the direction of causation is restricted by the other equation, the $[u]$-equation, since for a frictionless steady-state stratosphere $f_0[v]_r = \nabla \cdot \vec{F}$. Mean flow can modify wave-breaking, but it does not *cause* waves to exist. Thus, after all, there is no consistent pathway for a radiatively-driven circulation where $[J]$ causes $[\omega]_r$, which causes $[v]_r$ by continuity in absence of eddies, all while maintaining a steady state. To be precise, not in this QG model, but this all is possible when non-linear terms are included in the $[u]$-equation. As will be seen later, $[v]_r \frac{\partial [u]}{\partial y} + [\omega]_r \frac{\partial [u]}{\partial p} \sim f[v]_r$ is a realistic dominant balance for slowly rotating planets, one that can be associated with $[J]$ causing $[\omega]_r$.

In the previous paragraph, wave-breaking was implicitly equated with $\nabla \cdot \vec{F}$ in the stratosphere. Ideal QG waves are always accompanied by a mean meridional circulation $([v], [\omega])$ which balances the Stokes drifts and the momentum/heat fluxes associated with the wave (Becker (2012)). Only non-ideal (e.g. breaking) waves can induce the residual circulation, which roughly corresponds to the true Lagrangian circulation of air parcels (Dunkerton (1978)), e.g. the Brewer-Dobson circulation known in Earth's stratosphere. Note that there are some alternative frameworks, e.g. the generalized Lagrangian mean, see Butchart (2014) for a review. Also note that when eddy forcing disappears, $([v]_r, [\omega]_r)$ trivially becomes $([v], [\omega])$.

2.7 Stratospheric dynamics and radiation

On Earth, the main driver of stratospheric meridional circulation are the upward propagating and breaking Rossby and gravity waves, some aspects of which were discussed in the previous two subsections. Another factor is radiation, which creates temperature gradients, which are especially pronounced around solstices in the winter hemisphere. Radiation determines the temperature structure in two main ways. First is the ozone layer, which absorbs the incoming solar UV radiation, and thus creates an unusually warm layer. This mechanism is restricted by the amount of incoming sunlight. During a solstice, it has a maximum at the summer pole, but it is still relatively high in the low latitudes of either hemisphere. However it is very low in winter mid-latitudes, and absent in the winter polar region. The second mechanism is caused by greenhouse gases such as CO_2. In particular the upper layers in the polar night region can very efficiently radiate their thermal energy away. Corresponding radiative (e-folding) timescale is roughly a month (Wang et al. (2019)). Radiatively determined state in January can be seen in figure 1 taken from Becker (2012), where it is compared to the actual temperatures during that time, as calculated by a model with in principle similar treatment of radiative processes to the one in this study. The differences between the two temperature profiles are entirely dynamically driven. The treatment of radiative processes that was just mentioned consists of de-coupling the dynamics and the radiation (or more generally the diabatic processes). This means that any dynamically induced temperature deviations from the radiatively determined state are relaxed back with a timescale, which is generally space-dependent and reflective of its true values on Earth. In my simulations, a similar radiatively determined profile to that in figure 1 is used as the restoration temperature field, see section 3.3 for the technicalities. If one assumes a similar total amount of ozone and greenhouse gases (and that the latter act as chemically passive tracers), and similar orbital period, this should be, with some exceptions, relatively generalizable to planets with different rotation rates. In particular, the structure of the polar night region should not be significantly changed, assuming that greenhouse gases are mixed evenly with the air. For the ozone, at least in the upper part of the ozone layer, the ozone distribution is photochemically controlled, i.e. it does not depend on transport as much as on the incoming UV. While the transport and redistribution processes can change with rotation rate because of different dynamics, the incoming UV should not. The upper part of the ozone layer is also the part which can alter the temperature most easily - unlike the ozone partial pressure, which peaks at about 25 km, the ozone mixing ratio peaks at about 40 km. Hence I deem it acceptable to re-use the same restoration temperature profile to planets with different rotation rates.

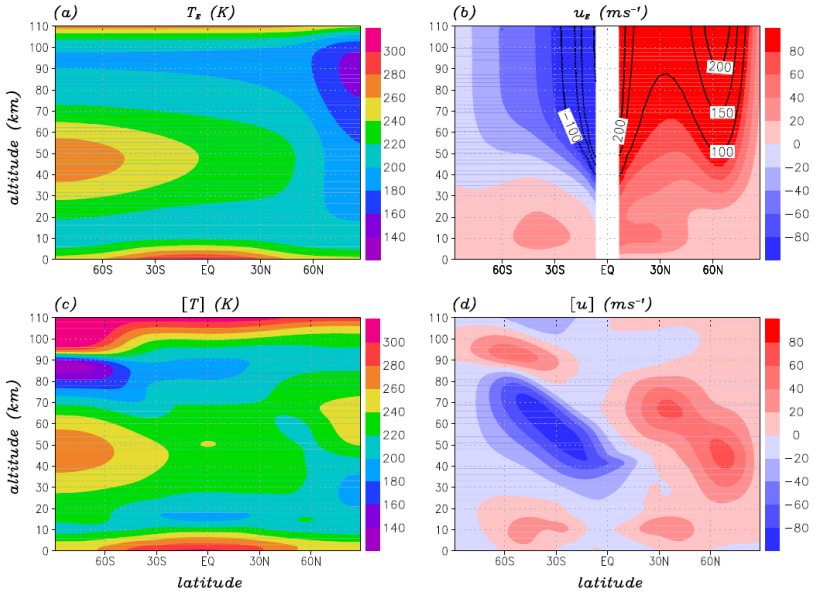

Figure 1: **taken from Becker (2012)**. At the top is a synthetic radiatively determined state for Earth in January and its associated geostrophic wind. At the bottom is a real temperature profile from a simulation which is nudged towards the radiatively determined state, the differences between the two profiles thus being entirely dynamically determined. On the bottom right is the wind field from the same simulation.

2.8 Superrotation

Superrotation is an atmospheric phenomenon documented on some slowly rotating Solar Sytem bodies (Read et al. (2018)), Venus and Titan. Local superrotation is a state in which a point in the atmosphere rotates around the planetary axis of rotation with more angular momentum than the solid surface at the equator. Even the weakest westerly winds above the equator thus amount to superrotation, just as any westerly winds away from the equator, if they are so strong that they could not have been simply transported there from a state of rest at the equator in an angular momentum conserving flow. In this work, superrotation is diagnosed with the local superrotation index $[s]$, which expresses the relative departure of angular momentum $[M]$ from its reference value. The reference value is Ωa^2, i.e. a state of solid body rotation at the equator:

$$[s] = \frac{[M]}{\Omega a^2} - 1 \tag{45}$$

For a given planet (fixed Ω), $[s]$ is just a conveniently scaled angular momentum.

The natural question is how is atmosphere able to generate and maintain such state, in other words where does the angular momentum come from. Hide's theorem (Vallis (2017)) tells us that a local maximum in angular momentum (e.g. superrotation) cannot be maintained by the mean flow. A local maximum in angular momentum implies upgradient eddy momentum fluxes (Vallis (2012)). In its general form, it is applicable to any quantity Q that is advected and diffused with coefficient κ in a steady state ($\frac{\partial Q}{\partial t} = 0$). Let us imagine a 2D incompressible flow with no source term:

$$\frac{\mathrm{D}Q}{\mathrm{D}t} = \nabla \cdot \kappa \nabla Q \implies \nabla \cdot (\vec{u}Q) = \nabla \cdot \kappa \nabla \tag{46}$$

Suppose there is a maximum of Q somewhere in the interior of the flow. Let us draw an area $\mathcal{A}$ around this maximum, delimited by a curve $\partial\mathcal{A}$, such that $\partial\mathcal{A}$ is an isoline of Q. Let us

now integrate the left hand side of 46 over this area, employing the Stokes theorem:

$$\int_{\mathcal{A}} \nabla \cdot (\vec{u}Q)\, d\mathcal{A} = \oint_{\partial\mathcal{A}} (\vec{u}Q) \cdot \hat{n}\, dl = Q \oint_{\partial\mathcal{A}} \vec{u} \cdot \hat{n}\, dl = Q \int_{\mathcal{A}} \nabla \cdot \vec{u}\, d\mathcal{A} = 0 \tag{47}$$

Let us integrate the right hand side:

$$\int_{\mathcal{A}} \nabla \cdot (\kappa \nabla Q)\, d\mathcal{A} = \oint_{\partial\mathcal{A}} (\kappa \nabla Q) \cdot \hat{n}\, dl \neq 0 \tag{48}$$

here the last inequality stems from the fact that $\partial\mathcal{A}$ contains an extremum somewhere inside it. Because of the contradiction between its left and right hand sides, equation 46 cannot hold in this setup. In physical terms, diffusion always dissipates an initial extremum, and advection can do nothing to stop it. The reason why an angular momentum extremum can exist at the ground is that only there are surface stresses that can balance the diffusive loss of westerly momentum into the fluid interior. This extremum value is Ωa^2, since winds are zero directly at the surface. Moving vertically up at the equator, angular momentum can only decrease. To be more precise, angular momentum is not an advective-diffusive quantity, since it is (linear) momentum that undergoes diffusion, but at a given latitude the two map one-to-one.

A way how to reconcile the left and right hand sides of equation 46 in a setup with an isolated maximum along the vertical, is to assign κ a different sign in various places. This would make the right hand side equal to zero. Physically, a steady axisymmetric state with a maximum along the vertical can be maintained by countergradient diffusive transport along the horizontal. This task can be accomplished by eddies (Read and Lebonnois (2018)). Note that $\frac{\partial[M]}{\partial t} = a\cos\theta \frac{\partial[u]}{\partial t}$, and by considering the eddy terms in the z.m. zonal momentum equation, it can be seen that they directly contribute to the angular momentum budget. By Hide's theorem, it is not possible for advective terms in the same equation to do so. Precise mechanisms of how the upgradient transfer is accomplished by eddies are not given here and vary among various planetary setups (Mitchell and Vallis (2010)).

2.9 Parameters affecting circulation patterns

Terrestrial atmospheric motions are primarily set by two important factors - by (i) meridional gradients due to differential diabatic heating, which is itself mainly due to solar radiation, and (ii) by fictitious (mainly Coriolis) forces due to planetary rotation. The former can be roughly described by an equator-to-pole potential temperature difference $\Delta\Theta_h$, the latter by the rotation rate Ω - or its dimensionless analog $\Omega^* = \Omega/\Omega_{Earth}$. These constitute a natural first guess for the basis of the parameter space of circulation regimes.

There exists a dynamical similarity (see e.g. Pinto and Mitchell (2014), albeit imperfect, between planets in various places of parameter space due to a simple scaling argument based on thermal wind scale

$$U_T = \frac{R\Delta\Theta_h}{\Omega a} \tag{49}$$

Here $\Delta\Theta_h$ represents the horizontal (i.e. equator-to-pole) temperature contrast, R is the molar gas constant, and a is planetary radius, which sets the horizontal length scale for the largest features. This velocity scale can be used to define thermal Rossby number, first mentioned in section 2.4, and repeated here for convenience:

$$\mathcal{R}o_T = \frac{R\Delta\Theta_h}{\Omega^2 a^2} \sim \frac{1}{\Omega^2} \tag{50}$$

As was seen in section 2.4, $\mathcal{R}o_T$ sets the latitudinal scale of the Hadley cell. Generally, since a wider Hadley cell on slower rotators means that larger areas of planetary atmosphere are being efficiently stirred, the effective result of slower rotation is a decreased $\Delta\Theta_h$, so unlike Ω, $\Delta\Theta_h$ is not an immutable externally imposed parameter. Here lies, in my opinion, a slight inconsistency never acknowledged in literature. For U_T and $\mathcal{R}o_T$, $\Delta\Theta_h$ has the meaning of actual equator-to-pole difference in actual physical temperature, one that is related to the

geopotential gradient that features in geostrophic balance equation. Note that it does not matter whether it is ΔT_h or $\Delta\Theta_h$, since on a given pressure level near the surface they are the same. However, studies such as Wang et al. (2019) at the very same time use this same quantity $\Delta\Theta_h$ as the *imposed* equator-to-pole temperature difference, which in that case refers to the radiative-convective restoration temperature profile they used as a Newtonian parametrization of radiative forcing (see 3.3). As will be seen in this work, the actual $\Delta\Theta_h$ in the model output can change significantly as one varies the rotation rate, even for the same prescribed $\Delta\Theta_h$ corresponding to radiative forcing.

There is a further physical reason for the importance of rotation rate, this time not related to its effect on the mean flow, but on eddies. Dominant baroclinic length scale is inversely proportional to the rotation rate (Walker and Schneider, 2006). Baroclinic instability is typically the primary source of eddies in the extratropics (Pedlosky, 2013). Smaller eddies are generally less efficient in ensuring meridional heat transport, which acts in the direction of larger $\Delta\Theta_h$ for faster rotators. This does not mean that there are more eddies on slower rotators, quite the opposite, since there is no baroclinic instability in most of the atmosphere because of the extensive and strong Hadley cell. Thus, the Hadley cell is not only responsible for most of the meridional heat transport by itself, but also in a way prevents eddies from "taking their part".

Except for $\mathcal{R}o_T$, other important non-dimensional numbers include Burger and Taylor number. Burger number

$$\mathcal{B}u = \frac{R\Delta\Theta_v}{2\Omega^2 a^2} \sim \frac{1}{\Omega^2} \tag{51}$$

is an analogy to $\mathcal{R}o_T$ that features the vertical (instead of meridional) temperature stratification and thus expresses the importance of baroclinic instability. The second important dimensionless number is the Taylor number $\mathcal{T}a$, which can be defined using the timescale τ of one of the two main damping processes, radiation (τ_r) and friction (τ_f).

$$\mathcal{T}a = 4(\Omega\tau)^4 \tag{52}$$

In previous studies (Wang et al. (2019), Goetz (2023a)), tropospheric circulation regimes were explored in the plane defined by $\mathcal{R}o_T$ and $\mathcal{T}a_f$.

It should be noted that since both $\mathcal{R}o_T$ and $\mathcal{T}a_f$ contain an explicit Ω-dependence, the sequences of simulated regimes on the main diagonals of figure 2 were obtained by changing purely Ω^*, not the other parameters like τ_f or the $\Delta\Theta_h$ of the forcing. Sporadic different values of $\mathcal{R}o_T$ for the same rotation rate and $\mathcal{T}a_f$ are caused by changing $\Delta\Theta_h$. According to Goetz (2023a), Goetz (2023b), small values of rotation rates ($\Omega^* < 1/10$) fall into the quasi-axisymmetric barotropic regime. A characteristic feature of this regime is a hemispheric-wide Hadley cell, overall lack/weakness of eddy motions and tropospheric superrotation. Hence it is often also called the superrotating regime. $1/10 < \Omega^* < 1/2$ is defined as the regular baroclinic regime. This is similar to Earth, but with overall more regular spatio-temporal pattern of midlatitude planetary waves. For $\Omega^* > 1/2$, this pattern is seemingly chaotic in time, and typically many zonal wavenumbers are present simultaneously. Wang et al. (2019) recognize also the multiple zonal jet flow for $\Omega^* > 3$, which, as the name suggests, supports multiple zonal bands of eddy-driven jets, similar to e.g. Jupiter in solar system. All the Ω^* values quoted here represent regions of $\mathcal{T}a_f$-$\mathcal{R}o_T$ plane, with the assumption that τ and $\Delta\Theta_h$ are similar to Earth. For all Ω^*, when either τ is small enough (strong damping), or $\Delta\Theta_h$ is small enough (weak forcing), the regime is termed "weak flow" by Goetz (2023a), or "axisymmetric flow" by Wang et al. (2019), both descriptions being accurate. These last two regimes are not of special interest here.

For the purposes of this study, I will mainly use Ω^* directly, as opposed to $\mathcal{R}o_T$ or $\mathcal{T}a$, since other parameters are fixed most of the time, but I might make occasional reference to these (or other) dimensionless numbers.

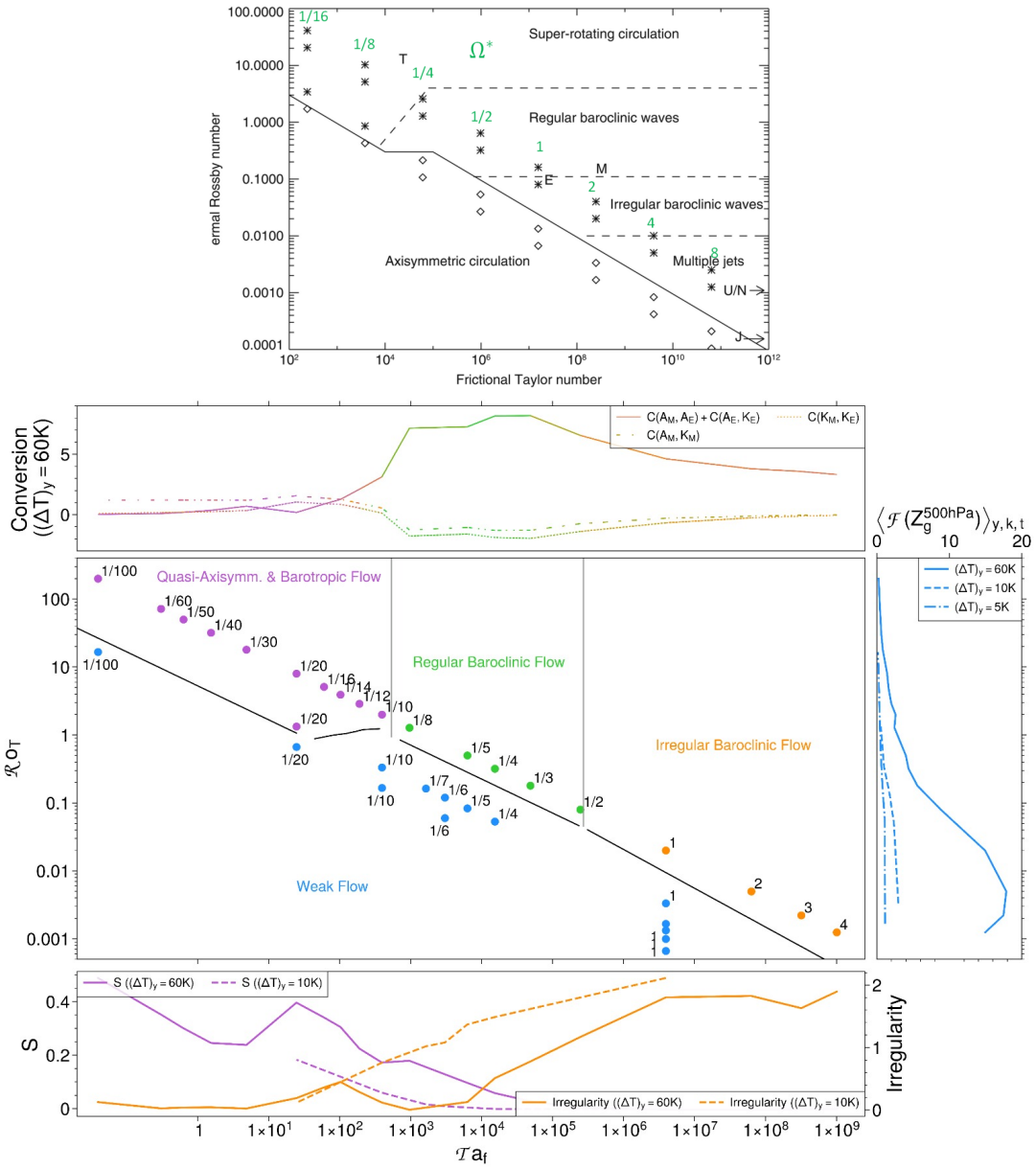

Figure 2: Top: **(taken from Wang et al. (2019))** Classification of tropospheric circulation regimes in $\mathcal{T}a_f$-$\mathcal{R}o_T$ plane. Green numbers near the points represent the relative rotation rate Ω^*, and these were added by me for additional clarity.
Bottom: **(taken from Goetz (2023b))** Another attempt at the same classification, this time more methodically - using K-means clustering. Side panels are not important for the purposes of this work.

3 Experiment setup

3.1 MESSy

The model framework used for simulations is Modular Earth Submodel System, from now on MESSy (Jöckel et al. (2005)). Its main feature is modularity and relative ease of combining submodels of various complexity, from box models, to full 3D Earth System Models. Interested reader is invited to consult the official website to learn the specifics `https://messy-interface.org/`.

3.2 ECHAM

The base model of MESSy is always a dynamical core coupled to individual physical or chemical submodels. Dynamical core used in this study is the 5th generation ECHAM (Roeckner et al. (2003)). It solves hydrostatic primitive equations using spectral transform method with triangular truncation. Prognostic variables include temperature, vorticity, divergence and surface pressure, expressed via a truncated series of spherical harmonics Roeckner et al. (2006). This work uses truncation at horizontal wavenumber 42, i.e. resolution T42. There are 128 grid points in longitude and 64 in latitude, or a horizontal resolution of roughly 300 km. This is not enough to resolve most of gravity waves (GWs), and because existing parametrizations are valid for Earth, they were not used in this work. GW-driven circulation features will be affected - for example the Brewer-Dobson circulation that feels also the GW effect (see e.g. Cohen et al. (2014)). However, as will become apparent, the influence of eddies on stratospheric circulation overall decreases. Radiation and non-linear advection are more important for more slowly rotating planets.

3.3 EMIL and RELAX

The acronym EMIL stands for ECHAM/MESSy IdeaLized Garny et al. (2020). EMIL uses ECHAM as the dynamical core, but with all the additional physical modules (in MESSy terminology *submodels*) inactive, all replaced by a submodel RELAX. RELAX does only two things:

(i) Newtonian cooling as a parametrization of diabatic processes

(ii) Rayleigh friction as a parametrization of momentum dissipation

Newtonian cooling is implemented as a relaxation towards a prescribed restoration temperature profile T_{eq}, whose precise form will be defined later. This profile is motivated by a radiatively determined state typical for Earth in January, with convective and latent heat effects being partially incorporated into the thermal structure of the troposphere, especially in low latitudes. Ground heat fluxes are also represented in this profile. In the stratosphere, it is essentially a radiatively determined state. The restoration profile is specific for a given latitude θ and pressure level p, and independent of time and longitude λ. With this parametrization, the diabatic term in the energy equation takes the form:

$$\frac{J}{c_p} = -\frac{T - T_{eq}(p,\theta)}{\tau(p,\theta)} \tag{53}$$

where T is the temperature computed by the model based on dynamics (a *prognostic* variable).

Boundary layer processes are represented by relaxation of near-surface winds towards zero, through a linear (Rayleigh) damping coefficient $k_{damp}(p,\theta)$. Another damping layer is present near model top to prevent undesired artifacts such as gravity wave reflection (the "sponge layer"). In either case, frictional force per unit mass takes the form:

$$\mathcal{F} = -k_{damp}(p,\theta)u \tag{54}$$

where k_{damp} takes non-zero values for $p > 700$ hPa to represent the boundary layer and $p < 0.8$ hPa to create the sponge layer. By using these simple parametrizations, atmospheric forcing can be easily modified and the response of the large-scale circulation to those isolated modifications can be studied separately. This plays into the theme of using simplified models where influence of relatively simple changes can be tracked in a relatively simple way. Along with the strict modularity of MESSy, it offers in principle a possibility of conducting studies in a hierarchical sequence of models, which, albeit beyond the scope of this work, might indeed be the best way of tackling problems such as this one. More information on EMIL can be found in (Garny et al., 2020).

A frequently used temperature profile $T_{eq}(p, \theta)$ (not yet the one used in this study!) is based on the model setup proposed by (Held and Suarez, 1994), abbreviated HS. It was originally designed as a tool for easy intercomparison of dynamical cores of different models, but has grown very popular beyond that purpose, in particular as a restoration temperature profile for parametrizing diabatic processes (e.g. Wang et al. (2019)). This profile can be seen in figure 3 on the right. Note that it is zoomed in compared to the profile in the center, but it is isothermal beyond the picture top at roughly 100 hPa. The underlying equation reads:

$$T_{eq}^{HS} = \max\left\{T_0,\ \left[T_1 - \delta_y \sin^2\theta - \varepsilon \sin\theta - \delta_z \log\left(\frac{p}{p_s}\right)\cos^2\theta\right]\left(\frac{p}{p_s}\right)^K\right\} \tag{55}$$

And the associated inverse relaxation timescale ($\mu = 1/\tau$):

$$\mu \equiv \kappa = \kappa_a + (\kappa_s - \kappa_a)\max\left(0, \frac{p/p_s - \sigma_b}{1 - \sigma_b}\right)\cos^4\theta \tag{56}$$

In these equations θ is latitude, p is the actual pressure, p_s is the current surface pressure, and $K = \frac{R}{c_p} = \frac{2}{7}$. In the standard HS setup, $\varepsilon = 0$, which results in a hemispherically symmetric profile (can be modified to simulate seasons). Near-surface Rayleigh damping coefficient takes the form

$$k_{damp}(p, \theta) = k_{max}^{HS}\max\left(0, \frac{p/p_s - \sigma_0}{1 - \sigma_0}\right) \tag{57}$$

with $\sigma_0 = 0.7$, i.e. the "boundary layer" top is at roughly 700 hPa.

This profile with suitable parameters can give rise to rather realistic tropospheric dynamics, but lacks the stratospheric thermal features needed to reproduce the behaviour of that layer (e.g. WSJ).

Polvani-Kushner setup (PK) extends HS into the stratosphere. It was first used by (Kushner and Polvani, 2004). As can be seen in figure 3, it is roughly representative of a January condition, unlike the HS profile, which represents an equinox limited to the troposphere. PK setup has the same relaxation timescale than HS. The PK temperature profile is similar to HS in the troposphere (except ε), but adds stratospheric features:

$$T_{eq}^{PK}(p, \theta) = \begin{cases} \max\left\{T_{US}(p_{Ts}),\ \left[T_1 - \delta_y \sin^2\theta - \varepsilon \sin\theta - \delta_z \log\left(\frac{p}{p_s}\right)\cos^2\theta\right]\left(\frac{p}{p_s}\right)^K\right\} & p \geq p_T(\theta) \\ [1 - W(\theta)]T_{US}(p) + W(\theta)T_{US}(p_{Ts})\left(\frac{p}{p_T(\theta)}\right)^{\frac{R\gamma}{g}} & p < p_T(\theta) \end{cases} \tag{58}$$

Here the stratospheric temperature is based on the US standard atmosphere temperature profile $T_{US}(p)$ (Atmosphere, 1976) in the summer hemisphere and exhibits a temperature decrease with lapse rate γ in the winter hemispher,e representing the region of the polar vortex. $W(\theta)$ is the weighting function that sets the transition from summer to winter structure:

$$W(\theta) = \frac{1}{2}\left[1 + \text{sign}(h_{fac})\tanh\left(\frac{\theta - \theta_0}{\delta\theta}\right)\right] \tag{59}$$

where h_{fac} is a parameter whose sign sets which hemisphere has winter (i.e. whether its "July" or "January"), and the latitude (in winter hemisphere) where this transition happens is θ_0. The

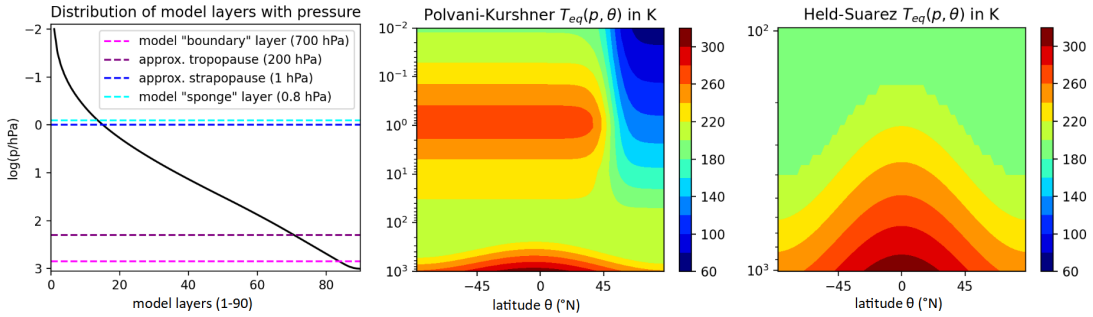

Figure 3: Left: vertical scheme of the atmosphere with regards to important pressure levels, and the distribution of the 90 model layers. Note that the cyan line (sponge layer base) should be higher up, at 0.43 hPa, not 0.8 hPa (this was a mistake). Center and right: the two restoration temperature profiles mentioned in this section, only the former being used in this study.

transition from tropospheric to stratospheric formulas happens at the transition pressure level $p_T(\theta) = (p_{Tw} - p_{Ts})W(\theta) + p_{Ts}$ where p_{Ts} and p_{Tw} are constants characteristic for summer and winter.

The following model-top damping profile is used:

$$k_{damp}(p(i_{lev}),\theta) = \begin{cases} 0 & i_{lev} > i_{lev}^{sp} \\ k_{drag} c^{i_{lev}^{sp} - i_{lev}} & i_{lev} \leq i_{lev}^{sp} \end{cases} \tag{60}$$

here, $k_{drag} = 5.02 \times 10^{-7}$ s^{-1} is enhanced by a factor $c = 1.5238$ at each level i_{lev} going upward from the base of the sponge layer ($i_{lev}^{sp} = 10$). Note that planetary surface is completely smooth and homogeneous. Some of the boundary layer thermodynamics is implicitly incorporated into the tropospheric part of the restoration temperature. Only dynamical exchange with the ground happens via k_{damp}.

See the Appendix A and the Supplement of (Garny et al., 2020) for more details, including the parameter values (they are all default unless otherwise stated).

3.4 Parameter space

The only parameter varied in this study was the rotation rate relative to the Earth, expressed as $\Omega^* = \frac{\Omega}{\Omega_E}$. Upper bound was $\Omega^* = 1$, i.e. an Earth-equivalent, and lower bound was $\Omega^* = \frac{1}{64}$. Simulations were done to cover the Ω^* space logarithmically in steps of two. The reason for the upper bound being set to Earth's value was that based on experience of Wang et al. (2019) and Goetz (2023a) significantly larger horizontal resolution is needed for $\Omega^* > 1$, mainly because of the emergence of a complicated and narrowly spaced pattern of zonal jets comparable to those on Jupiter (rotation period about 10 hours), c.f. Wang et al. (2019), top rows of figure 4 for an illustration of this behaviour. The strict lower end at 1/64 was mainly because of increasingly large problems with the assumption of a longitudinally symmetric restoration temperature field (i.e. a neglect of day-night contrasts).

Since $\Omega^* = 1$ is the fast edge of our region of interest, these planets and planets nearby in a logarithmic sense will sometimes be referred to as "fast rotators", or "intermediate rotators" (all the way to 1/8), while planets nearer to the slow edge (1/64, 1/32, 1/16) will be referred to as "slow rotators". These also correspond quite well with the two main tropospheric regimes (quasi-axisymmetric superrotation vs. regular/irregular baroclinic regime, see section 2.9). As follows from that section, for a large enough temperature gradient $\Delta\Theta$, one can cover all the tropospheric circulation regimes in diagram 2 just by changing Ω^*, since both dimensionless numbers that constitute the respective axes depend on it.

All planets had Earth-like radius, gravitational acceleration, atmospheric mass and mean surface temperature. It should be noted that the bulk composition of the atmosphere was also assumed to be Earth-like, since the molar gas constant R featured in the geophysical fluid equations is adjusted to Earth-like mean molecular mass, and this was not changed in the dynamical core. This does not invalidate the stated aim of maximal generality of the setup, since atmosphere needs to have *a* composition, and the Earth's one is the obvious default choice. A reader interested in a more exhaustive search of parameter space of tropospheric circulations, including atmospheric mass and composition, is referred to Kaspi and Showman (2015).

3.5 Temporal convergence

Table 1 summarizes the simulation years that were used for analysis of the steady state. The main criterion for the steady state was full development of zonal winds, since from the phenomena studied for this purpose (including eddy transports or the meridional circulation), this took the longest time, in particular for slowest rotators. Even though the half-times $\tau_{1/2}$ level off at around 6 months as one traverses the second column of the table, the subsequent spin-up is much slower for the very slow rotators (top of the table). That is reflected in numbers in the right column. For $\Omega^* = \frac{1}{64}$, the steady state was barely achieved in the last years of the simulation. Note that the averaging windows are quite short for a climatologic study. There are some longer scale variations in the steady state that will necessarily get ignored. However, the temporal variability of the steady state was not of particular interest in this study, which only aimed to get a very rough view of the dominant processes (and possessed limited computational resources).

Ω^*	$\tau_{1/2}$ (months)	years used
1/64	4	17-20
1/32	6	5-15
1/16	7	5-10
1/8	3	2-5
1/4	2	2-5
1/2	1	2-5
1	1	2-5

Table 1: Timescale of growth to 50% of maximum for the zonal winds (middle column, in months), and the time of the steady-state simulation used for temporal and zonal mean analysis (right column, in years).

4 Overview of simulation results

This section presents a quick overview of the relatively raw simulation output. The aim here is two-fold:

(i) To provide readers an intuitive picture of the consequences of changing Ω^*, and potentially start forming their own ideas about the dynamics, before being presented with mine. I attach my comments and put the results one by one into the context of earlier work, but these discussions are for now strictly separated from the description of results.

4.1 Zonal winds

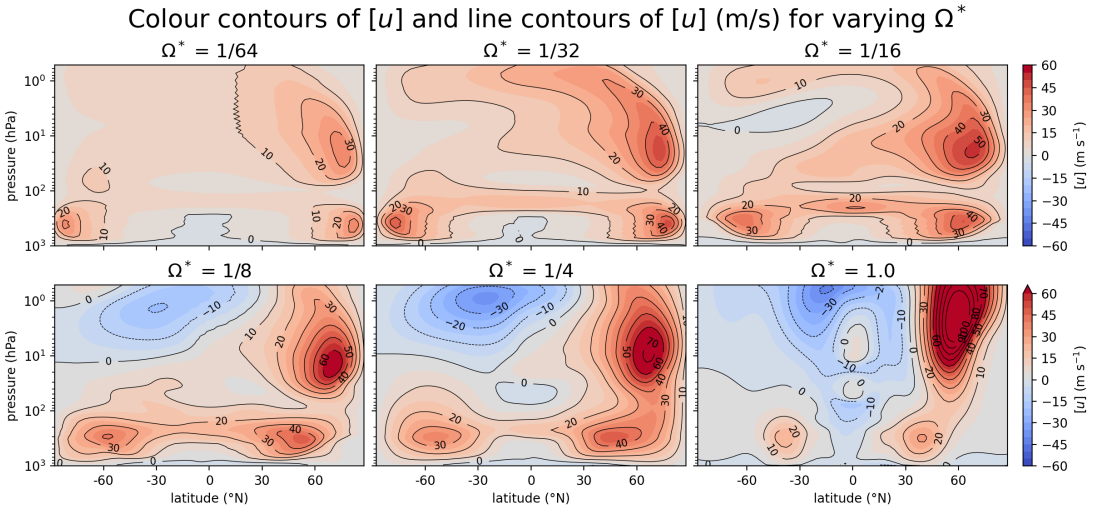

Figure 4: Structure of the t.m.z.m. zonal winds $[u]$. Line contours are spaced by 10 m/s all the way to 100 m/s and colours are spaced by 5 m/s until 60 m/s.

Figure 4 shows the pattern of t.m.z.m. zonal winds $[u]$ for varying Ω^*. Noteworthy features include:

1. With decreasing Ω^*, tropospheric jets migrate poleward and initially intensify, reaching maximum around $\Omega^* = \frac{1}{4}$ to $\frac{1}{8}$. There is a slight tendency for the tropospheric jets to migrate to higher pressure.

2. With decreasing Ω^*, the intensity of the winter stratospheric jet (WSJ) monotonously decreases, it moves to higher pressures. Its connection to the tropospheric jets at first strengthens, later it becomes more separated.

3. With decreasing Ω^*, the easterlies in equatorial and summer stratosphere are gradually replaced by westerlies, that peak around $\Omega^* = \frac{1}{16}$ and $\frac{1}{32}$.

4.2 Meridional circulation

Figure 5 shows the pattern of t.m.z.m. Eulerian streamfunction Ψ for varying Ω^*. Noteworthy features include:

4. With decreasing Ω^*, first the thermally direct polar cell disappears ($\Omega^* = \frac{1}{4}$), then the Ferrel cell - between $\Omega^* = \frac{1}{8}$ and $\frac{1}{16}$.

5. With decreasing Ω^*, the Hadley cell intensifies and expands to higher latitudes, until it spans the entire globe. It somewhat shrinks in the vertical.

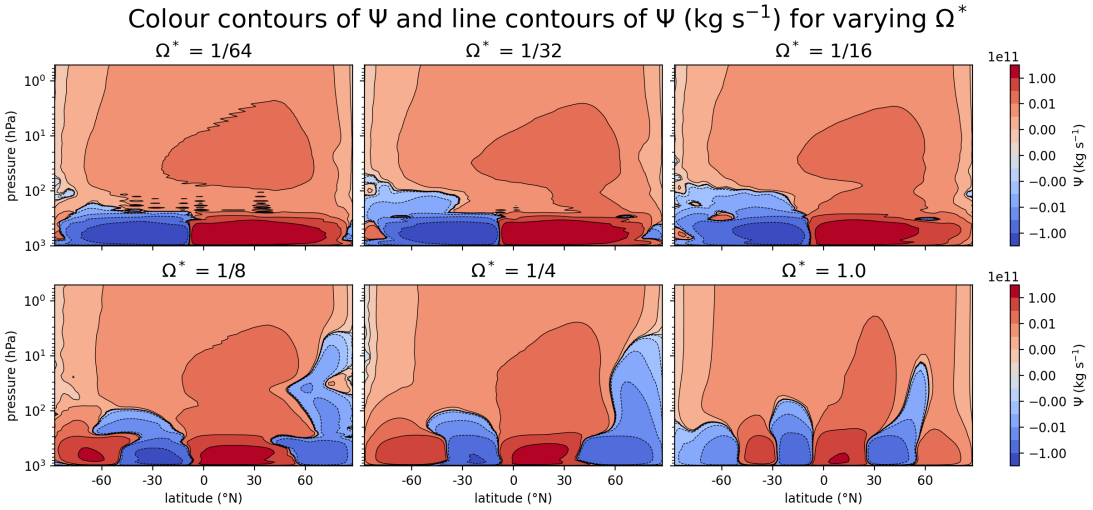

Figure 5: Structure of the t.m.z.m. Eulerian streamfunction Ψ on a logarithmic scale.

6. Ψ in the stratosphere is mostly positive, appears as an extension of the Hadley cell. A negative Ψ in winter hemisphere appears as an "extension" of the Ferrel cell, until it disappears below $\Omega^* = \frac{1}{8}$. With decreasing Ω^*, Ψ in the stratosphere gradually detaches from the tropospheric cell, in the sense that there is a separate stratospheric maximum.

4.3 Temperature profile

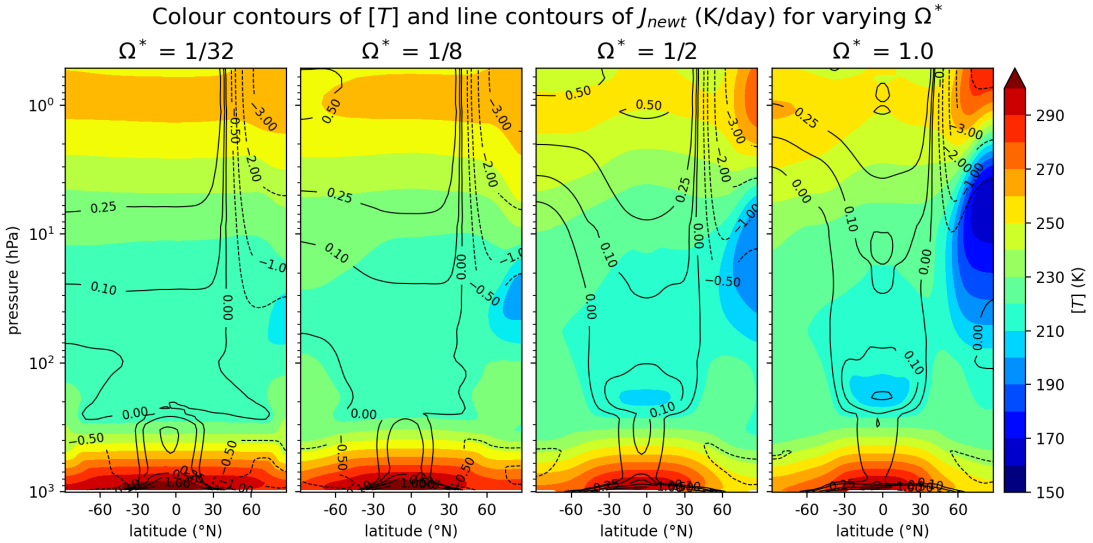

Figure 6: Temperature structure $[T](\theta, p)$ of the atmosphere in colour, overlaid with selected contours of diabatic (Newtonian) heating in K/day, positive values being in full contours, and negative values in dashed contours.

Figure 6 shows the structure of the fields of temperature $[T]$ and the parametrized diabatic heating $\frac{[J]_{newt}}{c_p}$. Noteworthy features include:

7. In the troposphere, low latitudes are diabatically heated, while the middle and high latitudes are diabatically cooled. This pattern is stronger for slower rotators.

8. With decreasing Ω^*, isotherms are flatter both in the troposphere and the stratosphere. Only areas with more significant tropospheric meridional temperature gradient for the slow rotators are in high latitudes, at the edges of the enhanced Hadley cell.

9. With decreasing Ω^*, the vertical edge of the polar night area that is radiatively cooled migrates to higher pressures, with the equilibriated (i.e. very cold) region weakening and itself moving to higher pressures.

4.4 Waves

Figure 7 shows a snapshot of the meridional section of the meridional wind at an arbitrary longitude, at an arbitrary time in the equilibrated phase of the simulation. Figure 8 shows a snapshot of the zonal wind at 3 pressure levels corresponding roughly to mid-troposphere (500 hPa), tropopause (200 hPa) and mid-stratosphere (10 hPa). Note that these snapshots serve merely as a first impression, and are not suitable for a quantitative comparison, that will be done later - in section 8. Also note that the raw velocity field v (not $v^* = v - [v]$) is plotted in figure 7, to show the dominance of the mean flow in the troposphere of slow rotators.

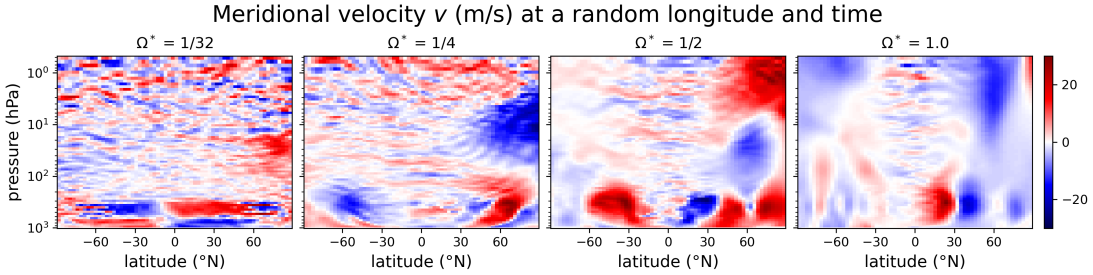

Figure 7: Snapshot of meridional velocity in both troposphere and stratosphere during the equilibriated phase at longitude 0 degrees. The colorbar is common for all four rotation rates.

Noteworthy aspects of these figures are:

10. Tropospheric meridional motion is dominated by baroclinic Rossby waves for slower rotators, while the mean flow in the form of overturning circulation is not strong enough to be visible by eye. This is reversed for the slowest rotators, where the Hadley cell overshadows any wave motions present in the troposphere.

11. For $\Omega^* = \frac{1}{4}$ and $\frac{1}{8}$, the jetstream is significantly fractured, at places into two bands per hemisphere.

12. With decreasing Ω^*, there is a general trend towards lower zonal wavenumbers, visible already in the regular baroclinic regime. For the slowest rotators in the quasi-axisymmetric regime, as the name suggests, there is little planetary wave activity, and it seems to be concentrated in zonal wave number 1, a behaviour not observed on Earth, or the $\Omega^* = 1$ simulation (figure 30).

13. With decreasing Ω^* from 1 to *at least* $\frac{1}{2}$, there is a widening pattern of equatorially-trapped waves in the stratosphere. It is possible that this extends to $\frac{1}{4}$ and beyond, the meridional scale of decay has simply reached the pole to equator distance.

4.5 Discussion of the observed features and the scope of this project

Let me briefly address each of the points made above, drawing on fundamental physics as well as results of previous studies:

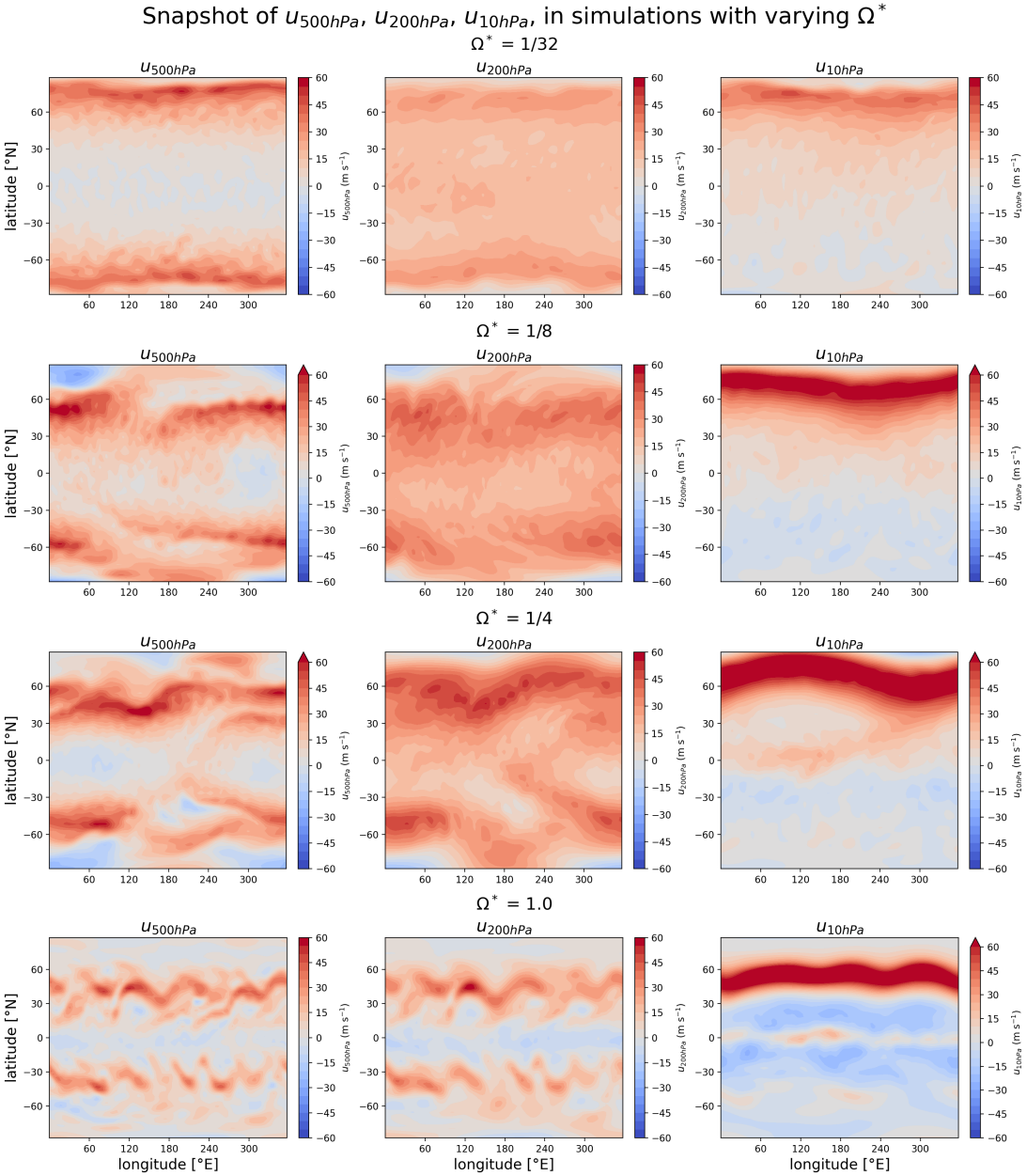

Figure 8: Snapshot of zonal wind at 500 hPa (left column), 200 hPa (middle column) and 10 hPa (right column) for varying rotation rate, from $\Omega^* = \frac{1}{32}$ (top row) to $\Omega^* = 1$ (bottom row).

1. Poleward movement of tropospheric jets is a natural consequence of the expansion of the Hadley cell, consistent with section 2.4. This result was independently verified in many studies, including Wang et al. (2019), Kaspi and Showman (2015), Goetz (2023a), Goetz (2023b), Williams (1988a) and others. With regards to their intensification, there are two balancing effects: (i) with decreasing Ω^*, Hadley circulation reaches further poleward, so a greater portion of planetary angular momentum gets transferred to the relative zonal movement w.r.t. the ground, and (ii) with decreasing Ω^*, the total available angular momentum is proportionally smaller. In our simulations, (i) dominates until roughly $\frac{1}{8}$, and as the poleward extension effect saturates, effect (ii) takes over. The jet for $\Omega^* = \frac{1}{16}$ is already weaker. This is quantitatively consistent with Wang et al. (2019). Note that related estimate cannot be easily done analytically, since the validity of the "small-angle"

Hou-Held model breaks down for $\Omega^* < 1$, and the formula provided in section 2.4 valid near the pole is still not sufficiently valid.

2. In figure 6, isobaric slope of isotherms in winter subpolar stratosphere is seen to diminish greatly, largely taking away the underlying reason for the emergence of the jet. This likely outweights the fact that Coriolis force becomes weaker. There were no similar studies of which I am aware of to which to compare this feature.

3. Westerlies above the equator mean that the atmosphere has, at least locally, more angular momentum than the solid surface. This is the concept of superrotation introduced in section 2.8, that is known to develop on real slowly-rotating planets and moons. It needs to be achieved by suitable eddy processes.

4. Decrease of the number of meridional cells is in good agreement with the results of studies cited in the first point. Disappearance of the Ferrel cell is associated with the overall decrease of eddy activity as the tropospheric regime transitions from regular baroclinic to quasi axisymmetric, when Ω^* is decreased below $\sim 10^{-1}$.

5. Poleward expansion and intensification of the Hadley cell is also in agreement with studies cited above, and is qualitatively consistent with the Hou-Held model introduced in 2.4.

6. The behaviour of streamfunction for $\Omega^* = 1$ can be compared with figure 2 of Becker (2012). This comparison suggests that the amount of "leakage" of the winter Ferrel cell is actually underestimated in my model. In either case, rather than the Eulerian picture, it is much more useful to study the stratospheric streamfunction in the Lagrangian picture. For this, however, I will first need to show, using the scales in the simulation output, that a variant of the widely used Transformed Eulerian Mean (TEM) is appropriate.

7. On Earth, the tropics *do* experience a net diabatic warming and the poles a net diabatic cooling. While for poles this is mostly radiative, for equator it is both radiation and latent heat release. Outside of the tropical troposphere, I will allow myself to use the terms *radiative* and *diabatic* quite interchangeably. The "elephant in the room" remains what are the assumptions behind the restoration temperature profile. Its authors (Held and Suarez (1994), p. 3) had this to say:

   "This radiative equilibrium is given some positive static stability, relatively large in the Tropics and decreasing to zero at the poles. One can think of this tropical static stability as taking into account the effects of moist convection, but this is potentially misleading, and it is better to think of it as simply an artifact that helps minimize the occurrence of gravitational instability."

   The goal of the authors was to create a framework for dynamical core intercomparison, and therefore they created a restoration temperature field that would work well with dynamical cores (such as ECHAM, the one used in this study) and take care of all the physical processes outside the realm of fluid dynamics. In my understanding, all that in a way that would mimic the Earth *well enough*, but it was not the primary goal. Since then, it has become a popular method of radiative-convective parametrization in idealized models. In the next subsection, when $\Omega^* = 1$ is compared to reanalysis data for Earth, it will become apparent that the Hadley cell is a few times weaker than on Earth, suggesting that the effect of latent heating is not present strongly enough, or there are other processes at play. On a philosophical ground, since the restoration temperature field is "reasonable", having no particular planet in mind for the study, it is no longer necessary to seek the specifics. It is a reasonable assumption that the restoration temperature field in the troposphere, based on diabatic effects of radiation and moderate amount of water vapour is given by a similar profile. It is also reasonable that it is given primarily by a (fixed) amount of greenhouse gases, and their long term concentration profile is independent of Ω^*. Presence and absence of water vapour modulates this profile.

8. Flatter isotherms for slow rotators can be explained by the expansion of the Hadley cell, which is efficient in redistributing the heat in the troposphere. Sharper gradients correspond to its edge, where at the same time the thermally driven jets occur. Figure 4 of Wang et al. (2019) shows a similar pattern of tropospheric isotherms, albeit in an equinoctal simulation, so they are more hemispherically symmetric. The stratospheric pattern is less clear, and could be associated to the enhanced stratospheric Ψ in the slow rotators, also due to advective heat redistribution.

9. Based only on the figures presented here, it is not clear what causes the shift in the thermodynamics of the polar stratosphere. Again, it might be linked to the meridional circulation pattern.

10. The reason for the prominence of Hadley cell over baroclinic waves for slower rotators is by now clear, since the former intensifies and the latter weaken.

11. Note that $\Omega^* = \frac{1}{4}$ and $\frac{1}{8}$ correspond to the regular baroclinic regime. It is in this regime and roughly these Ω^* that the separation between the eddy-driven and the standard tropospheric angular-momentum-driven ("thermal") jet is the greatest, according to Goetz (2023a). This explains the double structure of the jet, and partially why it is so meridionally spread out in figure 4. Note that this is a very different case from the multiple jet regime at $\Omega^* \gg 1$, because there all the jets are eddy-driven. The expected number of eddy-driven jets based on the Rhines scale for the case $\Omega^* = \frac{1}{4}$, i.e. $\mathcal{R}o_T \sim 0.5$, is just roughly 0.3. Of course this should not be taken too literally, but when and where eddy-driven jet does happen, it is at latitudes 60-80 degrees, while the angular momentum jet is around 40-50 degrees. See section **??** for an overview of these concepts, and figure 5.7 in Goetz (2023a) for the data on the separation between the two types of jets.

12. The subject of the zonal scale of tropospheric eddies was reviewed and treated extensively in Wang et al. (2019). In the stratosphere, Charney-Draizin criterion introduced in section 2.5 is at play, and will be discussed later, in section 8.

13. The length scale of amplitude decay for equatorially trapped waves increases with decreasing Ω^*. This will also be discussed in section 8.

From the list above, it begins to be seen where lie the opportunities for this research project. In general, tropospheric patterns are to a large extent understood and do not need so much new treatment. After all, my tools are at best similar to previous works, at times poorer, e.g. Kaspi and Showman (2015) have better radiative scheme. Still, in section 5, the troposphere is addressed, to give a more detailed, term-by-term analysis of the zonal mean geophysical fluid equations and how the balances change with changing Ω^*. However, at the heart of this work is the stratosphere. In particular, the mechanisms and consequences of the stratospheric circulation on slower rotators are explored in section 6. Some attention is then given to the origin of stratospheric superrotation, in particular in winter hemisphere. Emergence of the strong downwelling which allows the stratospheric circulation cell to form, and why it is specific for slower rotators, is then explored in section 7 with a massively-simplified mathematical model. Up to and including that moment, all zonal asymmetries are abstracted to terms like $[v^*T^*]$ etc., and the nature of the underlying wave motion is not explored. This changes in section 8, where the zonal mean picture is abandoned and an attempt is made to better understand those waves.

4.6 Comparison to Earth

It would be a severe simplification to equate the case $\Omega^* = 1$ with Earth. There are several major reasons for this. Perhaps the main reason is because it is an aquaplanet. This above all limits the diversity of the wave phenomena present in the simulation, with consequences for the wave-driven circulation. There are no land-sea contrasts available for the formation of stationary planetary waves - especially the small wavenumber modes that propagate most

easily into the stratosphere (Charney and Drazin (1961)). Tropospheric baroclinicity remains the only source of Rossby waves. Also the gravity wave spectrum is affected. The model is course (horizontal resolution $\sim$ 300 km), so a large part of the gravity wave spectrum is missing altogether. There is no topography to create orographic waves, and there is no gravity wave parametrization, since it would not generalize well to other Ω^*. The sole exception is the mesospheric sponge layer, which in a way is a gravity wave parametrization. Note that mesosphere is not studied here, and that the purpose of the sponge layer within these simulations is to prevent gravity wave reflection from the upper boundary, see section 3.3. In this light, it is not surprising that there are significant differences. Figure 9 summarizes the noteworthy ones:

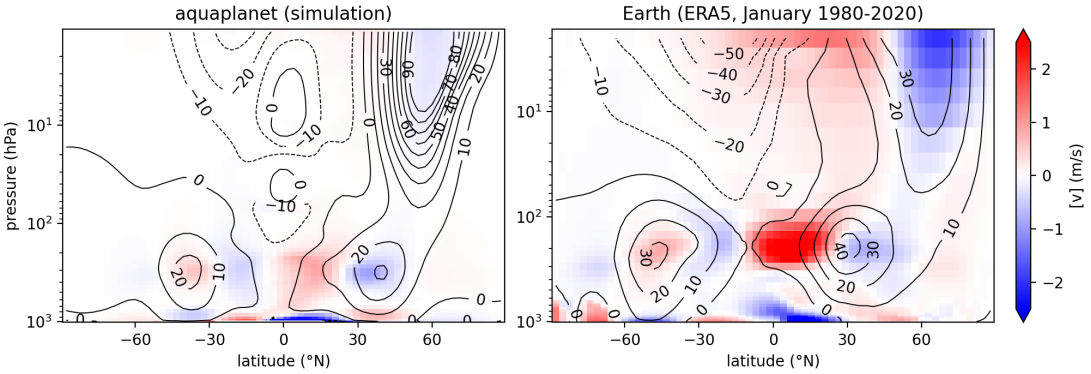

Figure 9: Comparison of climatology of t.m.z.m. meridional wind component $[v]$ (colour, m/s) and t.m.z.m. zonal wind component $[u]$ (contours, m/s).

1. Winter stratospheric jet (WSJ) is much stronger than on Earth. This is mainly because of the lack of sea-land contrasts, WSJ in southern (i.e. ocean) hemisphere is actually quite close to the simulated values of above 100 m/s.

2. Hadley cell is a few times weaker and reaches significantly less high than on Earth. This is likely related to the issues with the slight arbitrariness or lack of realism of the restoration temperature field.

3. Meridional overturning in the stratosphere is much weaker than on Earth. This is related to the above mentioned lack of certain wave types.

It should be emphasized that despite large quantitative differences, the simulation $\Omega^* = 1$ qualitatively captures the circulation regime on Earth, and is a useful stepping stone for comparisons with simulations with $\Omega^* < 1$.

5 Temporal and zonal mean dynamics: general aspects and the troposphere

This study, and similar studies before it, takes a dynamical core with approximations designed for Earth, and takes it to planets with different rotation rates. This section starts with taking a step back, and if not justifying, than at least plausibly motivating without reference to the simulation results, why this is still a valid approach in this case. Then it takes the reader from the laws of nature to the suitably approximated yet quantitatively correct zonal mean equations. These are then used to analyze the dynamics in detail.

5.1 Introduction: assumptions and justifications

In section 2.6, the following simplified system was used to introduce the meridional overturning circulation induced by eddies and radiative processes:

$$\frac{\partial[u]}{\partial t} + \frac{\partial}{\partial y}[v^* u^*] - f_0[v] = [\mathcal{F}_x] \tag{61}$$

$$\frac{\partial[T]}{\partial t} + \frac{\partial}{\partial y}[v^* T^*] - S_p[\omega] = \frac{[J]}{c_p} \tag{62}$$

While these budgets capture the critical processes, they cannot be expected to close when applied to the simulation output. The reasons for this are rather trivial, but let me state them briefly:

1. equations above are on a mid-latitude plane, so value of $f = f_0$ does not vary with latitude as it should
2. all the geometrical corrections for the convergence of meridians towards the poles are missing
3. metric terms in velocity components are missing because of implicit scaling arguments: e.g. for terrestrial purposes $\frac{uv\tan\theta}{a}$ is usually much smaller than fv etc.
4. advective terms are missing, as they are not crucial for the mid-latitudes on Earth
5. also some eddy flux terms are missing, only the dominant ones on Earth are retained. It is not guaranteed that same scaling applies to other planets.

It is no surprise that these zonal mean equations are lacking, since they were derived from simplified QG equations on mid-latitude plane. There are of course ready-made formulas for a more quantitative and complete treatment of the Earth. In our case, it is however the most interesting option to start from scratch, and think about all the assumptions involved and how they relate to Ω^*. To have sound theoretical grounding, we should start the zonal averaging procedure from the full equations of geophysical fluid dynamics, this time also including the

diabatic and frictional effects:

$$\frac{\mathrm{D}u}{\mathrm{D}t} - \left(2\Omega + \frac{u}{r\cos\theta}\right)(v\sin\theta - w\cos\theta) = -\frac{1}{\rho r\cos\theta}\frac{\partial p}{\partial\lambda} + \mathcal{F}_x \tag{63}$$

$$\frac{\mathrm{D}v}{\mathrm{D}t} + \frac{wv}{r} + \left(2\Omega + \frac{u}{r\cos\theta}\right)u\sin\theta = -\frac{1}{\rho r}\frac{\partial p}{\partial\theta} + \mathcal{F}_y \tag{64}$$

$$\frac{\mathrm{D}w}{\mathrm{D}t} - \frac{u^2+v^2}{r} - 2\Omega u\cos\theta = -\frac{1}{\rho}\frac{\partial p}{\partial r} - g + \mathcal{F}_z \tag{65}$$

$$\frac{\partial\rho}{\partial t} + \frac{1}{r\cos\theta}\frac{\partial(u\rho)}{\partial\lambda} + \frac{1}{r\cos\theta}\frac{\partial}{\partial\theta}(v\rho\cos\theta) + \frac{1}{r^2}\frac{\partial}{\partial r}\left(r^2 w\rho\right) = 0 \tag{66}$$

$$\frac{\mathrm{D}}{\mathrm{D}t}\left[T\left(\frac{p_0}{p}\right)^{\frac{R}{c_p}}\right] = \frac{J}{c_p} \tag{67}$$

$$p = R\rho T \tag{68}$$

$$\frac{\mathrm{D}}{\mathrm{D}t} \equiv \frac{\partial}{\partial t} + \frac{u}{r\cos\theta}\frac{\partial}{\partial\lambda} + \frac{v}{r}\frac{\partial}{\partial\theta} + w\frac{\partial}{\partial r} \tag{69}$$

These are more complete than the numerical model itself, which uses primitive equations. It is also a goal here to motivate why the model could have been used in the first place. I make the assumption that primitive equations are good enough for Earth, since they are such a gold standard in Earth system modelling. Let me now address why the 3 assumptions in section 2.1 that are the bridge between full and primitive equations should hold in my study of slowly rotating planets *at least as well* as on Earth:

(i) *The shallow fluid approximation*:
For Earth, the atmospheric scale height $H = \frac{RT}{g}$ is much smaller than the radius of the planet. This might not be the case anymore if I either (i) made R larger by having a more volatile atmosphere (e.g. H_2), (ii) made T higher by changing the radiative parametrization, (iii) made g smaller, or (iv) made the planetary radius a smaller. None of these parameters has reason to be affected by rotation rate. Note that if hydrostaticity was violated by orders of magnitude, the formula for H would no longer hold. There is no physical reason for such a drastic and large-scale violation of hydrostaticity due to a weaker Coriolis effect, appreciable violations happen on Earth only in strong localized events such as convective storms.

(ii) *The hydrostatic approximation*:
How about smaller deviations from hydrostaticity? Looking at the full vertical momentum equation and ruling out the Coriolis term, it can come from $\frac{u^2+v^2}{r}$ or $\frac{\mathrm{D}w}{\mathrm{D}t}$. Considering that $g \sim 10^1$ ms^{-2}, U would have to be supersonic and $\frac{U^2}{a}$ would still fall short of g at least by an order of magnitude. No such winds are physically viable on any planet. $\frac{\mathrm{D}w}{\mathrm{D}t} \sim g$ means a free-fall like condition with only small buoyancy. Again, this is physically implausible. Finally, note that since the atmospheric mass is the same in all simulations and scale height must be always at the same order of magnitude, $\frac{\partial p}{\partial z}$ must always be the same order of magnitude as g.

(iii) *The traditional approximation*:
This approximation is the hardest to reason about *a priori*. All Coriolis terms approach zero as $\Omega \to 0$, so those Coriolis terms that are negligible for Earth are almost surely negligible for slowly rotating planets. Regarding the metric terms, while wv should be negligible compared to u^2 almost certainly in the meridional momentum equation, how many times is uv larger than uw is harder to guess not knowing the scales beforehand.

I assumed that any model error on velocity components commited by neglecting these terms is not large enough to alter the velocity components to such a degree to affect whether their combinations into the "negliglible" terms described here are indeed much smaller than the "non-negligible" terms. In this way, it was determined *a posteriori* (by looking at the simulation

output) that presence or absence of terms neglected in (iii) does not change the budget. Only the largest - the one derived from $2\Omega w \cos\theta$ - was barely present in the budget for Earth rotation speed, some 1-2 orders of magnitude below the dominant balance. It quickly disappeared for slower rotators. Metric terms eliminated in (iii) were utterly negligible, i.e. not visible on a linear colour scale. We can therefore safely start from primitive equations, repeated here already in their form in pressure coordinates (section 2.2), and with diabatic and damping effects included. This is the final system, that is used from now on:

$$\frac{\mathrm{D}u}{\mathrm{D}t} - 2\Omega \sin\theta v - \frac{uv\tan\theta}{a} = -\frac{1}{a\cos\theta}\frac{\partial\Phi}{\partial\lambda} + \mathcal{F}_x \tag{70}$$

$$\frac{\mathrm{D}v}{\mathrm{D}t} + 2\Omega \sin\theta u + \frac{u^2\tan\theta}{a} = -\frac{1}{a}\frac{\partial\Phi}{\partial\theta} + \mathcal{F}_y \tag{71}$$

$$\frac{\partial\Phi}{\partial p} = -\frac{RT}{p} \tag{72}$$

$$\frac{1}{a\cos\theta}\frac{\partial u}{\partial\lambda} + \frac{1}{a\cos\theta}\frac{\partial(v\cos\theta)}{\partial\theta} + \frac{\partial\omega}{\partial p} = 0 \tag{73}$$

$$\frac{\mathrm{D}T}{\mathrm{D}t} - \frac{RT}{c_p p}\omega = \frac{J}{c_p} \tag{74}$$

5.2 Derivation of the zonal mean equations

Now the zonal mean of the system of equations 70 -74 is taken. Let us first derive the zonal mean of material derivative, using a generic quantity Q. This notation is to avoid any chance of confusion of positions of the differentiated quantity (e.g. u) with its positions in other terms of these equations (like the term $\sim u\frac{\partial u}{\partial\lambda}$). We use the equation in flux form, which can be achieved by adding the continuity equation scaled by Q:

$$\left[\frac{\mathrm{D}Q}{\mathrm{D}t}\right] = \left[\frac{\partial Q}{\partial t} + \frac{1}{a\cos\theta}\frac{\partial(uQ)}{\partial\lambda} + \frac{1}{a}\frac{\partial(vQ)}{\partial\theta} - \frac{vQ\tan\theta}{a} + \frac{\partial(\omega Q)}{\partial p}\right] \tag{75}$$

$$= \frac{\partial[Q]}{\partial t} + \left(\frac{1}{a}\frac{\partial}{\partial\theta} - \frac{\tan\theta}{a}\right)\left([v][Q] + [v^*Q^*]\right) + \frac{\partial}{\partial p}\left([\omega][Q] + [\omega^*Q^*]\right) \tag{76}$$

$$= \frac{\partial[Q]}{\partial t} + \frac{[v]}{a}\frac{\partial[Q]}{\partial\theta} + [\omega]\frac{\partial[Q]}{\partial p} + [Q]\overbrace{\left(\frac{1}{a}\frac{\partial[v]}{\partial\theta} - \frac{\tan\theta[v]}{a} + \frac{\partial[\omega]}{\partial p}\right)}^{=0,\text{ by continuity eqn.}} + \tag{77}$$

$$+ \left(\frac{1}{a}\frac{\partial}{\partial\theta} - \frac{\tan\theta}{a}\right)[v^*Q^*] + \frac{\partial}{\partial p}\left([\omega^*Q^*]\right) \tag{78}$$

We can now compute the zonal means. After regrouping some terms:

$$\frac{\partial[u]}{\partial t} + [v]\frac{\partial[u]}{\partial y} + [\omega]\frac{\partial[u]}{\partial p} + \left(\frac{\partial}{\partial y} - \frac{2\tan\theta}{a}\right)[v^*u^*] + \frac{\partial}{\partial p}[\omega^*u^*] - \left(2\Omega\sin\theta + \frac{[u]}{a}\tan\theta\right)[v] = [\mathcal{F}_x] \tag{79}$$

$$\frac{\partial[v]}{\partial t} + [v]\frac{\partial[v]}{\partial t} + [\omega]\frac{\partial[v]}{\partial p} + \left(\frac{\partial}{\partial y} - \frac{\tan\theta}{a}\right)[v^*v^*] + \frac{\partial}{\partial p}[\omega^*v^*] + \frac{\tan\theta}{a}[u^*u^*] + 2\Omega\sin\theta[u] + \frac{\tan\theta}{a}[u]^2 = -\frac{1}{a}\frac{\partial[\Phi]}{\partial\theta} + [\mathcal{F}_y] \tag{80}$$

$$\frac{\partial[T]}{\partial t} + [v]\frac{\partial[T]}{\partial t} + [\omega]\left(\frac{\partial[T]}{\partial p} - \frac{R[T]}{c_p p}\right) + \left(\frac{\partial}{\partial y} - \frac{\tan\theta}{a}\right)[v^*T^*] + \left(\frac{\partial}{\partial p} - \frac{R}{c_p p}\right)[\omega^*T^*] = \frac{[J]}{c_p} \tag{81}$$

These were the three prognostic equations. The two diagnostic equations are linear, thus simple:

$$\frac{\partial[\Phi]}{\partial p} + \frac{R[T]}{p} = 0 \tag{82}$$

$$\frac{1}{a\cos\theta}\frac{\partial([v]\cos\theta)}{\partial\theta} + \frac{\partial[\omega]}{\partial p} = 0 \tag{83}$$

In the zonal momentum equation, note that the factor of 2 in front of "$-\frac{\tan\theta}{a}$" not present in other equations is not a typographic error. The $(1\times)\left(-\frac{\tan\theta}{a}\right)$ - which is present in all

equations - comes from the material derivative. A further $-\frac{\tan\theta}{a}$ in the $[u]$ equation comes from the metric term $-\frac{uv\tan\theta}{a}$, i.e. from outside the material derivative. In the $[T]$-equation, the vertical advective term is extended with what was before the adiabatic cooling term, into the zonal mean stability parameter $S_p \equiv \frac{R[T]}{c_p p} - \frac{\partial[T]}{\partial p}$.

For reference, if approximation number (iii) in the list (i.e. the traditional approximation) had not been made in the derivation, extra terms would appear in horizontal ($[u]$, $[v]$) momentum equations. As it was mentioned, I had no suspicion of approximations (i) and (ii) being problematic, so I only tested (iii). Therefore, the full version of e.g. the $[u]$-equation that I initially used for data analysis was as above in eqn. 79, but with the following extra terms ϵ on the left-hand side:

$$\epsilon = \left[2\Omega w\cos\theta + \frac{uw}{a}\right] \qquad \text{(convert to } p\text{-coordinates)} \tag{84}$$

$$= -\frac{R}{pg}\left[2\Omega\omega T\cos\theta + \frac{u\omega T}{a}\right] \tag{85}$$

$$= -\frac{2R\Omega\cos\theta}{pg}([\omega][T] + [\omega^*][T^*]) \tag{86}$$

$$-\frac{R}{pga}([u][\omega][T] + [u][\omega^*T^*] + [\omega][u^*T^*] + [T^*][\omega^*u^*] + [u^*\omega^*T^*]) \tag{87}$$

5.3 Tropospheric Eulerian mean circulation

Here, the system of equations 79 is used to diagnose the dynamics of the tropospheric Eulerian mean (EM) circulation. Reader is encouraged to refer back to figures 4 and 5 for the structure of zonal wind and Eulerian streamfunction. For interpretation of all subsequent figures, it is important to note and keep in mind the sign convention. All the right hand sides of EM equations for $[u]$ and $[T]$ are reserved to only two types of terms: (i) error terms $[\epsilon_x]$ and $[\epsilon_J]$, and (ii) parametrized terms $[\mathcal{F}_x] = -k_{damp}[u]$ and $\frac{[J]}{c_p} = -\frac{[T]-T_{eq}}{\tau}$. For the $[v]$-eqn., the same applies, hence also $\frac{\partial[\Phi]}{\partial y}$ is from now on the left. This sign convention is especially important when thinking e.g. about the acceleration $\frac{\partial[u]}{\partial t}$ that a given term on the left would cause on its own: it is of opposite sign to "what the colour suggests", i.e. blue is a positive acceleration. Basic values of Ω^* are in relative steps of 4: (1/64, 1/16, 1/4, 1). The value 1/ 32 will be added in the stratosphere because of the strange "barcode" behaviour of the temporal mean $[v]$ in the 1/64 case (c.f. fig. 5 or fig. 10). Also, 1/64 starts seriously violating assumptions about the negligible day-night temperature differences (see section **??**). The value of 1/8 is sometimes added, because it shows the transition between baroclinic and barotropic regimes (c.f. figure **??**). In all cases, the temporal averaging periods are those stated in table **??** in section 3.5. Note that the cyclostrophic frequency is sometimes not written out, but labelled with $[\phi] = \frac{[u]\tan\theta}{a}$.

5.3.1 Eulerian mean of the $[u]$-equation in the troposphere

Let us now analyse figure 10. Its features of interest are:

1. The main balance shifts from being between $[v^*u^*]$ and ficticious forces $-(f+[\phi])[v]$ for $\Omega^* = 1$ to between $[v]\frac{\partial[v]}{\partial y}$ and $-(f+[\phi])[v]$ for $\Omega^* = \frac{1}{64}$. In Earth midlatitudes, eddies accelerate the mean zonal flow, which is counteracted by the Coriolis effect associated with the meridional Ferrel cell. Looking at the top two rows of 10), on the slowest rotators, mid-latitude mid-tropospheric zonal flow is accelerated by ficticious forces caused by the poleward branch of the Hadley cell. This is counteracted by advection from the regions of weaker zonal flow.

2. Relative influence of $f[v]$ and $[\phi][v]$ transitions from the latter being negligible for $\Omega^* = 1$, to being slightly more important poleward of 45° for the slowest rotator. So in terms of the main dynamical balance in the meridional overturning circulation, planetary rotation

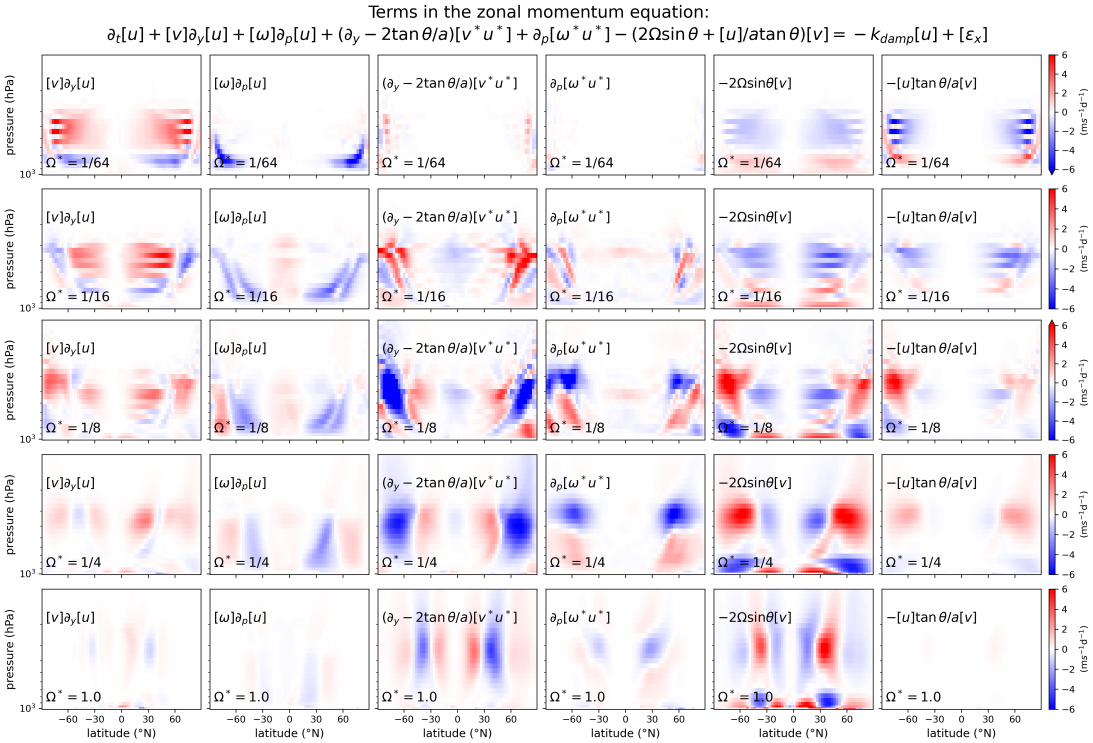

Figure 10: Terms in the zonally averaged zonal momentum equation in the troposphere and lowermost stratosphere, i.e. from the surface at around 1000 hPa to the pressure level of 100 hPa. Rotation rates are organized in rows and terms in columns. Terms that are too small to be seen or barely seen but irrelevant for all rotation rates are not shown. Damping is not shown, since it is only active in the ("imaginary") boundary layer, and has predictable shape $\sim -[u]$. In this figure, every row has the same colour scheme, see the colourbars on the right. This will generally *not* be the case in every similar subsequent plot, reader should always check these colourbar scales.

is the main or at least roughly equitable component of the main balance, even very deep in the slowly rotating quasi-axisymmetric regime. As we will see, the same does not hold for the meridional momentum budget.

3. Acceleration pattern caused by $[v^*u^*]$ is similar in magnitude down to $\Omega^* = \frac{1}{8}$, decreases significantly below that Ω^*.

4. Vertical eddy momentum $[\omega^*u^*]$ convergence is even stronger and more important in the regular baroclinic regime ($\Omega^* = \frac{1}{8}, \frac{1}{4}$) than in the irregular baroclinic regime.

5. Vertical momentum advection $[\omega]\frac{\partial[u]}{\partial p}$ from upper regions with faster winds is important for accelerating the zonal flow in the downwelling region of the Hadley cell both in the regular baroclinic regime and the quasi-axisymmetric regime. This make sense, since the Hadley cell is generally stronger and wider for smaller Ω^*.

6. Despite the fact that $\Omega^* = \frac{1}{16}$ is classified in the quasi-axisymmetric regime because of its single Hadley cell and the zonal wind pattern, in particular the strong superrotation, mid-latitude eddies still play a significant role in the zonal momentum balance.

5.3.2 Eulerian mean of the $[T]$-equation in the troposphere

Now let us describe the figure 11, featuring the temperature equation. The main features of interest are:

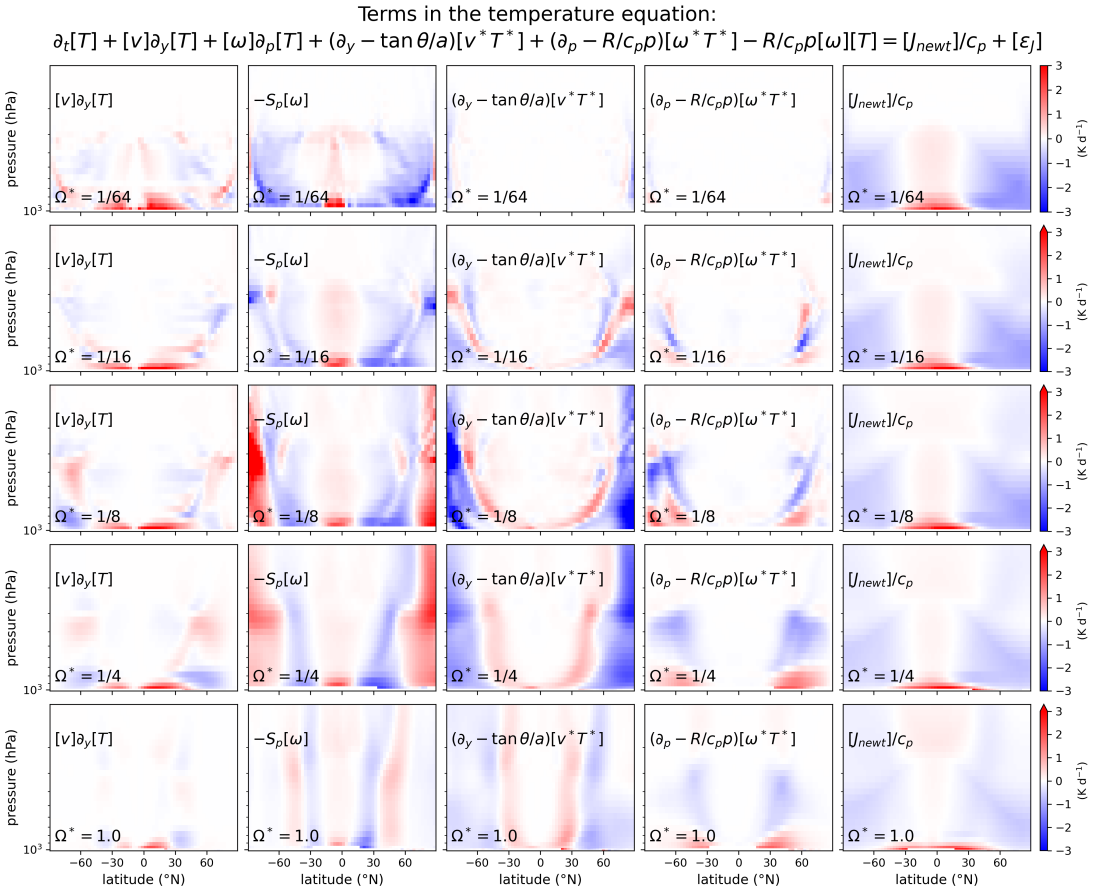

Figure 11: Terms in the zonally averaged temperature equation in the troposphere and lowermost stratosphere, i.e. from the surface at around 1000 hPa to the pressure level of 100 hPa. Rotation rates are organized in rows and terms in columns. Terms that are too small to be seen or barely seen but irrelevant for all rotation rates are not shown. In this figure, every row has the same colour scheme, see the colourbars on the right. This will generally *not* be the case in every similar subsequent plot, reader should always check these colourbar scales.

1. The main thermodynamical balance in the middle and upper troposphere in mid-latitudes shifts from being essentially a 3-way balance between eddies, $[J]$ and $[\omega]$ for $\Omega^* = 1$, to being a simple 2-way balance between $[J]$ and $[\omega]$ for $\Omega^* = \frac{1}{64}$. The most complicated balance is however in the intermediate cases, mostly in the regular baroclinic regime, where vertical eddy transports are at their most important.

2. As expected, the stronger Hadley cell for smaller Ω^* is able to redistribute the excess radiative heat over a larger meridional range also via *horizontal* advection in its equatorward lower branch. In lower troposphere, horizontal heat advection is a very important process.

3. Tropospheres of slower rotators are in general maintained further away from radiative balance than those of faster rotators. This is because of the efficient advective mixing, which causes meridional temperature gradients to vanish in most parts of a slowly rotating troposphere.

4. Again, eddies are still an important factor for $\Omega^* = \frac{1}{16}$.

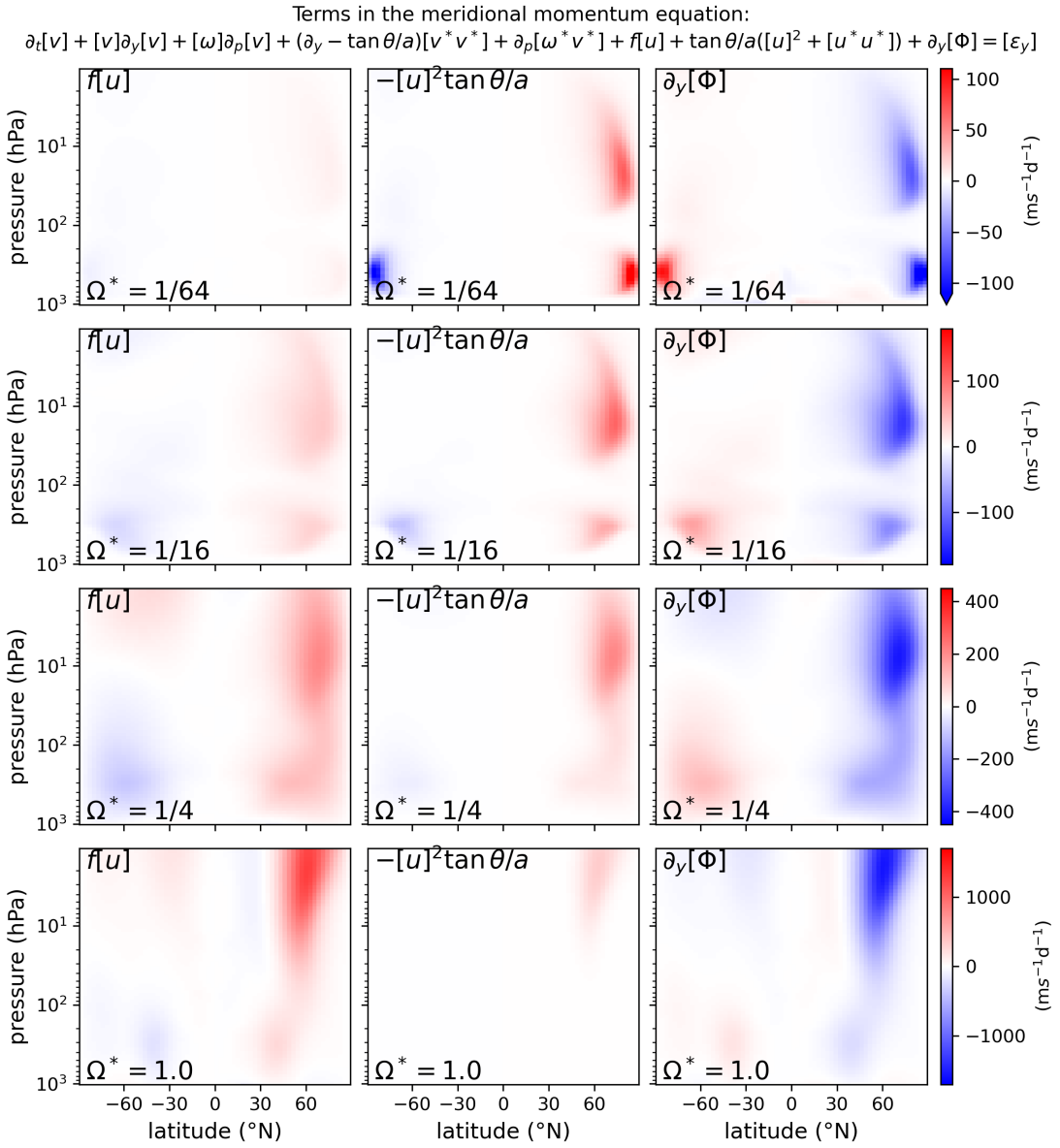

Figure 12: Terms in the zonally averaged meridional momentum equation through the entire atmospheric column, i.e. from the to the pressure level of 1 hPa. Rotation rates are organized in rows and terms in columns. Terms that are too small to be seen or barely seen but irrelevant for all rotation rates are not shown. In this figure, every row has different colour scheme, since values of meridional acceleration are order-of-magnitude different. Inside a row, all the columns share this colour scheme.

5.3.3 Eulerian mean of the $[v]$-equation in both troposphere and stratosphere

Now let us describe the figure 12, featuring the meridional momentum equation. Unlike in the cases of $[u]$- and $[T]$-equations, here the picture is extended all the way to the stratopause region at 1 hPa. These previous two were split because the values of most terms were order-of-magnitude different in the stratosphere and troposphere, thus making a single plot for both regions impractical. This is not the case for the $[v]$-eqn. The main features of interest are:

1. Only 3 terms are seen in the figure, because all the advective, temporal and error terms are negligible, at least an order of magnitude below the main balance for all Ω^*.

2. Unlike the balance between $\frac{u \tan\theta}{a} v$ and fv in the $[u]$-eqn., in this case the cyclostrophic term $\frac{u^2 \tan\theta}{a}$ is clearly dominant over fu for the slowly rotating planets. So for the large-scale zonal winds, it is rather accurate to say that they are in cyclostrophic balance with the meridional geopotential gradient, even though the same cannot be said for the strength of this effect in determining the meridional overturning. While talking about cyclostrophic balance on slowly rotating planets, this is really what is meant. This concludes the discussion of the $[v]$-eqn. in this work.

5.4 Discussion of tropospheric circulation regimes

Let us first briefly look at how well the budgets close. As an example, figure 13 compares the extent of the error term to one of the terms of the dominant balance of the $[T]$-equation. The dominant term was chosen to be $\frac{[J]}{c_p}$, since it is substantial for all Ω^*. As is the case for other equations and rotation rates, errors tend to be strongest near the surface. These is likely attributable to numerical issues with boundary conditions in the data analysis, and the fact that the ground varies over time in pressure coordinates. This is because since the ground is a complicated, time-dependent surface in pressure coordinates, some derivatives are corrupted. Although not very prominent in this picture, other areas of occasional stronger errors are the grid cells very near the poles. In general, and especially inside the domain, error terms are much smaller than the leading-order balance.

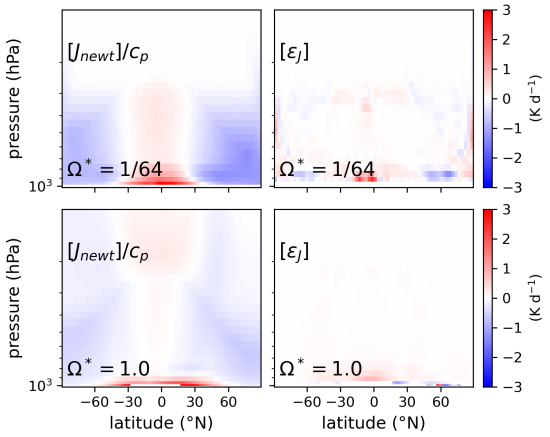

Figure 13: Error term vs. a term in the dominant balance of the $[T]$-equation.

As noted in section 2.9, a few previous studies already addressed the issue of qualitatively different circulation regimes in the troposphere - unlike the stratosphere, which is the main focus of this study. According to Goetz (2023a), which was the closest to this study in the sense that similar radiative parametrization was applied (only) to the troposphere, but which studied the Ω^*-space with finer resolution, a fundamental transition happens between $\Omega^* = \frac{1}{14}$ and $\Omega^* = \frac{1}{8}$. For $\Omega^* < \frac{1}{14}$, an approximately baroclinic-free, superrotating circulation with dominant Hadley cell is observed. Some baroclinicity appears between $\Omega^* = \frac{1}{14}$ and $\Omega^* = \frac{1}{12}$, a thermally indirect Ferrel cell appears in this regime for the first time, so do the eddy-driven jets. Between $\Omega^* = \frac{1}{10}$ and $\Omega^* = \frac{1}{8}$, eddies and baroclinicity start dominating the circulation, which becomes increasingly irregular. It is not the aim of this work to demonstrate all these transitions again, yet it can be seen that simulations with different Ω^* values in this study are consistent with where these fall in terms of these regimes. The study Goetz (2023a) is attributed the most importance in this regard, since it uses a very similar tropospheric setup as is used here, but also published, peer-reviewed articles, such as Kaspi and Showman (2015) and in particular Wang et al. (2019) reach similar conclusions. Some quantitative differences however do remain. For instance, $\Omega^* = \frac{1}{8}$ is seen in figure 4 of Wang et al. (2019) to not exhibit any appreciable Ferrel cell, while it does in my simulations, just like those of Goetz

(2023a). Also, figures 2 and 3 of Wang et al. (2019) suggest that $\Omega^* = \frac{1}{8}$ is classified in the quasi-axisymmetric regime, while according to the clustering of Goetz (2023a), it should be among the regular baroclinic cases. These differences are present despite both models having been set up as aquaplanet Earth-analogs with similar ideas behind radiative parametrizations and similar horizontal resolution. It is beyond the focus and scope of this work to pursue the precise origins of those differences, and it should be stressed that defining these regimes is still a work in progress.

What this work brings on top of previous tropospheric studies is that it shows explicitly the changing roles of various processes represented through terms in the zonal mean equations. It is also a reminder that while the developing view of distinct circulation regimes is a useful conceptual tool, it should be taken with a grain of salt. Even circulation patterns that might look qualitatively similar can have much distinct dynamical balances, e.g. the cyclostrophic term $\frac{uv\tan\theta}{a}$ cannot be neglected in a serious dynamical analysis of a $\Omega^* = \frac{1}{4}$ atmosphere, even though the atmosphere is well within the eddy-dominated baroclinic regime in either Goetz (2023a) or Wang et al. (2019). Also vertical eddy momentum transport, attributable presumably to upward propagating Rossby waves, is dramatically affected by the changing value of f within the baroclinic regime.

It seems that the zonal mean budgets are at their most complicated around $\Omega^* \sim 10^{-1}$, where both advection and eddies have similar importance for meridional transports. Not surprisingly, this is the approximate boundary between the quasi-axisymmetric regime and the baroclinic regime. The fact that this transition in importance between eddy and mean flow transports is not particularly sharp also motivates why one should not expect a particularly sharp and consistent regime transition, despite what regime diagrams might suggest. This is especially true since, as was noted, the precise boundaries differ between models set up in slightly different ways, mainly in terms of representations of sub-grid scale processes used. None of this is to suggest that the qualitatively distinct regimes do not exist, there is clearly much stronger variations in dynamical behaviour in the regions of parameter space near supposed boundaries, it is rather that the regimes are not *quite* so internally homogeneous.

Even though faster rotators than the Earth were not covered in this study, both extrapolating the trends from figures 10 and 11 and inspecting previous work, one can postulate that the complexity when viewed via the lens of the zonal mean equations only decreases with further increasing of Ω^* beyond 1. This is of course by no means suggesting that the *dynamics* is less complex, quite the contrary. It has more to do with this zonal-mean approach becoming less revealing, since all important transports come from eddies, which are however themselves less efficient (recall 2.9), and any large-scale mean meridional flow is suppressed by the strong Coriolis force. Also note that for very strong Rossby waves, the decomposition into the mean flow and eddies becomes problematic, as discussed at the end of this work. As was noted before, cases $\Omega^* > 1$ were not included because of the higher computational cost caused by smaller eddy lengthscales, and the fact that the scope of this work was semi-arbitrarily restricted to planets rotating more slowly than the Earth.

6 Temporal and zonal mean dynamics: the stratosphere

This section is a natural continuation of the previous section, taking the tools introduced there and "tested" on the troposphere to tackle the less known Ω^*-dependence of stratospheric dynamics.

6.1 Stratospheric Eulerian mean circulation

Here I partially repeat the tropospheric analysis for the stratosphere. As previously noted, this had to be separated because of the order-of-magnitude difference in the scale of accelerations and heating rates present in the stratosphere. Eulerian mean (EM) analysis for the stratosphere is given less emphasis, since the EM circulation in general does not represent the true (Lagrangian) motion of air parcels, only the local mean wind components. Knowing the Lagrangian motion is crucial e.g. for knowing the distribution of short-lived species. The difference stems from Stokes drifts due to waves (Matsuno (1980)). We can expect that this effect should become less important in the quasi-axisymmetric regime, provided that this axisymmetry extends to the stratosphere - and it should, since stratospheric waves are normally generated in the troposphere (Becker (2012)).

In figure 5, it was noted that there is a separate maximum of streamfunction in the stratosphere. Below $\Omega^* = 1/8$, there is a relatively well-separated stratospheric cell. It should be noted that since that plot shows the streamfunction on a logarithmic scale, the true separation of the stratospheric blob of positive streamfunction is even stronger than suggested in that figure (but also it is much weaker than the tropospheric circulation). To imagine the circulation in a more intuitive, linear perspective, reader can refer to figure 14.

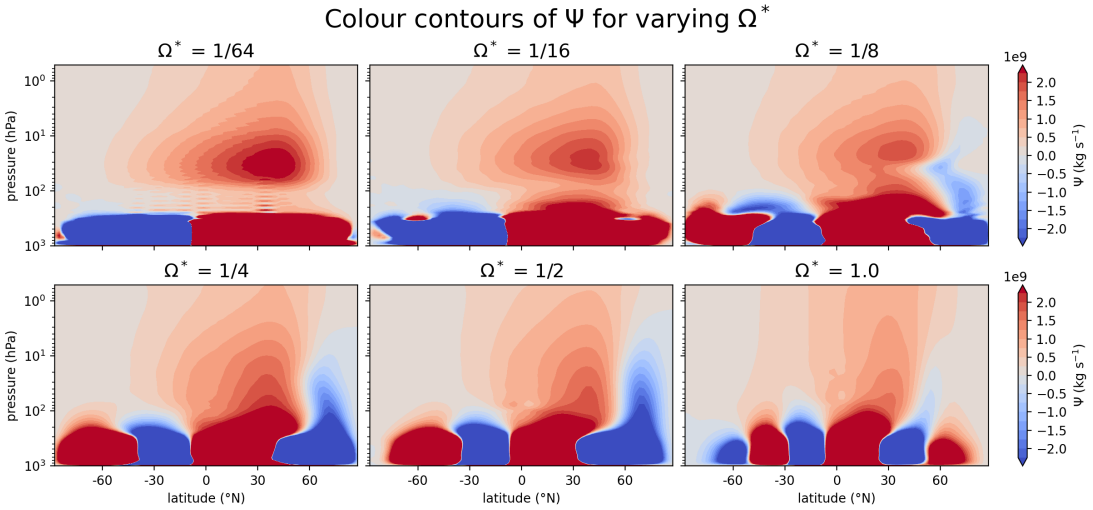

Figure 14: Stratospheric Eulerian-mean mass streamfunction with a linear colour scheme. Note that the colour sheme is fitted to the stratospheric values of Ψ, and tropospheric ones are up to two orders of magnitude above this.

Existence of substantial heat transports in the stratosphere of slow rotators is required based on the shape of isotherms in figure 6. Stratosphere experiences a very uniform temperature, which is at odds with radiatively determined state from figure 3 (Polvani-Kushner). Overturning circulation seems to be a likely candidate for these heat transfers. These cues are further developped in figures 15 and 16, especially since eddy heat transports disappear for slowest rotators. These two figures are equivalents of 10 and 11, except plotted between pressure levels of 200 and 1 hPa. Since the the simulation of $\Omega^* = \frac{1}{64}$ shows a suspicious pattern of nodes alternating with neighbouring pressure levels, its credibility is somewhat compromised - even though it adheres to the trend of other simulations without this strange feature. $\Omega^* = \frac{1}{32}$

is added into the figure to form an uppermost bound on the subset of the parameter space that can be trusted.

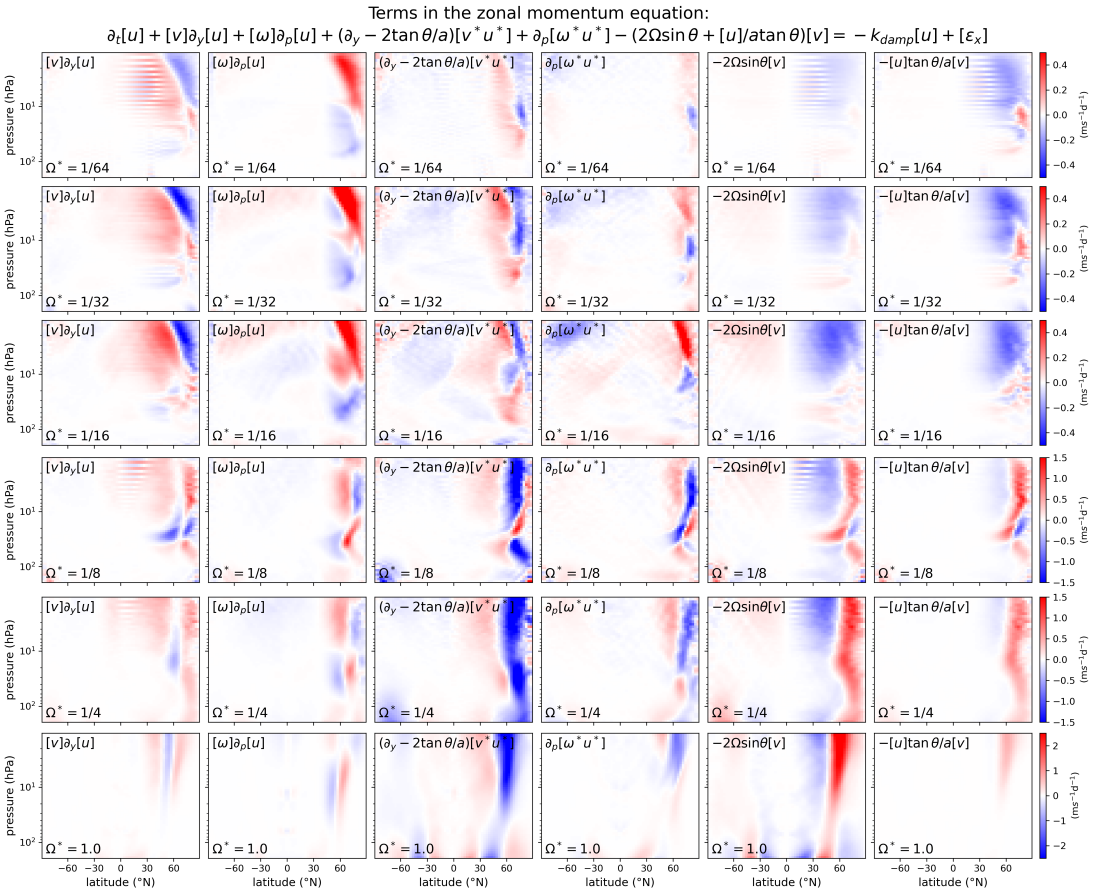

Figure 15: Terms in the zonally averaged zonal momentum equation in the stratosphere, i.e. between 200 hPa and 1 hPa. Rotation rates are organized in rows and terms in columns. Terms that are too small to be seen, or barely seen but irrelevant for all rotation rates are not shown. Damping is not shown, since the "sponge layer" only starts above the upper boundary of what is shown here. In this figure, every row can have different colour scheme, since the values of zonal acceleration are order-of-magnitude different between rows. Inside a row, all the columns share this colour scheme.

Figure 15 shows the stratospheric $[u]$-equation. The features of interest are:

1. In the winter hemisphere of slowly rotating planets, there is a strong pattern of meridional advection of zonal momentum $[v]\frac{\partial[u]}{\partial y}$, that is associated with the edge of the stratospheric overturning cell. This pattern bears similarity to the termination of the Hadley cell especially for $\Omega^* = \frac{1}{16}$ in the troposphere (figure 10).

2. Strong vertical advection $[\omega]\frac{\partial[u]}{\partial p}$ is not surprising, this spatial pattern is a necessary consequence of downwelling ($[\omega] > 0$) meeting the zonal jet at the edge of the stratospheric cell. The most intense zonal winds are generally in the region 5-30 hPa, and this is also where the sign of this term changes. Above, zonal winds are decelerated (red pattern) by downwelling bringing in air with smaller zonal velocities, while below the maximum of the jet, the opposite effect takes place.

3. As in the troposphere, eddy-induced acceleration is stronger for faster rotators. Here, a note about the nature of the ever-present winter stratospheric jet (WSJ) can be made.

For faster rotators, eddy flux convergence (blue) appears to contribute to driving the jet, while it is negligible for slower rotators. This is clarified later in the TEM view, where it will turn out that the net t.m.z.m. effect of all eddy processes is to decelerate the WSJ across all Ω^* in almost all places in winter hemisphere. In any case, the main positive contributor of zonal momentum are the ficticious forces induced by the overturning. Diagnosis of what *causes* the overturning is delayed to the TEM analysis.

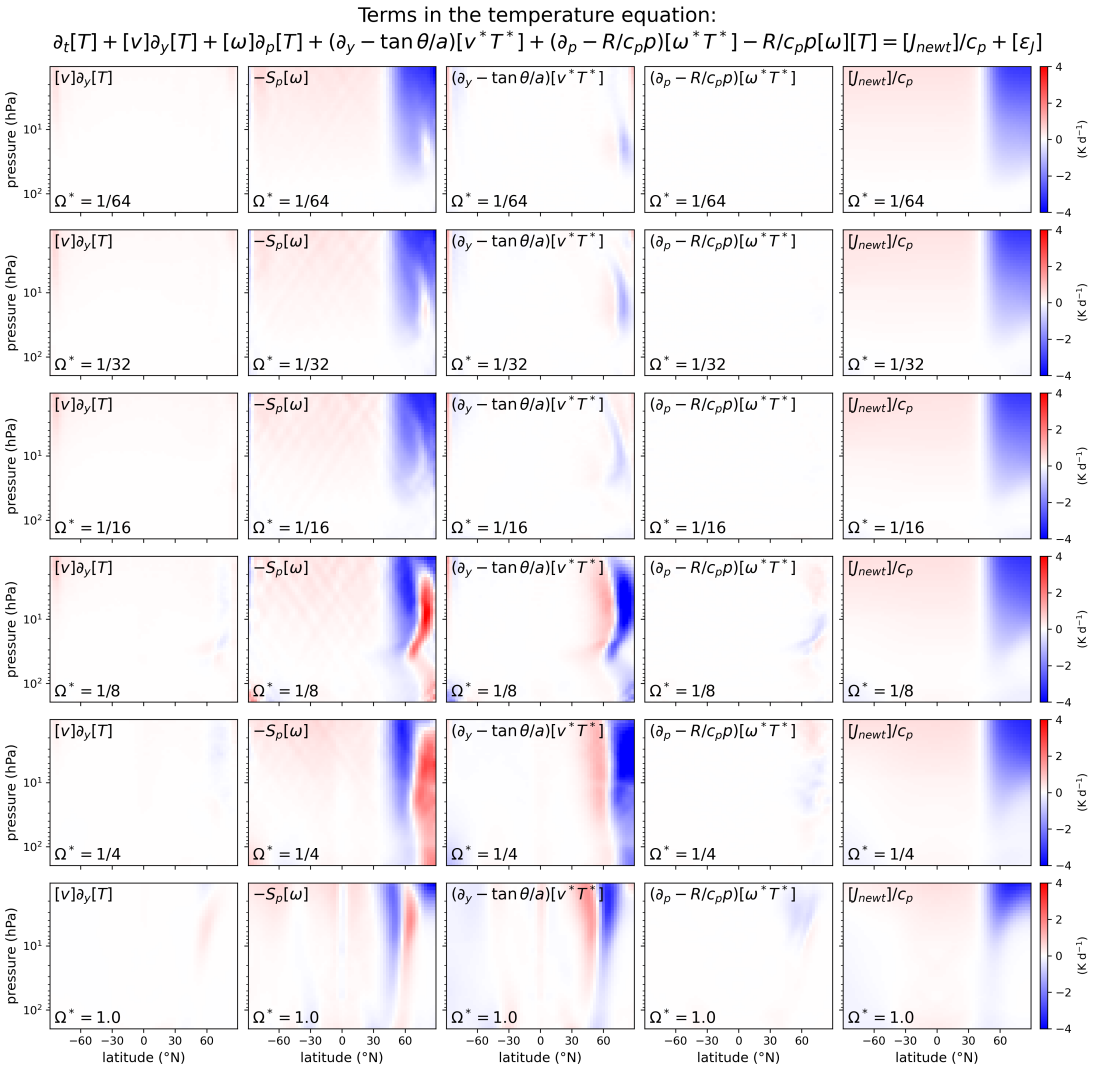

Figure 16: Terms in the zonally averaged temperature equation in the stratosphere, i.e. between 200 hPa and 1 hPa.. Rotation rates are organized in rows and terms in columns. Terms that are too small to be seen or barely seen but irrelevant for all rotation rates are not shown. In this figure, every row has the same colour scheme, see the colourbars on the right. This will generally *not* be the case in every similar subsequent plot, reader should always check these colourbar scales.

Figure 16 shows the stratospheric $[T]$-equation. The features of interest are:

1. Relative importance of eddy heating collapses sharply between $\Omega^* = \frac{1}{8}$ and $\frac{1}{16}$, i.e. precisely on the transition from baroclinic to quasi-axisymmetric tropospheric flow regime. This is so far the clearest indication in this work of how important the tropospheric transition is for the stratosphere.

2. The transition from a state of no net radiative forcing to a strong radiative deficit in (sub)polar winter stratosphere happens at roughly constant height for given Ω^*. This height and the sharpness of the transition increase with increasing Ω^*.

3. Despite the presence of the overturning cell, *meridional* heat advection is irrelevant even for slowest rotators. This will be developped in the section on temporally dependent processes, where it will be shown that it is not only a feature of the steady state, which has flat isotherms for small Ω^* (thus small $[v]\frac{\partial[T]}{\partial y}$), but it holds equally well in an example of a *transient* state (albeit slightly unrealistic one).

4. EM adiabatic heating pattern for faster rotators is composed of downwelling in mid-latitudes and upwelling in the polar region. This is not a surprising result, it traces back all the way to Vincent (1968), who tried to calculate the EM meridional stratospheric circulation based on observations. The paradoxical mismatch between such EM circulation and the circulation derived by mass was only resolved by Andrews and Mcintyre (1976) and their subsequent works , see e.g. Butchart (2014) for a very useful overview of developments of our understanding of Brewer-Dobson circulation. As can be seen from my figure 5, or e.g. figure 2 in Becker (2012), the mid-latitude downwelling part is due to the poleward end of the positive streamfunction region (spatially) connected with the tropospheric Hadley cell, while the upwelling in high latitudes is due to a negative streamfunction region (spatially) connected to the winter Ferrel cell, which is sharper on its equatorward edge. Just as the Ferrel cell in the troposphere, this polar EM upwelling is also an eddy effect. This is consistent with the fact that the pattern of $[v^*T^*]$ convergence is almost exactly opposite to $-S_p[\omega]$.

5. With the collapse of eddy heating below $\Omega^* = \frac{1}{8}$, the now largely radiative-driven EM circulation must be very similar to what would the TEM circulation look like. Furthermore, the qualitative pattern seen in the figure even on the slowest rotators is slightly similar to Brewer-Dobson circulation on Earth (i.e. a "fast" rotator), as will be better illustrated in figure 17.

6.2 Stratospheric Transformed Eulerian mean circulation

TEM circulation first defined by Andrews and Mcintyre (1976) is often used for approximating the Lagrangian motions. A very simplified version was presented in section 2.7. Here, the task is to determine a similar framework valid across our Ω^*-space, one that is sufficiently accurate, but also not unnecessarily complicated. Since the aim of the transformation is to eliminate terms from the $[T]$-equation in such way to leave there only the residual vertical motion $[\omega]_r$, which is the response to diabatic heating $[J]$, let us recall the stratospheric $[T]$-equation recently presented in figure 16. Unlike in the troposphere, where all terms are important for at least some Ω^* , stratospheric thermodynamics seem simpler throughout the Ω^*-space. Horizontal advection $[v]\partial_y[T]$ and vertical eddy transport $[\omega^*T^*]$ can be neglected to a very good approximation. With these simplifications, the $[T]$-equation becomes:

$$\frac{\partial[T]}{\partial t} + \left(\frac{\partial}{\partial y} - \frac{\tan\theta}{a}\right)[v^*T^*] - S_p[\omega] = \frac{[J]}{c_p} \tag{88}$$

This is already much easier to work with, and only differs from the form in section 2.7 by the presence of geometrical correction for the convergence of meridians. Note that this and all the subsequent treatment applies *strictly* to stratospheric dynamics, since this ad-hoc empirical approximation is not valid in the troposphere!

Recall that the transformation done in section 2.6 was:

$$[\omega]_r = [\omega] - \frac{\partial}{\partial y}\left(\frac{[v^*T^*]}{S_p}\right) \tag{89}$$

Since the equation 88, which is good-enough for the stratosphere, only contains terms in $[v^*T^*]$, all that is needed is a trivial extension to spherical geometry.

$$[\omega]_r = [\omega] - \frac{\partial}{\partial y}\left(\frac{[v^*T^*]}{S_p}\right) + \frac{\tan\theta}{a}\frac{[v^*T^*]}{S_p} \tag{90}$$

With this equation, eliminating $[\omega]$ from 88, we get:

$$\frac{\partial[T]}{\partial t} + \frac{[v^*T^*]}{S_p}\frac{\partial S_p}{\partial y} - S_p[\omega]_r = \frac{[J]}{c_p} \tag{91}$$

Thus the influence of eddy terms has been eliminated from the $[T]$-equation, apart from a small correction featuring $\frac{\partial S_p}{\partial y}$. The correction is negligible everywhere except at the polar front of faster, Earth-like rotators, and practically vanishes elsewhere and for slow rotators. Thus to a good approximation, the steady-state balance is:

$$-S_p[\omega]_r \approx \frac{[J]}{c_p} \tag{92}$$

The suggested form of $[\omega]_r$ can thus be seen as a suitable form of residual velocity in stratospheres studied in this work. For $([v]_r, [\omega]_r)$ to be a consistent velocity vector, it must satisfy the continuity equation in pressure coordinates, i.e. be divergence-free. This can be used to formally find the remaining component. Let us assume the following form, inspired by equation 90:

$$[v]_r = [v] + \frac{\partial}{\partial p}\frac{[v^*T^*]}{S_p} + \Delta(\theta, p) \tag{93}$$

Here the function $\Delta(\theta, p)$ is the difference between $[v]_r$ for this system and that in 2.7. Substituting $([v]_r, [\omega]_r)$ defined in 93 and 90 into the continuity equation 82, and finally using the continuity equation of $([v], [\omega])$ leads to a lot of cancellation, leaving only:

$$\frac{1}{a\cos\theta}\frac{\partial}{\partial\theta}(\Delta(\theta, p)\cos\theta) = 0 \implies \Delta(\theta, p) = \frac{\tilde{\Delta}(p)}{\cos\theta} \tag{94}$$

Let us take the simplest choice $\tilde{\Delta}(p) = 0$. For summary, the system is:

$$[v]_r = [v] + \frac{\partial}{\partial p}\left(\frac{[v^*T^*]}{S_p}\right) \tag{95}$$

$$[\omega]_r = [\omega] - \frac{\partial}{\partial y}\left(\frac{[v^*T^*]}{S_p}\right) + \frac{\tan\theta}{a}\frac{[v^*T^*]}{S_p} \tag{96}$$

The transformed Eulerian mean (TEM) equations can be derived by eliminating $([v], [\omega])$ in favour of $([v]_r, [\omega]_r)$ in the EM $[u]$- and $[T]$-equations. TEM $[T]$-equation is already derived, see equation **??**. The $[u]$-equation takes the form:

$$\frac{\partial[u]}{\partial t} + [v]_r\frac{\partial[u]}{\partial y} + [\omega]_r\frac{\partial[u]}{\partial p} - (f + [\phi])[v]_r = [G] + [X] \tag{97}$$

Here, $[\phi] = \frac{[u]\tan\theta}{a}$ is cyclostrophic frequency, $f = 2\Omega\sin\theta$ is Coriolis frequency, $[X] = -k_{damp}[u]$ is the parametrized friction and $S_p = \frac{R[T]}{c_p p} - \frac{\partial[T]}{\partial p}$ is the static stability parameter. $[G]$ is the total eddy driving, within this approximation composed only of eddy terms involving $[v^*T^*], [v^*u^*], [\omega^*u^*]$:

$$[G] = -\left\{\left(f + [\phi] - \frac{\partial[u]}{\partial y}\right)\frac{\partial}{\partial p} + \frac{\partial[u]}{\partial p}\left(\frac{\partial}{\partial y} - \frac{\tan\theta}{a}\right)\right\}\frac{[v^*T^*]}{S_p} - \left(\frac{\partial}{\partial y} - \frac{2\tan\theta}{a}\right)[v^*u^*] - \frac{\partial}{\partial p}[\omega^*u^*] \tag{98}$$

Note that under QG scaling and a mid-latitude plane geometry, this would reduce to $[G] = -\frac{\partial[v^*u^*]}{\partial y} - f_0\frac{\partial}{\partial p}\frac{[v^*T^*]}{S_p}$, i.e. the same form as in eqn. 43 in section 2.6. The reasoning, and

the decisions which assumptions to make and which not, is unique to the specific nature of this study. Still, there are many examples of use of TEM equations with various degrees of complexity in the literature. Note that if one starts from the primitive equations and makes no further assumptions, terms with $[\omega^* T^*]$ must be present in the $[T]$-equation, and also the horizontal advective term. This would make the entire transformation more complicated. Fortunately, this was not the case in my Ω^* space, but it is very possible that for even smaller Ω^*, horizontal advection would be strong enough to make my current treatment inadequate.

Another question is whether the formula 98 represents a divergence of a vector-valued flux quantity, as it should within the generalized Eliasen-Palm theorem (Andrews and Mcintyre (1976)). Although they do not explicitly state their assumptions, or the final formula for the eddy forcing term, Andrews et al. (1983) use the Eliassen-Palm flux (EPF) vector in pressure coordinates on the sphere with similar eddy terms present/absent than in my work:

$$\vec{F} = F_\theta \hat{e}_\theta + F_p \hat{e}_p \tag{99}$$

$$= a\cos\theta \left(-[v^* u^*] - \frac{[v^* T^*]}{S_p} \frac{\partial [u]}{\partial p} \right) \hat{e}_\theta \tag{100}$$

$$+ a\cos\theta \left(-[\omega^* u^*] - \frac{[v^* T^*]}{S_p} \left(\frac{\partial ([u]\cos\theta)}{a\cos\theta \partial\theta} - f \right) \right) \hat{e}_p \tag{101}$$

This can be used to verify the form of $[G]$ in equation 98 that I found above by comparing with established literature. Taking the isobaric divergence

$$\nabla \cdot \vec{F} = \frac{\partial (F_\theta \cos\theta)}{a\cos\theta \partial\theta} + \frac{\partial F_p}{\partial p} \tag{102}$$

it can be shown that "my" $[G]$ is indeed consistent with "their" EPF divergence, in the sense that $\nabla \cdot \vec{F} = a\cos\theta [G]$.

Let us define the TEM mass streamfunction Ψ_r in an analogy to its EM counterpart Ψ:

$$\Psi_r = \frac{2\pi a \cos\theta}{g} \int_0^p [v]_r dp \tag{103}$$

Ψ_r can be seen in figure 17, which is a TEM analog of figure 14. In figures with Ψ/Ψ_r, larger resolution was given to the higher end of Ω^* space, to see how the positive stratospheric streamfunction detaches from the tropospheric region. The qualitative nature of the separated stratospheric cell does not change anymore for $\Omega^* \leq \frac{1}{16}$. Apparent "countercirculations" at high latitudes around 400 hPa for Ω^* values $\frac{1}{8}$ and $\frac{1}{4}$ result from specific features in $[v^* T^*]$. Note that the equations for $[v]_r$ and $[\omega]_r$ were only derived assuming stratospheric scales, so these strange tropospheric features are not in themselves disturbing and will be addressed no further.

Now, equations 91 and 97 can be used to diagnose stratospheric dynamics in the TEM picture.

In figure 18, the term-wise budget of equation 91 is presented. Interpretation is aided with figure 17 which shows the stratospheric TEM streamfunction. Things to note here, in addition to what was seen in the EM picture, are:

1. as expected, the eddy inluence in higher winter latitudes that was creating a local upwelling in EM is now absent. Downwelling dominates the entire region poleward of roughly +45 degrees.

2. Upwelling is weaker and spread out over the entire region southward of +45 degrees, at least for slower rotators (see the point just below).

3. Downwelling is present also over the *summer* pole of fast rotators. For $\Omega^* = 1$, it extends higher than the 10 hPa level. This feature is precisely what is observed on Earth, c.f. the ERA interim climatology of TEM streamfunction in the December-January-February

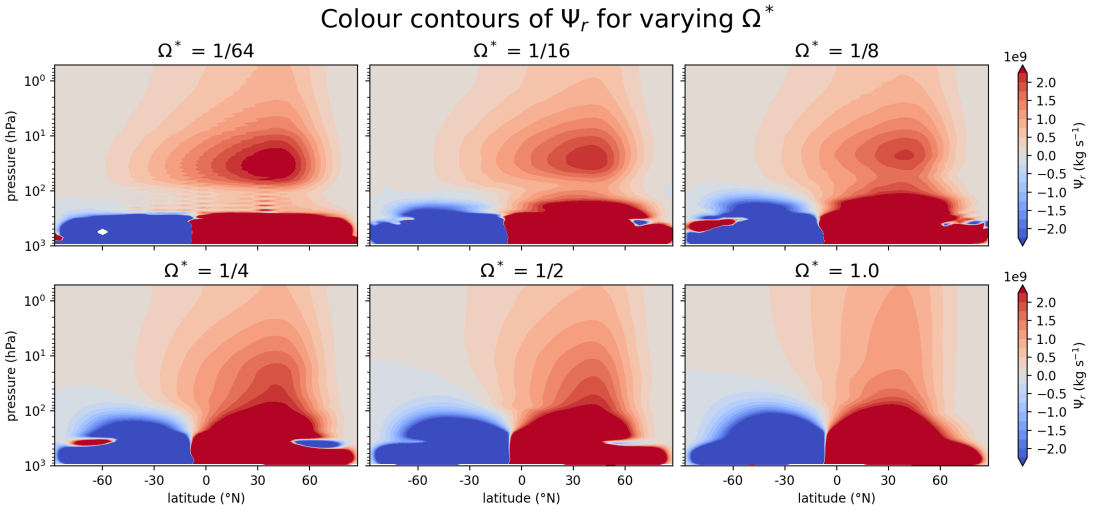

Figure 17: Stratospheric Eulerian-mean mass streamfunction with a linear colour scheme.

season in figure 5 of Butchart (2014). It is reassuring to see that this pattern agrees with Earth so well. As Ω^* decreases, this weaker summer-hemisphere cell however extends lower and lower, until it disappears from the stratosphere altogether, and becomes one with the tropospheric Hadley cell in the summer hemisphere, which is itself somewhat less high for slower rotators.

4. In summary, for slower rotators, the entire stratosphere is dominated by a single TEM circulation cell, with downelling North of 45 degrees, and upwelling elsewhere.

In figure 19, the term-wise budget of equation 97 is presented. Important points include:

1. Compared to the EM picture, the two advective terms $[v]_r \frac{\partial [u]}{\partial y}$ and $[\omega]_r \frac{\partial [u]}{\partial p}$ were merged into one, to provide clearer picture about the net effect of advection. Note that for slower rotators, where advection is important, TEM and EM velocity components are similar, so this can be viewed as a continuation of discussion of advection from the EM picture. For slow rotators in middle and upper stratosphere, the supply of air from more southern regions with smaller zonal speed is the main contributor to mean flow deceleration. This is somewhat complemented by positive eddy deceleration $-[G]$ by waves on the jet itself. Regardless of the main source of deceleration, it compensates the meridional circulation.

2. So far, nothing was said about *causation*. On Earth, baroclinicity in the troposphere creates Rossby waves that propagate upward and (with some GW contribution) largely drive the stratospheric meridional circulation. In the "classical" TEM picture on Earth (see e.g. Becker (2012)), very roughly reconstructed here for $\Omega^* = 1$, $f[v]_r + [G] \approx 0$, so it can be said that the meridional motion is driven by eddies, which causes vertical motions simply due to continuity, which then causes radiative deficit via $\frac{[J]}{c_p} \approx -S_p[\omega]_r$. So radiation is in a sense almost an afterthought.

3. The mechanism just outlined for Earth, and with it the main motivation of the TEM picture, breaks down in slowly rotating stratospheres: $f[v]_r + [G]$, or rather $(f + [\phi])[v]_r + [G]$ is not anywhere close to zero. It was stated in the first point that "momentum advection is counteracted with ficticious forces from the meridional circulation". But this is a throwaway sentence which could have equally been made the other way around. Advection *is* the meridional circulation, so the statement carries no explanatory value on its own, and does not address the issue *why*. This cannot be achieved by analyzing figure 19, since the only process captured in this figure which can cause overturning are eddies.

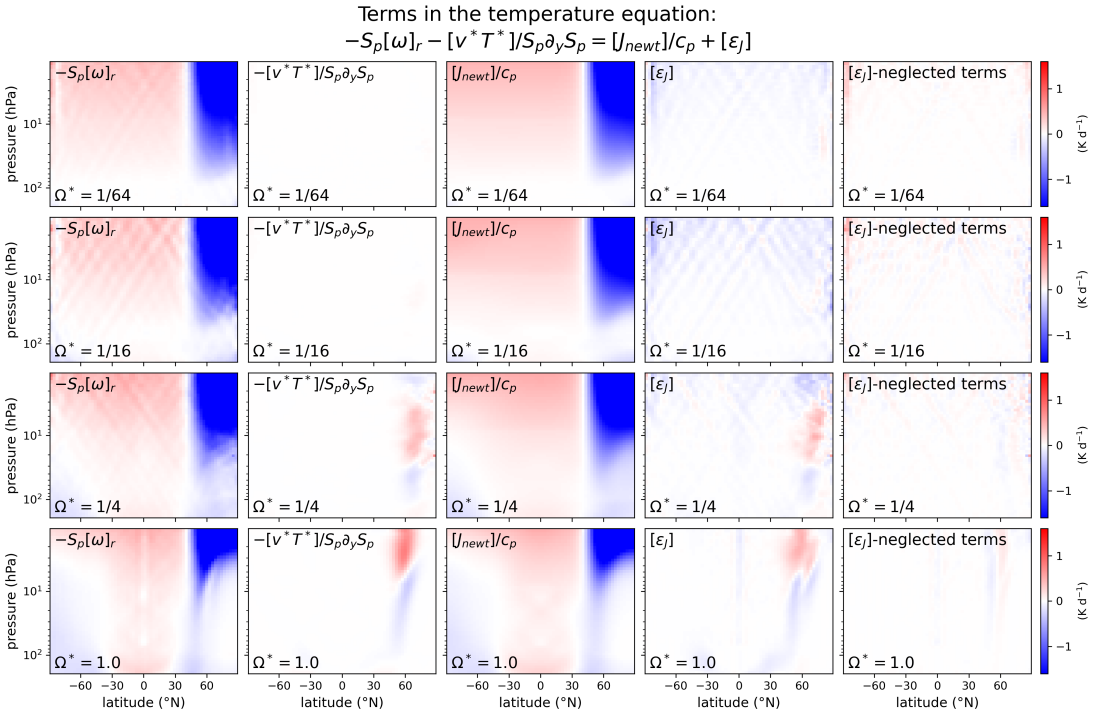

Figure 18: Terms in the TEM temperature equation in the stratosphere, i.e. between 200 hPa and 1 hPa.. Rotation rates are organized in rows and terms in columns. Unlike in the Eulerian zonal mean plots up to this point, now the error terms are shown explicitly. Because of the approximations made, they are systematic and no longer negligible. The error term in the right-most column, called "$[\epsilon_J]-$neglected terms", is the error that could be achieved if the terms neglected from the full $[T]$-eqn. were added to the equation in the title of this figure, i.e.: $[v]\frac{\partial[T]}{\partial y} + \left(\frac{\partial}{\partial p} - \frac{R}{c_p p}\right)[\omega^* T^*]$. The second column from the right, labelled $[\epsilon_J]$ is the error of the simplified equation without these terms, i.e. the error that is actually propagated to the zonal momentum equation and the residual streamfunction, after substitution of $[\omega]_r$ defined via the equation in the title. In this figure, every row has the same colour scheme, see the colourbars on the right.

4. For slow rotators whose tropospheres are relatively eddy-free, the eddy forcing of stratospheric circulation is a second order effect. There is a thermally direct, globe-spanning Hadley-like cell centered at winter mid-latitudes between 100 hPa and 10 hPa. Unlike the Hadley cell in the Earth's troposphere, the spatially more confined region corresponds to downwelling in the polar night region, and upwelling is more spread out over the rest of the globe.

5. The proposed causation chain is now "turned on its head": it is the radiative deficit that causes downwelling, while the meridional motion follows from continuity. This closes the overturning cell and causes zonal momentum advection, which assures that the atmosphere is maintained in a steady state ($\langle \frac{\partial[u]}{\partial t} \rangle_t \approx 0$). This causation direction is not sufficiently supported at this stage, and will be given more attention in section 7.

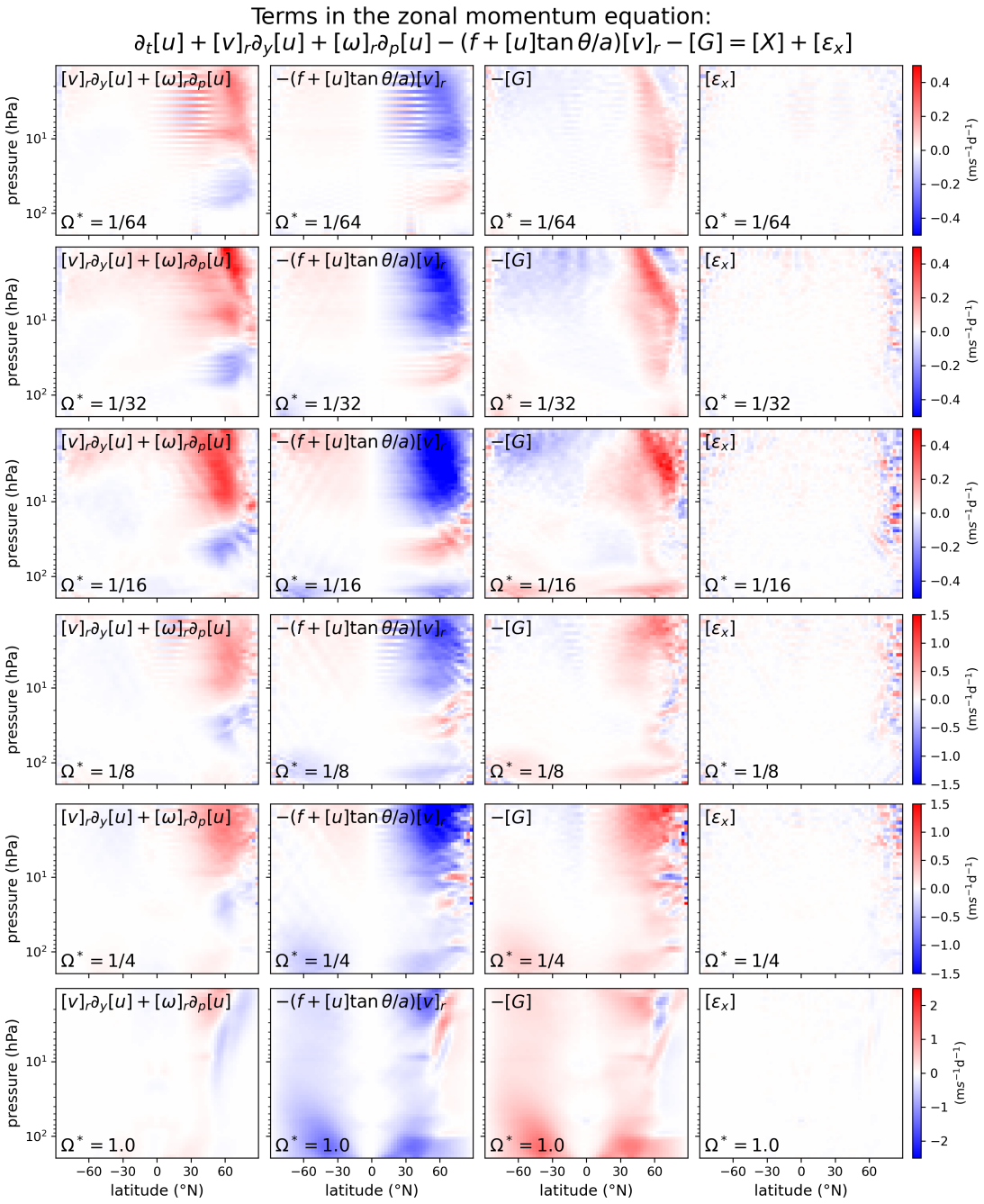

Figure 19: Terms in the zonally averaged residual zonal momentum equation in the stratosphere, i.e. between 200 hPa and 1 hPa. Rotation rates are organized in rows and terms in columns. $[\epsilon_x]$ is mostly propagated from the error in the definition of $[\omega]_r$ that is slightly inconsistent with the temperature equation itself. The reader is reminded that different (groups of) rows have different colour schemes, as always consistent inside those rows.

6.3 Superrotation

Let us analyze the t.m.z.m. zonal specific angular momentum $[M]$, defined as usual:

$$[M] = a\cos\theta([u] + \Omega a\cos\theta) \tag{104}$$

Superrotation will be diagnosed using the superrotation index s defined in 2.8 and repeated here for convenience:

$$s \equiv \frac{[M]}{\Omega a^2} - 1 \tag{105}$$

In this way, s expresses the excess angular momentum with regards to the solid body rotation at the equator.

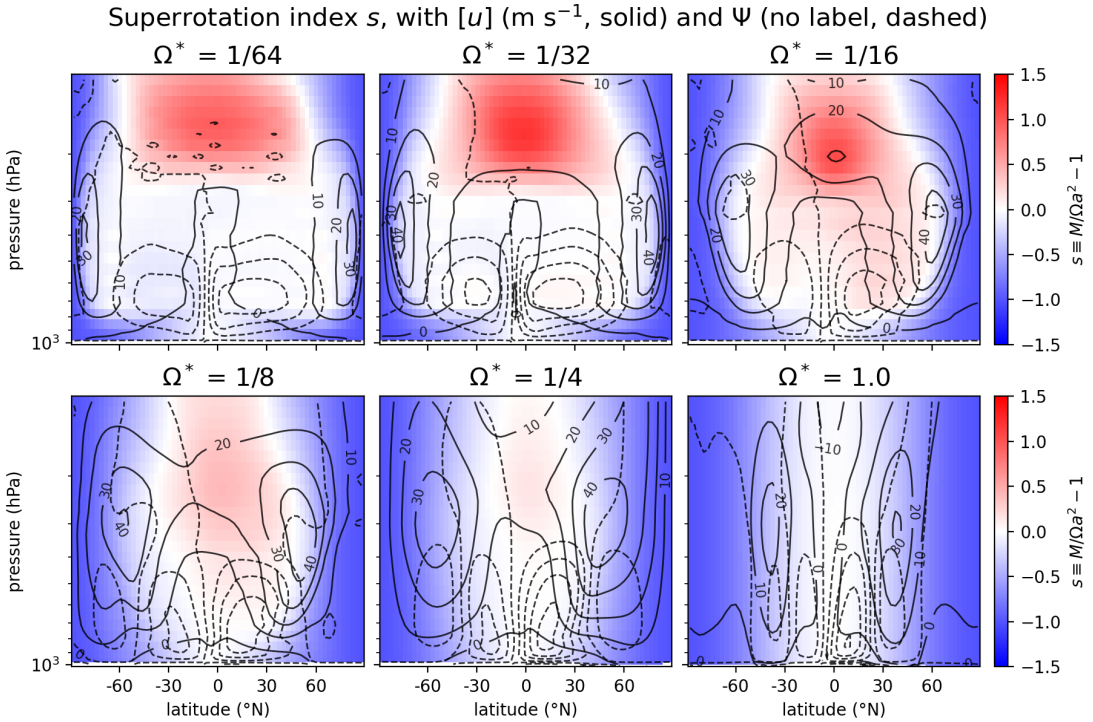

Figure 20: Tropospheric t.m.z.m. superrotation index $s = \frac{M}{\Omega a^2} - 1$ for various rotation rates in colour contours, with fixed colour scheme. Labelled solid contours indicate the t.m.z.m. zonal wind in m/s, and the unlabelled dashed contours indicate the Eulerian mean streamfunction, but with contour levels fitted for each frame separately (i.e. contour values not comparable between subplots).

Figure 20 shows the t.m.z.m. tropospheric angular momentum pattern, expressed using s. Fast rotators do not exhibit superrotation anywhere in the t.m. view, since $s < 0$. Tropospheric superrotation appears from $\Omega^* = \frac{1}{4}$ and appears to not enhance further below $\Omega^* = \frac{1}{32}$. Dashed pattern shows the overturning cells. Hadley cells are to a good degree angular momentum-conserving for fast rotators, but excess angular momentum appears around $\Omega^* = \frac{1}{16}$ even within the cell. It is noteworthy that for Ω^* from $\frac{1}{4}$ down to $\frac{1}{16}$, superrotation extends to relatively high pressures, while for $\Omega^* > \frac{1}{16}$, it appears sharply restricted to above roughly 250 hPa. Tropospheric superrotation was addressed in other studies, including Goetz (2023a), and is not analyzed further in this work.

Figure 21 shows the t.m.z.m. stratospheric angular momentum pattern, again using s. The stratospheric superrotating region consistently appears divided from the upper tropospheric region, by a gap with weaker winds, seen also in figure 4.The middle-stratospheric region is spatially correlated with the stratospheric radiatively-driven cell. For slowest rotators the

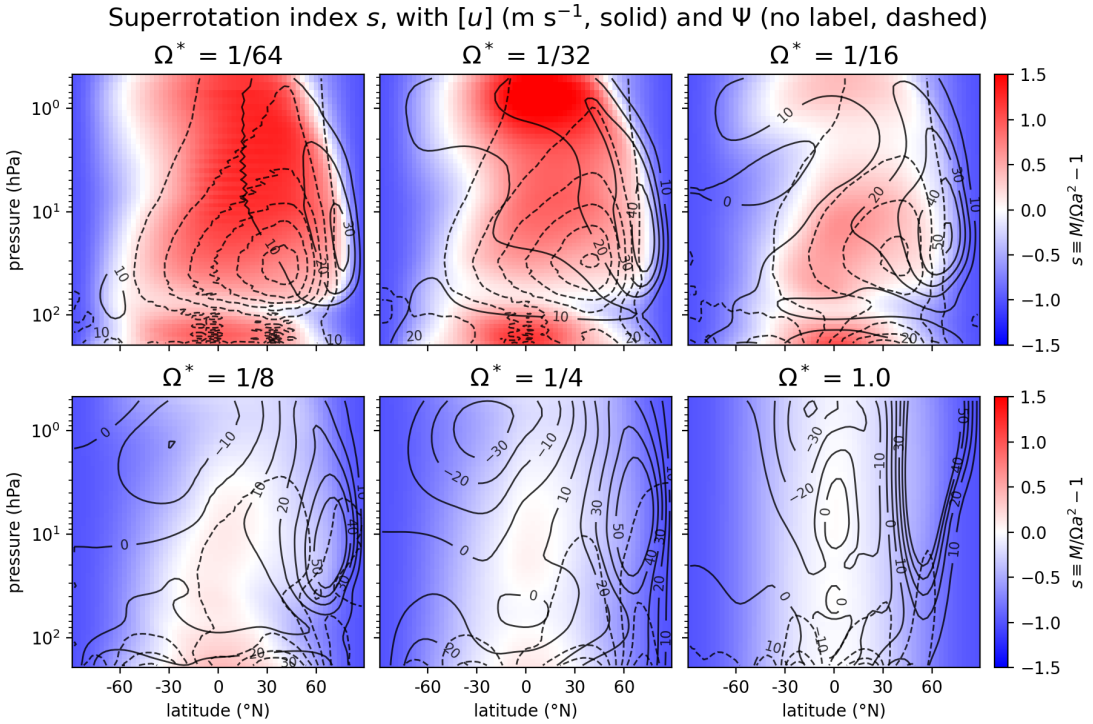

Figure 21: Stratospheric t.m.z.m. superrotation index $s = \frac{M}{\Omega a^2} - 1$ for various rotation rates in colour contours, with fixed colour scheme. Labelled solid contours indicate the t.m.z.m. zonal wind in m/s, and the unlabelled dashed contours indicate the Eulerian mean streamfunction, but with contour levels fitted for each frame separately (i.e. contour values not comparable between subplots).

stratospheric cell (or at least its, longer, upper branch) is roughly angular momentum conserving, just as the tropospheric Hadley cell. The difference is that the angular momentum of this entire mixed region is significantly above what it "should" be. Note also that the superrotating region extends significantly more southward in upper stratosphere than the streamlines would suggest if superrotation was related to the cell itself.

The natural question is where this stratospheric angular momentum - in other words excess zonal wind - comes from. According to Hide's theorem introduced in section 2.8, in an axisymmetric system, a local extremum of angular momentum can only occur at the lower boundary. In practice, this means that superrotation requires eddies. Getting back to figure 19, we see that there is a substantial eddy acceleration of the zonal wind in upper southern stratosphere, peaking at $\Omega^* = \frac{1}{16}$, spatially somewhat coinciding with the southward extension of the superrotating region beyond the area of elevated streamfunction. A slight problem is that this eddy region does not extend into the northern (i.e. winter) stratosphere, i.e. only covers the southward edge of the superrotating region. In winter stratosphere, eddies are either absent, or decelerating the mean flow. Looking at the rows $\Omega^* = \frac{1}{16}$ and $\frac{1}{32}$ in figure 19, an explanation offers itself: the "red" (mean flow decelerating) areas of $[v]_r \frac{\partial [u]}{\partial y}$ in lower northern latitudes and the "blue" (mean flow accelerating) areas of $-[G]$ in the southern hemisphere meet and touch somewhere in the tropics between 10 and 1 hPa. Positive zonal momentum can thus be generated by wave activity of yet unspecified nature in summer upper stratosphere, be picked up by the northward upper branch of the radiatively driven stratospheric circulation, and end up in northern hemisphere. When approaching the equator from the South, the *decelerating* effect of the background gradient of planetary angular momentum counterbalances the eddy-induced anomaly in relative angular momentum, causing a negligible net advective effect on local zonal winds. In figure 19 in the southern hemisphere for $\Omega^* = \frac{1}{16}$ and $\frac{1}{32}$, $-[G]$ and $-(f + [\phi])[v]_r$

are indeed seen to cancel each other. This compensation leaves no place for substantial $[v]_r \frac{\partial [u]}{\partial y}$ in the steady state, and indeed it is not seen in the southern hemisphere. The further North from the equator the parcel travels when being advected away from its source region, the more it is zonally *accelerated* by the ficticious forces, but at the same time this starts manifesting as a decelerating advective effect on the mean flow. This is exactly what is seen in figure 19: in northern mid-latitudes, the main balance is not eddies vs planetary effects, but planetary effects vs advection. Eddy deceleration becomes appreciable (and this time positive) only at the very edge of the stratospheric cell, presumably from wave breaking at the jet which forms its boundary.

6.4 Section summary

This section adressed two main aspects of the stratospheric dynamics of slowly rotating planets:

1. Emergence of planetary-wide radiatively driven overturning cell, centered in winter mid-latitudes in middle stratosphere. Upwelling and downwelling that makes up this cell helps in keeping the winter stratospheric temperature gradients low, thus maintaining the region in the radiative deficit that allows the circulation to exist. I also call this circulation the "stratospheric Hadley cell".

2. Emergence of westerlies above the equator and the summer hemisphere, and a planetary-wide superrotating state in the stratosphere. Potentially due to gravity wave breaking in the middle and upper summer stratosphere, positive angular momentum is deposited, and likely advected by the mean flow across the equator, thus forming the superrotating region. This region corresponds very well with the extent of the cell, especially on its sharp northern edge.

These two ideas are not yet complete. A causal mechanism for the stratospheric overturning was proposed in this section, but it could not be sufficiently backed-up by looking at the steady state alone. Understanding the timescales at which various aspects of the stratospheric flow develop would help make this point. Also, the steady state was built by running a simulation with *seasonal* radiative forcing pattern for *several years* (!). Although one can in principle argue that there can be terrestrial planets with Earth-like net insolation on much longer orbital periods (e.g. around hotter and more massive stars), this is both rare in terms of the known exoplanet populations, and it also constitutes a rather excessive hiding behind the liberty of this kind of parametric research. Ideally, the atmospheric conditions described in this section should arise, at least in a qualitative way, within the seasonal cycle of an Earth-like planet, i.e. within a few months. This all will be the goal of the next section. To understand the nature of the waves that have originally deposited the positive angular momentum necessary for the superrotating state, one needs to abandon the zonal mean perspective, which will be done in section 8.

7 Temporal variations of the zonal mean state

In subsection 7.1, the *spin-up* phase is discussed, i.e. the sequence of processes that lead from the initial state to the equilibrated state. It reveals important differences in time scale when various processes set in, and how they influence the evolution of observed fields. This subsection then motivates the theoretical subsection 7.2, which is the pinnacle of this section. It shows mathematically why the radiatively-driven circulation appears only on slowly rotating planets. The theory is in a very rough agreement with what is seen in the simulations, which will be shown in subsection 7.3.

7.1 The spin-up phase

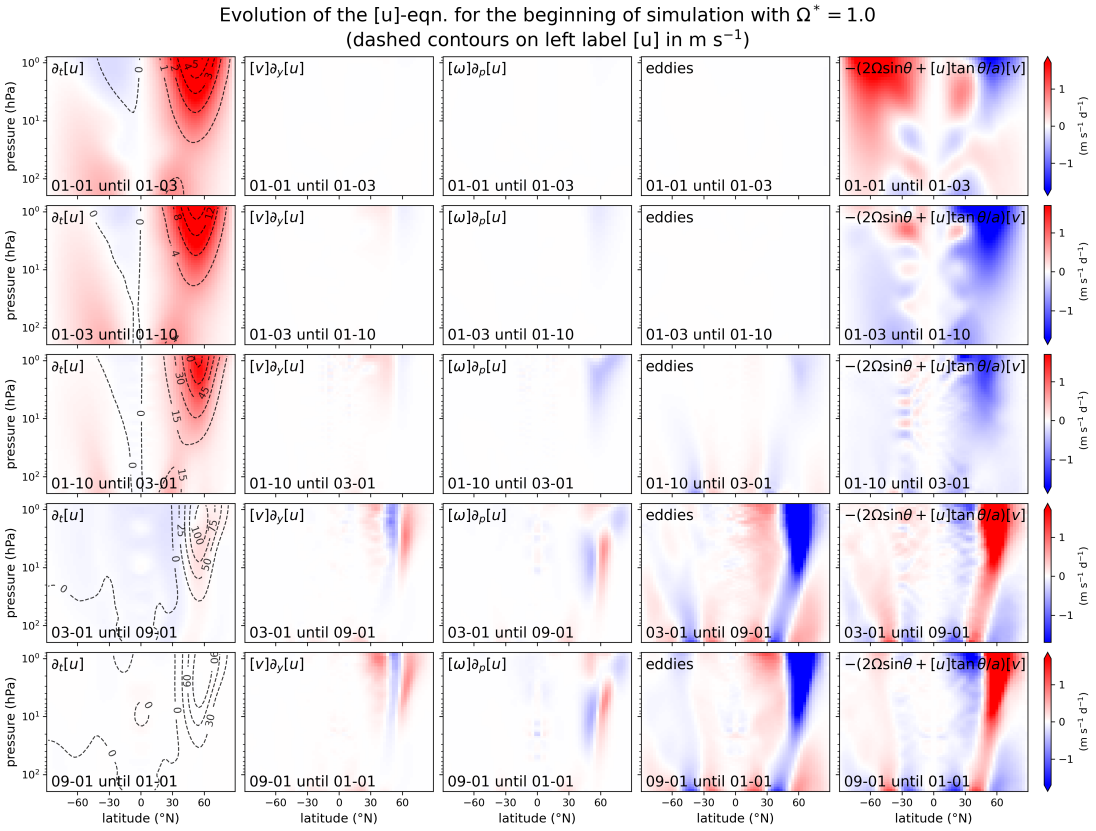

Figure 22: Temporal evolution of relevant terms in the EM $[u]$-eqn in the first days to years of the simulation for $\Omega^* = 1$. Sign convention is such that all the terms are on the LHS of the equation. Terms, ordered by columns, are displayed in the top left corner of each picture. Each row represents a t.m.z.m. state for the given time period (format mm-dd), indicated on the bottom left. Note that the end of the last period (01-01) is the start of the third year, while all dates before are in the first year.

In this subsection the similarities and differences between the spin-up phases of runs with $\Omega^* = 1$ and $\Omega^* = \frac{1}{16}$ are outlined. The simulation always begins to evolve from a stationary and isothermal state, which initially evolves because of the applied restoration temperature, which results in immediate strong radiative deficit over the winter latitudes poleward of roughly 45° N, and a slight radiative excess over the remainder of the globe. This then drives the dynamics, by (i) creating the radiatively driven overturning circulation and (ii) building up geopotential gradients, that result in zonal winds and baroclinic wave generation. In particular the relative strengths and timescales of these two processes are of interest. To take the time-dependent

constraints of seasonality into account more carefully than in previous sections, the values of Ω^* were chosen so that the "slow rotator" ($\Omega^* = \frac{1}{16}$) is very safely within the requirement that the half-period of rotation (8 days) be much smaller than the stratospheric radiative relaxation timescale (40 days). Another useful feature of $\Omega^* = \frac{1}{16}$ is that within the first roughly one month, its meridional balance is dominated by the Coriolis force rather than the centrifugal force, making the linear analytic treatment of the next subsection more plausible than for e.g. $\Omega^* = \frac{1}{64}$, where cyclostrophic balance sets in sooner than the processes of interest take place, considerably complicating the mathematics.

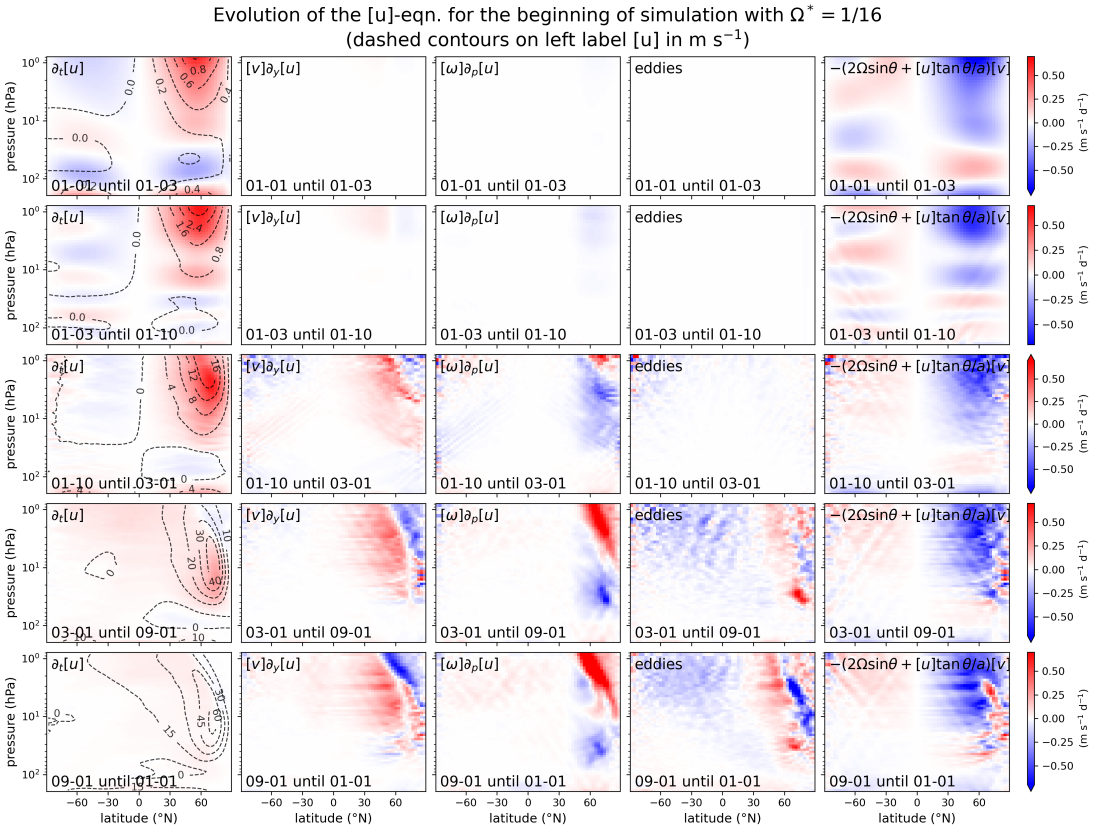

Figure 23: Analog of figure 22, but for $\Omega^* = \frac{1}{16}$. Note that the end of the last period (01-01) is the start of the third year, while all dates before are in the first year.

In figures 22 and 23, we see that the momentum balance in the first weeks is almost purely between zonal acceleration and the combined Coriolis-cyclostrophic force, a case of geostrophic adjustment (with a minor cyclostrophic component). For the slow rotator, momentum advection in the form of the overturning circulation builds up relatively quickly - on timescales characteristic for the duration of seasons on Earth, i.e. up to a few months. In the last row, the slow rotator already exhibits the advective structure seen in equilibriated simulations, associated with the stratospheric Hadley cell. Also the corresponding "subtropical" jet at around 70° N is built up to more than 1/2 of its steady-state value on these timescales. However, the superrotation is negligible even on timescales of 3-9 months, which is already a timescale on the optimistic side of a typical season. It strongly appears only in the last row, which corresponds to a timescale of 1-2 years, when all other phenomena are relatively stationary. This is mainly because significant momentum-depositing eddy processes only emerge and start accelerating the flow on timescales of 3-6 months.

The overall spin-up process is much slower for the slower rotator. This is consistent with Table 1 in section 3.5, which shows that both a half and a full buildup of the zonal wind for the fast-rotator takes takes shorter than for the slow rotator. This is the opposite of what

one would expect by considering the role of Ω^* in the geostrophic balance. As will become apparent very soon, the main reason is because the buildup of geopotential gradient for a given initial radiative forcing is much faster for the faster rotator.

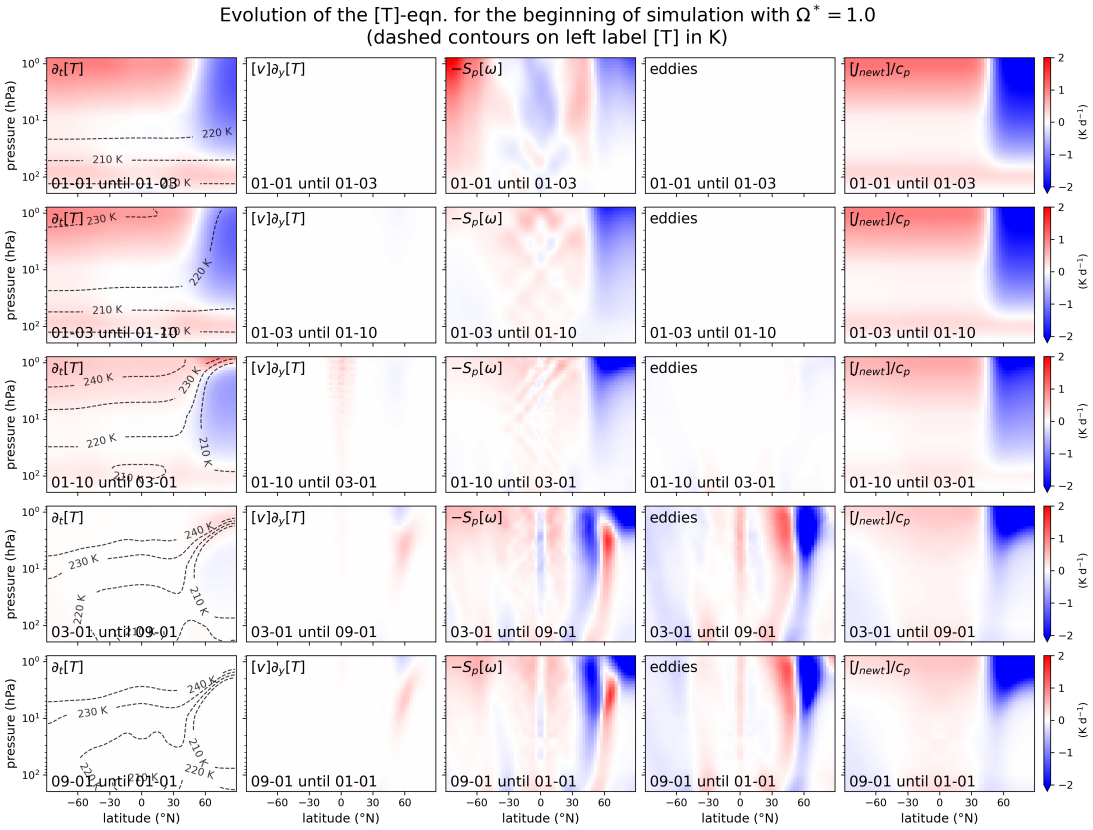

Figure 24: Analog of figure 22, but for the $[T]$-eqn. Sign convention is that all terms except the diabatic heating $\frac{[J_{newt}]}{c_p}$ are on the left hand side of the equation, with the last being on the right hand size. Note that the end of the last period (01-01) is the start of the third year, while all dates before are in the first year.

For the evolution of the Eulerian mean temperature equation, refer to figures 24 and 25, which are analogs of 22 and 23. Meridionally isothermal initial condition means that both simulations begin with a significant radiative deficit over the winter pole. In the first weeks, there is only a 3-way balance between temperature changes $\frac{\partial[T]}{\partial t}$, adiabatic heating $S_p[\omega]$ associated to downwelling, and diabatic heating $\frac{[J_{newt}]}{c_p}$ - advective and eddy transports not having set off yet. Radiative forcing from the radiative deficit over the winter pole is initially the same in both cases because of the initial conditions, but both the initial response to it and the subsequent evolution are very different. For the slow rotator, a strong downwelling compensates most of the radiative forcing, maintaining stratospheric temperatures surprisingly stable throughout the simulation, and never allowing a substantial meridional temperature gradient. Stratosphere is maintained very far from radiative equilibrium via this mechanism, which survives with little change to the equilibriated simulation displayed in figure 16, which is well approximated already by the last row of figure 25. The northern downwelling region is also the downward branch of the planet-wide stratospheric Hadley cell described in previous chapter on the t.m.z.m. circulation. Note that the buildup of eddies takes more than 12 months. Thus for $\Omega^* = \frac{1}{16}$ on seasonal timescales, $[\omega]_r \approx [\omega]$, an equality that only becomes more true for even smaller Ω^*.

For the fast rotator, the downwelling, while present, is very weak, insufficient to compensate

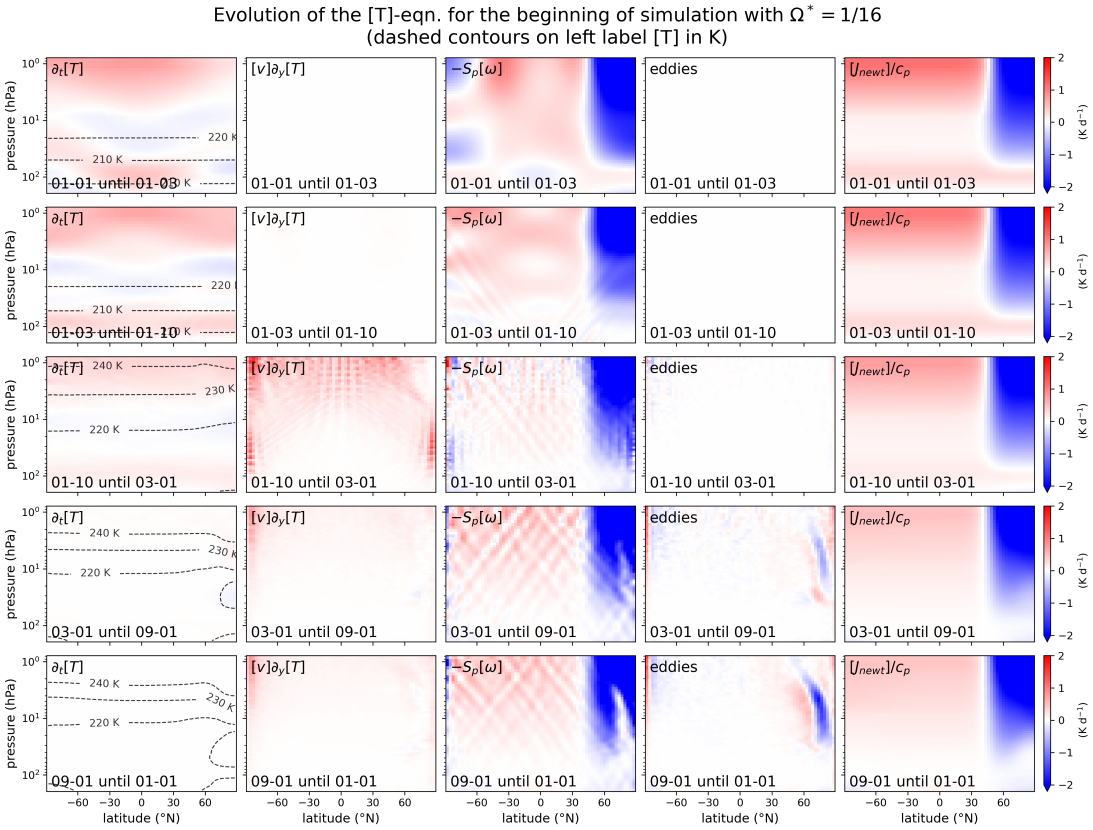

Figure 25: Analog of figure 24, but for $\Omega^* = \frac{1}{16}$. Note that the end of the last period (01-01) is the start of the third year, while all dates before are in the first year.

the radiative forcing. Only at the very top of the domain, above 2 hPa, it offsets a large portion of the forcing. In the first few months of this run, the northern polar stratosphere reaches a nearly steady thermal state, which is much closer to radiative balance than the initial state. An overturning has little reason to develop, since all of the radiative forcing goes into temperature changes, and eddies are absent. Beyond this period however, the eddies start being a first-order driver of stratospheric motion. Thus the pattern of $-S_p[\omega]$ is no longer a good proxy for the Lagrangian circulation, for which the reader can refer back to figure 18 (onset of eddies roughly coincides with the timescale on which the steady state is achieved).

In short, different strength of downwelling resulting from the same initial radiative forcing is the reason behind the differences in thermal structure between the stratospheres of fast and slow rotators. Now, the said differences in downwelling are qualitatively explained using a minimalist analytical model.

7.2 Theoretical explanation of the differences in the radiatively driven stratospheric circulation between fast and slow rotators

As described in the previous section, the main difference between the adjustment of a fast and a slow rotator is that the downwelling, which is a first response to the diabatic forcing (preceding the buildup of advection and eddies), is much stronger for the slow rotator. In both cases, there is initially a 3-way balance between $\frac{[J]}{c_p}$, $\frac{\partial[T]}{\partial t}$ and $-S_p[\omega]$. The goal of this section is to understand in an idealized mathematical model, how precisely the ratio between the second and the third of these terms depends on the rotation rate.

For an illustration of the principles at play, let us study the following linear problem. A motionless atmosphere with no meridional temperature gradients is subjected to a sudden

onset of diabatic forcing - to be precise, radiative cooling. Let this effect be restricted to a rectangular region of strong cooling near the winter pole in a latitude range $\Delta\theta = \frac{\pi}{2} - \theta_{min}$ and over a pressure range $\Delta p = p_{max} - p_{min}$, where $p_{max} \gg p_{min} \approx 0$. The corresponding set of linear mid-latitude f-plane equations for the short-term response is as follows:

$$\frac{\partial[u]}{\partial t} - f[v] = 0 \tag{106}$$

$$\frac{\partial[v]}{\partial t} + f[u] = -\frac{\partial[\Phi]}{\partial y} \tag{107}$$

$$\frac{R[T]}{p} + \frac{\partial[\Phi]}{\partial p} = 0 \tag{108}$$

$$\frac{\partial[T]}{\partial t} - S_p[\omega] = -\mu([T] - T_{eq}) \tag{109}$$

$$\frac{\partial[v]}{\partial y} + \frac{\partial[\omega]}{\partial p} = 0 \tag{110}$$

Note that $\frac{\partial[\Phi]}{\partial y}$ is determined either directly by cooling or indirectly by processes that arise from it , so the sole true forcing of this system is the right hand side of 109, which assumes the form of Newtonian cooling present in the simulations in the rectangular region defined above. Recall that $\mu \equiv \frac{1}{\tau}$ is the inverse radiative relaxation timescale. Let us simplify this forcing term as $-\mu[\tilde{T}] \equiv -\mu([T] - T_{eq})$. The goal is to determine how the short-term response to $-\mu[\tilde{T}]$ is distributed among the terms $-S_p[\omega]$ and $\frac{\partial[T]}{\partial t}$. The system is linear and well-defined, so solving it is trivial, one only needs to differentiate the equations a number of times and suitably combine and eliminate the mixed partial derivatives. Note that $\frac{\partial S_p}{\partial y}$ and $\frac{\partial \mu}{\partial y}$ are very small, and both μ and S_p are treated as constant with latitude. The result of the tedious but straightforward procedure of solving the system has the following form:

$$\frac{1}{f^2}\frac{\partial^4[\omega]}{\partial t^2 \partial p^2} + \frac{S_p R}{f^2 p}\frac{\partial^2[\omega]}{\partial y^2} + \frac{\partial^2[\omega]}{\partial p^2} = \frac{\mu R}{f^2 p}\frac{\partial^2[\tilde{T}]}{\partial y^2} \tag{111}$$

Technically, this not a finished solution, since the twice-differentiated diabatic term on the right still displays the variable $[T]$ inside $[\tilde{T}]$. Complete solution is not the aim here, instead let us look on the left. The term with $\frac{\partial^2[\omega]}{\partial y^2}$ can be traced back to the term $-S_p[\omega]$ in equation 109. The term $\frac{\partial^2[\omega]}{\partial p^2}$ can be traced back to the term $\frac{\partial[T]}{\partial t}$ in the same equation. The term with the mixed degree 4 derivative can be traced back to $\frac{\partial[v]}{\partial t}$ in the meridional balance. If the time scale Δt is much larger than $\frac{1}{f}$, in other words, if the time scale in *days* is much larger than $\frac{1}{\Omega^*}$, then the degree 4 term is much smaller than the term $\frac{\partial^2[\omega]}{\partial p^2}$. This is equivalent to saying that the atmosphere is close to thermal wind balance. For the case $\Omega^* = \frac{1}{16}$, and even more easily for $\Omega^* = 1$, this criterion is very well met for the seasonal timescales Hence, for now neglecting the degree 4, one is left with:

$$\nabla_*^2[\omega] = \mu\frac{\partial^2[\tilde{T}]}{\partial y^2} \tag{112}$$

where $\nabla_* \equiv \left(\frac{\partial}{\partial y_*}, \frac{\partial}{\partial p_*}\right) \equiv \left(\sqrt{S_p}\frac{\partial}{\partial y}, \sqrt{\frac{pf^2}{R}}\frac{\partial}{\partial p}\right)$. This is an elliptic equation, describing the non-local response of the downwelling to the spatial pattern of radiative cooling. Physically, radiative cooling produces two possible chains of reactions:

(i) drop of temperature $\frac{\partial[T]}{\partial t} \rightarrow$ buildup of geopotential gradient $\frac{\partial[\phi]}{\partial y} \rightarrow$ zonal wind acceleration $\frac{\partial[u]}{\partial t} \rightarrow$ meridional circulation $[v] \rightarrow$ vertical motion $[\omega]$ via continuity

(ii) downwelling $S_p[\omega] \rightarrow$ meridional circulation $[v]$ via continuity $\rightarrow$ mean flow acceleration $\frac{\partial[u]}{\partial t} = f[v]$ & gradual buildup of momentum advection $[v]\frac{\partial[u]}{\partial y}$

The ratio of $S_p[\omega]$ to $\frac{\partial[T]}{\partial t}$ for a given initial radiative forcing $-\mu[\tilde{T}]$ is crucial for the subsequent development of the stratosphere. In the steady state, the term $\frac{\partial[T]}{\partial t}$ is on average zero, and the main balance is always between $-\mu[\tilde{T}]$ and $S_p[\omega]$ (and, for faster rotators, also the eddies). However, if the system got to that steady state primarily via mechanism (i), e.g. on figure 24, then this steady state is close to the restoration temperature profile, and both $S_p[\omega]$ and $-\mu[\tilde{T}]$ are small in this state. Energy deficit went into bringing the air parcels to a state of no net radiative forcing, not moving them around (again, eddies are now ommited, yet essential in the steady state for $\Omega^* = 1$). On the other hand, if the system got to the steady state primarily via mechanism (ii), then the steady state is far from the restoration temperature profile, and downwelling $S_p[\omega]$ and hence the overturning circulation is strong. Adiabatic heating associated with the downwelling does relatively good job at keeping the temperature almost unchanged despite the significant forcing, refer back to figure 25.

Note that this linear system of equations cannot be used to analyze the steady state itself, since it lacks both the eddies, crucial for fast rotators, and the momentum advection term, crucial for slow rotators. However, it *can* be used to qualitatively understand how the ratio of $S_p[\omega]$ to $\frac{\partial[T]}{\partial t}$ for a given initial $-\mu[\tilde{T}]$ depends on Ω^*. And now comes the crucial argument of this subsection. Getting back to the equation 111 and inspecting the f-dependence, one can answer whether $S_p[\omega]$ or $\frac{\partial[T]}{\partial t}$ are the dominant response to forcing. We see that the term coming from $S_p[\omega]$ has f^{-2} in front of it. This scaling predicts that $S_p[\omega]$ dominates for smaller Ω^*, and $\frac{\partial[T]}{\partial t}$ for larger Ω^*. This is in perfect agreement with what is seen in the simulation in figures 25 and 24, respectively.

At this place, it would be appropriate to talk about the truly *heroic* set of assumptions that went into the original linear and axisymmetric equations used for this analysis. By extension, to judge whether it applies in some reasonable real-world scenario, i.e. whether the analysis was useful at all. The absence of non-linear terms is in itself easily justifiable by being close to the beginning of the simulation, where thermal gradients and winds are still small. As is seen in figures 24, 25, 22, 23, eddies only set start playing a role in the $\Omega^* = 1$ case, which happens after 3-9 months, so this is the time scale on which this analysis breaks down in that simulation. For $\Omega^* = \frac{1}{16}$, significant momentum advection steps in during the first 3 months, however figure 23 might be misleading, because it shows $[v]\frac{\partial[u]}{\partial y}$ and $[\omega]\frac{\partial[u]}{\partial p}$ separately to demonstrate the strength of the circulation cell. Their net effect in the $[u]$-equation is much weaker - especially in the third row, the two spatial patterns cancel out near perfectly. So in reality the mathematical model is quite adequate at least for the first 3 months. This is also the seasonal timescale on Earth, and the timescale on which the degree 4 term safely disappears for the slow rotators. In this sense, the model seems *good enough* to draw qualitative insights.

7.3 Numerical ansatz

What has been shown mathematically so far is only that two regimes should exist for "large enough" and "small enough" values of f, and that the expected behaviour is roughly in line with the simulation. It remains to be shown that it is plausible that the simulation is in indeed in the respective regime for $\Omega^* = \frac{1}{16}$ and for $\Omega^* = 1$. Let us make a very simplified ansatz for the forcing, one that will behave conveniently in the elliptic equation:

$$[J](p,\theta) = \begin{cases} \mathcal{J}_0 \sin\left(\frac{\pi(\theta-\theta_{min})}{2\Delta\theta}\right) \exp\left(\frac{-p}{\Delta p}\right) & \text{, if } \begin{cases} \theta \in (\theta_{min}, \theta_{min}+\Delta\theta) \\ \text{p}\in (p_{min}, p_{min}+\Delta p) \end{cases} \\ 0 & \text{, otherwise} \end{cases} \tag{113}$$

This qualitatively resembles the winter stratosphere seen in figures at the top two rows of figures 24 or 25. Suitable spatial scales Δp, θ_{min} and $\Delta\theta$ are 20 hPa, and 40 and 50 degrees. We are interested in $[\omega]$, not just its forcing. We can make a further simplification, which is that even for fast rotators, there is a response $S_p[\omega]$ with a similar Δp than the forcing. This might seem as a fatal inconsistency that forces the same $S_p[\omega]$ for the given $[J]$ irrespective of

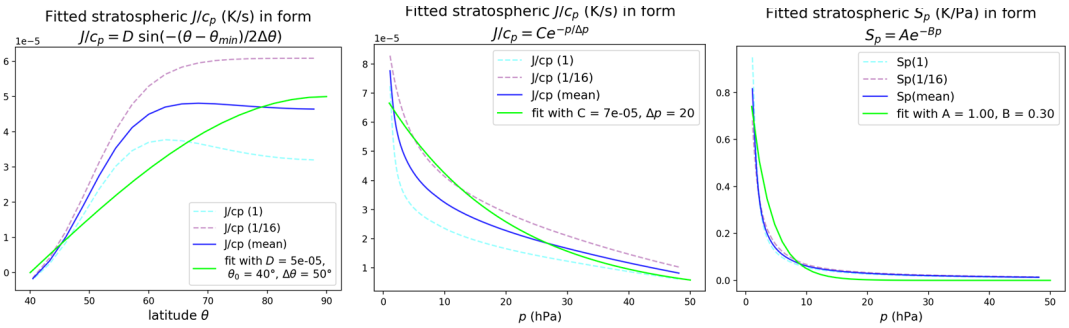

Figure 26: Partial structure functions that arise from equations 113 and 114.

Ω^*. However there is still the constant amplitude $\mathcal{W}_0$ that can vary among different Ω^* and which is expected to make the entire $[\omega]$ profile smaller for larger Ω^* (the remaining power being in $\frac{\partial[T]}{\partial t}$). Under this assumption, we can write the following profile for the response:

$$[\omega](p,\theta) = \begin{cases} \mathcal{W}_0(\Omega^*) S_p^{-1}(p) \sin\left(\frac{\pi(\theta-\theta_{min})}{2\Delta\theta}\right) \cos\left(\frac{\pi(p-p_{min})}{2\Delta p}\right) & \text{, if } \begin{cases} \theta \in (\theta_{min}, \theta_{min}+\Delta\theta) \\ \text{p}\in (p_{min}, p_{max}) \end{cases} \\ 0 & \text{, otherwise} \end{cases} \tag{114}$$

T.m.z.m. structure of the (partial) structure functions $J(\theta) = D \sin\left(-\frac{\pi(\theta-\theta_{min})}{2\Delta\theta}\right)$, $J(p) = Ce^{-p/\Delta p}$ and $S_p(p) = Ae^{-Bp}$ during the first 90 days of the simulation can be found in figure 26. By $J(\theta)$ is meant the meridional structure of $[J]$ in the region $(\theta_{min}, \theta_{min}+\Delta\theta) = (40°, 90°)$, when averaged in the vertical over $(p_{min}, p_{max}) = (1$ hPa, 50 hPa$)$. $J(p)$ means the vertical structure of $[J]$ in the region (p_{min}, p_{max}), when averaged in the horizonal over $(\theta_{min}, \theta_{min} + \Delta\theta)$. $S_p(p)$ is fitted as an exponential function, which is the worst of the approximations made here, yet it was done for mathematical convenience - to make the entire structure function $\omega(p)$ exponential, otherwise the trick that is coming would not be possible. When these fits are inserted into equation 112, one gets:

$$-\left\{\frac{Ae^{-Bp}R}{a^2 f^2 p}\frac{\pi^2}{4(\Delta\theta)^2} + \left(B - \frac{1}{\Delta p}\right)^2\right\}\mathcal{W}_0(\Omega^*) = -\frac{R}{a^2 f^2 p}\frac{\pi^2}{4(\Delta\theta)^2}\mathcal{J}_0 \tag{115}$$

Recall that $f = 2\Omega_E \Omega^* \sin\theta$ and a midpoint value of θ is 65° N. The right hand side is not relevant in our treatment, instead we require the equality of the two terms in curly braces on the left hand side. It is now a question at which pressure this occurs.

The result is an implicit equation for the transition pressure p_{tran} that can be easily solved numerically to obtain:

$$p_{tran} \approx \begin{cases} 2 \text{ hPa}, \Omega^* = 1 \\ 13 \text{ hPa}, \Omega^* = \frac{1}{16} \end{cases} \tag{116}$$

Higher in the atmosphere than this pressure level, downwelling should dominate, and below it the lowering of temperature should dominate. Checking back with figures 24 and 25, we see that this is very roughly what happens in respective simulations. In particular the third row (01-10 to 03-01), which corresponds (i) to the time scales in the fitting functions used here, as well as (ii) to the seasonal timescales, and also (iii) to the timescales on which this linear model is acceptable. For easier access, check figure 27.

Note that the inadequacy of the exponential fit of S_p is the main bottleneck of the accuracy of this estimation, introducing an error of up to a factor of 2 into the estimates - as can be verified by fiddling the parameters that still provide a roughly equally (un)reasonable

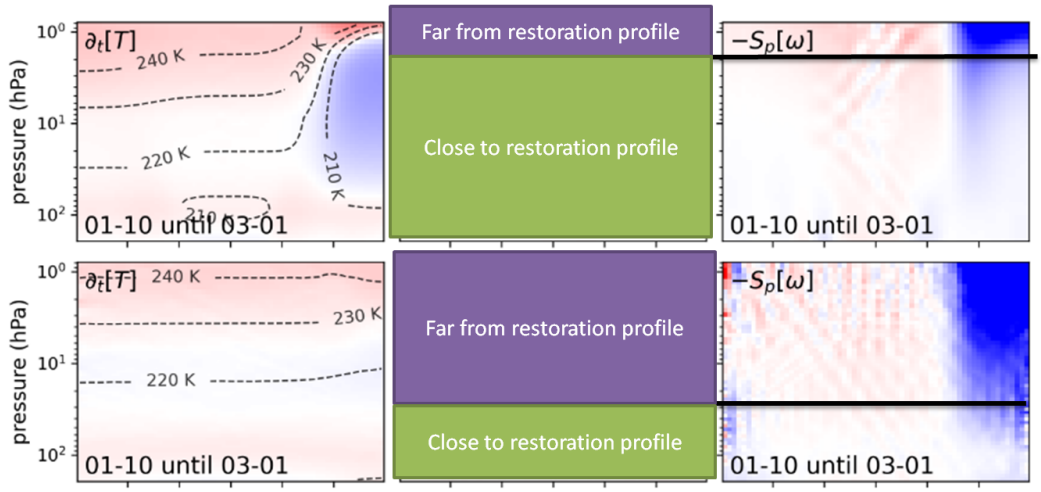

Figure 27: Excerpt from figure 24 for $\Omega^* = 1$ (top row) and from figure 25 for $\Omega^* = \frac{1}{16}$ (bottom row), for sub-seasonal timescales of 10 days to 3 months. The black line is a very rough estimate of p_{tran}. Note that the structure of $-S_p[\omega]$ in the case of $\Omega^* = \frac{1}{16}$ seems to show two transitions, one around 30-40 hPa and other around 8 hPa. The more likely p_{tran} is the 30-40 hPa one, since $\frac{\partial[T]}{\partial y}$ is so small.

fit. An alternative is to make a separate exponential fit to S_p in the lower and middle stratosphere, where the transition pressure is expected to be found for slow rotators, and near the stratopause, where it is expected to be found for fast rotators. Naturally, this leads to a much better fit. With new parameters $(A_1, B_1) = (1.5, 0.6)$ for near the stratopause, in the units as in figure 26, and $(A_2, B_2) = (0.25, 0.1)$ in the lower and middle stratosphere, we get a somewhat numerically different results:

$$p_{tran} \approx \begin{cases} 0.6 \text{ hPa}, \Omega^* = 1 \\ 46 \text{ hPa}, \Omega^* = \frac{1}{16} \end{cases} \tag{117}$$

An even better alternative would be to solve equation 111 with some initial forcing, e.g. that from equation 113. Note that the forcing itself is reasonably constant even for the simulation with $\Omega^* = 1$ in the first three months, it is only modified by the emergence of steady state on timescale of 3-9 months (see figure 24). This means that this approach could be useful. For our purposes, let us satisfy ourselves with noting that despite the gross inaccuracy of the functions substituted into the equation 112, it still gives somewhat reasonable estimates for the transition pressure. This fact, and the theoretical arguments in support of the validity of the linear set of equations used in this analysis (on suitable timescales), together make it likely that this mechanism is the essence of why stratospheric Hadley cell emerges and persists for the slow rotating simulations, but not for the fast rotating ones.

7.4 Section summary

One of the deficiencies of this entire work is its usage of a permanent-January-like condition in the restoration temperature profile. This condition is applied over several years of the simulation until a steady state is achieved. This is not what would happen on a planet with Earth-like orbital period, where seasons last ~ 3 months. One needs to consider which of the processes are likely to develop on these timescacles and which not. This was done looking at cases $\Omega^* = 1$ and $\Omega^* = \frac{1}{16}$. In summary:

1. Winter stratospheric jet and the stratospheric Hadley circulation get to 50% of their steady state strengths over the 3 month period of radiative forcing.

2. Eddy-induced superrotation spanning from summer to winter mid-latitudes in the mid- and upper-stratosphere needs at least 12 months to develop, since eddies that generate it need 3-6 months.

In a later part of this section, a simplified mathematical model was used to show that downwelling is the preferred initial response to radiative forcing in most of the stratosphere for slow rotators, while temperature adjustment is prefered at the other end of the Ω^* range. Only the former can lead to a strong steady-state radiatively driven circulation in the stratosphere, since the latter smooths out the forcing. A very crude numerical ansatz showed that it is plausible that the Ω^* values studied here indeed lie on the opposite ends of this regime transition, as the figures in part 7.1 suggest.

In some of its aspects, and in a very rough and qualitative sense, the spin-up phase can be regarded as related to what happens when seasons change during autumn. The obvious caveat that the change in radiative forcing should be continuous. The more fundamental caveat is that eddies from the troposphere do propagate upward during autumn, so processes that require eddies - like the superrotation - might be present after all (despite them not developping on seasonal timescales from the intitial state of the simulation). Hence, one needs to be very careful when interpreting the spin-up state, since it certainly does not map to the transition from autumn to winter, even disregarding the temporal discontinuity. More about this will be said in the final discussion section.

8 Zonal asymmetries

The focus of this chapter are phenomena that possess not only a temporal (like in the last chapter), but also a zonal variability. Naturally, zonally asymmetric processes were crucial for the dynamics presented in previous chapters, where they acted through eddy transport terms like e.g. $[v^*T^*]$. However, the nature of the particular motions that caused these was never examined. Same restoring forces associated to buoyancy and rotation are present, and lead to same kinds of wave motions as seen on Earth, however their amplitude, wavelength, frequency, refractive index, and spatial patterns of all these can change dramatically with changing the rotation rate. Unlike in previous chapters, where the pressure coordinates were used, this chapter uses log-pressure coordinates. This was decided because they are more natural especially when thinking about vertical wavenumbers, since they roughly correspond to the physical height, unlike pressure - which changes by 2 orders of magnitude in the stratosphere. In this chapter the *integer zonal wavenumber* $k_* = ka\cos\theta$ is used, where $k = \frac{2\pi}{L_x}$ is the wavenumber in inverse meters and $2\pi a\cos\theta$ is the circumference of the Earth at given latitude.

Note this section goes much less deep than previous sections, and resorts to a very descriptive overview and tests of a few back-of-the-envelope estimates. In a longer project, deeper understanding of the nature of waves in the simulation output of slower rotators would be among the priorities, in particular with regards to stratospheric superrotation, likely initiated by wave breaking in upper summer stratosphere.

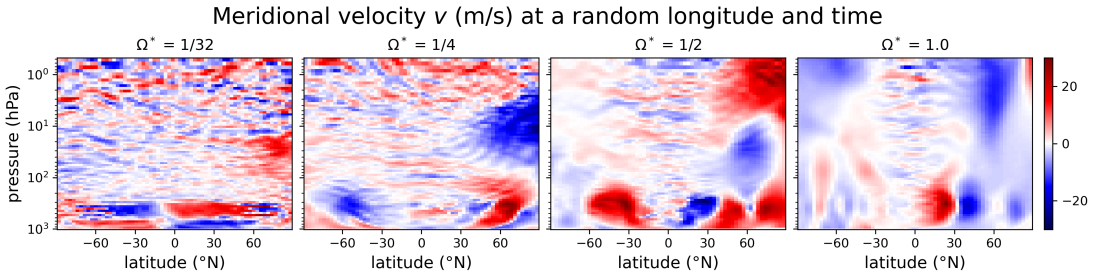

Figure 28: Snapshot of meridional velocity in both troposphere and stratosphere during the equilibriated phase at longitude 0 degrees. The colorbar is common for all four rotation rates.

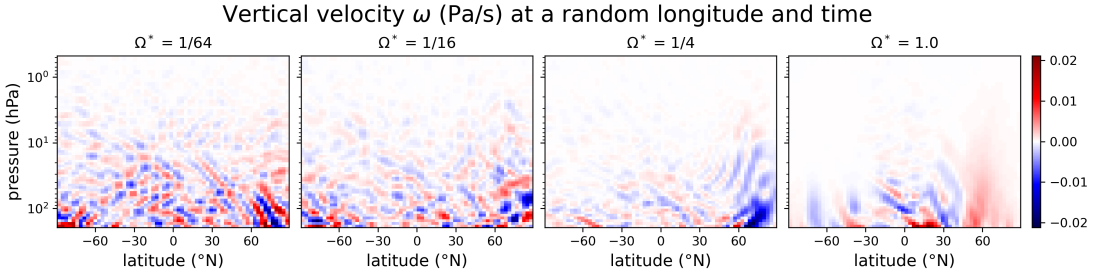

Figure 29: Snapshot of vertical velocity in the stratosphere during the equilibriated phase at longitude 0 degrees. The colorbar is common for all four rotation rates.

8.1 Vertical propagation of Rossby waves

Since no topography and no land-sea contrasts in albedo and heat capacity are present in the simulations, stationary Rossby waves have little reason to form. This has implications for the wave-driven part of the stratospheric circulation, since stationary waves are a dominant source of transmitted energy (Charney and Drazin (1961)). However, there are still baroclinic Rossby waves, especially evident e.g. in figure 28 around tropospheric jets, and these can propagate

to the stratosphere, as restricted by the criterion outlined and motivated below - also called the Charney-Draizin criterion.

8.1.1 Standard quasigeostrophic theory

This is a condensed overview of the underlying theory, sourced mainly from Chapter 12.3 in Holton and Hakim (2012) and may be skipped by a reader familiar with the topic. In log-pressure coordinates (see 2.2) and within the standard QG PV equation:

$$\left(\frac{\partial}{\partial t} + u_g\frac{\partial}{\partial x} + v_g\frac{\partial}{\partial y}\right) q = 0 \tag{118}$$

with the QG PV defined as

$$q \equiv f + \nabla_h^2\psi + \frac{f_0^2}{\rho_0 N^2}\frac{\partial}{\partial z}\left(\rho_0\frac{\partial\psi}{\partial z}\right) \tag{119}$$

through the QG streamfunction $\psi = \frac{\Phi}{f}$, one can derive a linearized perturbation equation for $q' \equiv q - [q], \psi' = \psi + [u]y$:

$$\left(\frac{\partial}{\partial t} + [u]\frac{\partial}{\partial x}\right) q' + \beta\frac{\partial\psi'}{\partial x} = 0 \tag{120}$$

where

$$q' \equiv \nabla_h^2\psi' + \frac{f^2}{\rho_0 N^2}\frac{\partial}{\partial z}\left(\rho_0\frac{\partial\psi'}{\partial z}\right) \tag{121}$$

One can look for harmonic waves of the form $\psi'(x,y,z,t) = \tilde{\psi}(z)e^{z/2H}e^{i(kx+ly-kc_xt)}$. After substitution, the vertical structure function ($\tilde{\psi}$) equation becomes:

$$\frac{\mathrm{d}^2\tilde{\psi}}{\mathrm{d}z^2} + \overbrace{\left\{\frac{N^2}{f^2}\left[\frac{\beta}{[u]-c_x} - (k^2+l^2)\right] - \frac{1}{4H^2}\right\}}^{\equiv m^2}\tilde{\psi} = 0 \tag{122}$$

This equation (akin to a simple harmonic oscillator) only allows vertical propagation if $m^2 > 0$, in which case the solution becomes $\tilde{\psi}(z) \sim e^{imz}$, i.e. m is the vertical wavenumber, whose sign gives the direction of phase propagation (NB: group velocity is always positive since energy propagates upwards, but phase velocity needs not be). The resulting condition for vertical propagation is:

$$0 < [u] - c_x < \frac{\beta}{k^2 + l^2 + \frac{f^2}{4H^2N^2}} \equiv U_c \tag{123}$$

It shows that vertical propagation can only happen if the winds are eastward and weaker than a critical strength U_c, and even then only waves for which the horizontal wavelength is longer than a certain value.

8.1.2 Ramifications for atmospheres of other planets

For now assume that the QG result is still good enough (although in reality almost certainly not for slowest rotators). Note that the rotation rate is featured both in the numerator and the denominator of U_c , since $\beta \sim \Omega$ and $\frac{f^2}{4H^2N^2} \sim \Omega^2$, the dominant effect being dependent on how $k^2 + l^2$ compares with $\frac{f^2}{4H^2N^2}$. Let us estimate these two terms at 45° N, where $k^2 + l^2 \approx k^2 \approx \frac{k_*^2}{a^2\cos^2\theta} \approx k_*^2 \times 5 \times 10^{-14}$ m^{-2}. A representative value of N^2 across most places in the stratosphere across all simulations can be taken as $3{\times}10^{-5}$ s^{-2} ($\pm$ 50%), and since global mean temperature is the same in all simulations, $H = \frac{RT_s}{g} = 8400$ m throughout. This makes the Ω-dependent term in the denominator into $\frac{f^2}{4H^2N^2} = (\Omega^*)^2 \times 1.3 \times 10^{-12}$ s^{-2}. For $k_* \sim$"a few" and $10^{-2} < \Omega^* < 10^0$, these terms are roughly equally important. For larger

wavenumbers and slower rotators, U_c initially increases with Ω^*, and on the faster side of Ω^* space, it decreases again with Ω^*. But it is important that when varying k_* and holding Ω^* still, U_c always decreases with increasing k_*, this decrease even being faster for smaller Ω^*, since the constant term $\frac{f^2}{4H^2N^2}$ in the denominator is much smaller. Thus Charney-Drazin filtering should still in principle hold for Rossby wave modes.

Naturally, QG theory is not an adequate description for the slowest rotators examined in this study. Getting back to the horizontal momentum equation:

$$\frac{\mathrm{D}u}{\mathrm{D}t} - 2\Omega v \sin\theta - \frac{uv\tan\theta}{a} = \frac{1}{a\cos\theta}\frac{\partial\Phi}{\partial\lambda} \tag{124}$$

that was previously abbreviated to

$$\frac{\mathrm{D}u}{\mathrm{D}t} - (f+\phi)v = \frac{\partial\Phi}{\partial x} \tag{125}$$

importance of Coriolis term is diminishing compared to the ϕ term. Which of the two balances is dominant depends on the ratio of f and ϕ. This is not so simple, since ϕ requires zonal wind u, and it can dominate in the regions with strong winds, but disappear elsewhere for a given slow rotating planet. While geostrophic balance is the dominant balance in the upper range of Ω^* values (roughly 1 down to 1/4), a mixed, gradient balance is applicable in the lower range (rougly 1/8 down to 1/64). None of the cases are purely cyclostrophic, although that component becomes larger for 1/64. This is in essence the same conclusion as was seen in previous figures with budgets like figure 10 or figure 15, where $f[v]$ and $[\phi][v]$ were seen separately.

8.1.3 Presence in the simulation

Figure 30 shows the distribution of spectral density among the integer zonal wavenumbers k_* in range 1-10. Tropospheric pattern is well comparable to figure 6 in Wang et al. (2019), which also shows the pattern at 500 hPa (albeit with a linear colour scale).

It is seen in the figure that Charney-Draizin criterion 123 filters out the wavenumbers 5-8 that are abundant in the midlatitude troposphere of the planet with $\Omega^* = 1$, only allowing wavenumbers 2 in the mid- and upper-stratosphere. This is also a familiar picture from the Earth (Hirota and Hirooka (1984)). However starting $\Omega^* = \frac{1}{4}$ and below, only wavenumber 1 is ever dominant in the stratosphere. This behaviour is not normally observed on Earth. A notable feature of the slowest rotator is the absence of waves at lower latitudes and pressure levels. From 100 hPa upwards in the stratosphere, the wavefield is dominated by Rossby waves at smaller wavenumbers, but it seems that inertia-gravity waves dominate for $\Omega^* \leq \frac{1}{16}$.

8.2 Equatorially-traped waves

Looking at figure 28, it is apparent that for fast rotators, there is a conical low-latitude stratospheric region where equatorially-trapped waves are the dominant wave process. On Earth, there are several well-known types of such waves: equatorial Kelvin waves and multiple Rossby-gravity wave modes. From 28, Kelvin waves can be ruled out, since they do not posses a meridional velocity component.

For a general case of a planet in a gradient wind balance, both the Coriolis and cyclostrophic effects contribute to the generalized β term, here labelled as $\tilde{\beta} = \beta_f + \beta_\phi$, not to be confused with $\beta \equiv \beta_f \equiv \frac{\partial f}{\partial y}$. The two components take the forms:

$$\beta_f \equiv \frac{\partial f}{\partial y} = \frac{1}{a}\frac{\partial}{\partial\theta} = \frac{2\Omega\cos\theta}{a} \tag{126}$$

$$\beta_\phi \equiv \frac{\partial\phi}{\partial y} = \frac{1}{a}\frac{\partial}{\partial\theta}\left(\frac{u\tan\theta}{a}\right) = \frac{u}{a^2\cos^2\theta} + \frac{\tan\theta}{a^2}\frac{\partial u}{\partial\theta} \tag{127}$$

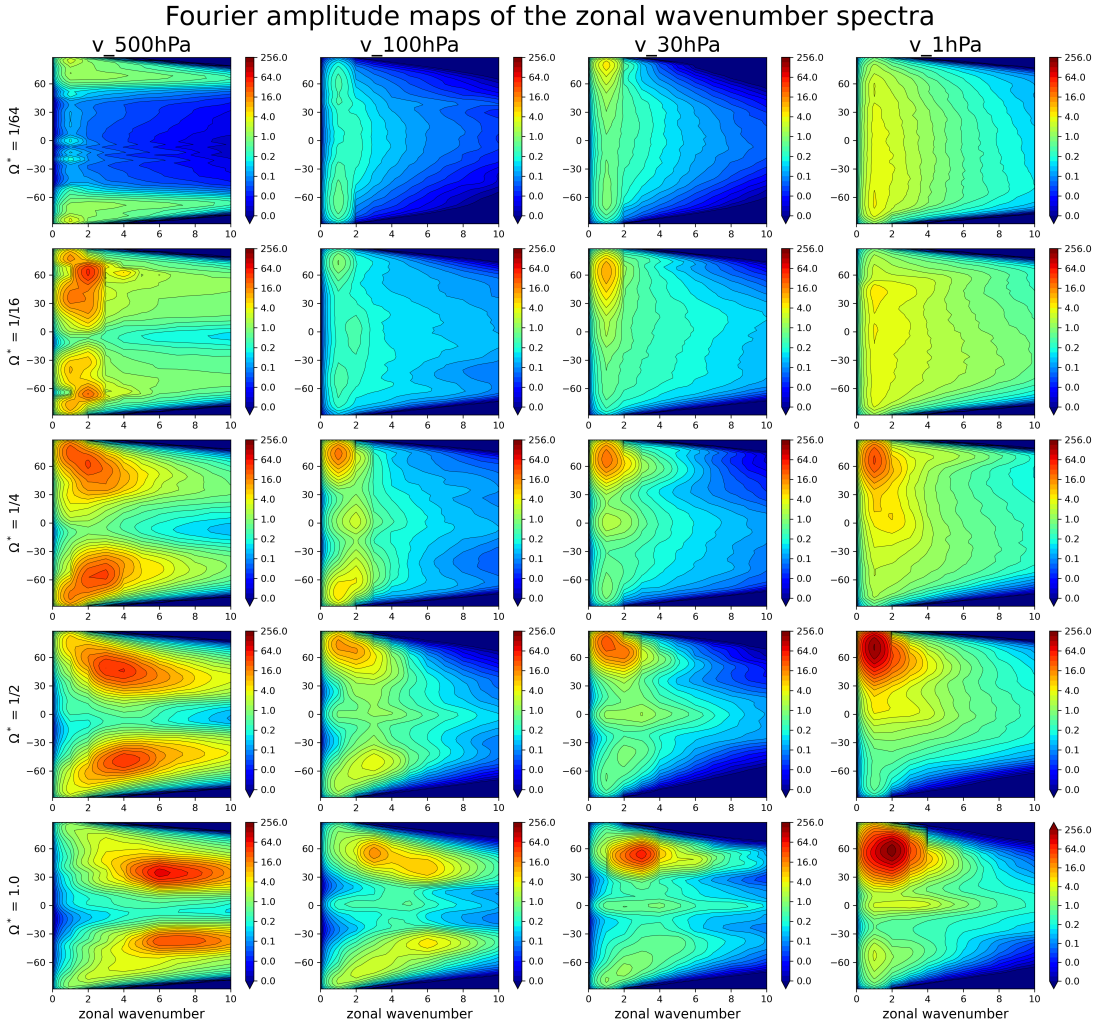

Figure 30: Integer zonal wavenumber $k_* = ka\cos\theta$ for different rotation rates (rows) and pressure levels (columns). Pressure levels are chosen to roughly represent the troposphere, and respectively lower, middle, and upper stratosphere. Note that the colour scale is logarithmic!

To be able to write linear perturbation equations on equatorial beta plane, we put $\tan\theta \approx 0$ and $\cos\theta \approx \cos^2\theta \approx 1$ (i.e. a somewhat stronger geometrical assumption is needed than just for β_f). Also, term $\beta_\phi yv$ is at present non-linear, so we need to assume that the zonal mean flow is not changed very much by the wave. In the zonal direction this holds sufficiently well. Fortunately, for the rotation rates considered in this study, the cyclostrophic component only ever becomes important when zonal wind is itself very large, so at least for a very qualitative

picture this approximation is admissible. Thus the system is as follows:

$$\frac{\partial u'}{\partial t} - \overbrace{\left(\frac{2\Omega}{a} + \frac{\bar{u}}{a^2}\right)}^{\tilde{\beta}} yv' = -\frac{\partial \Phi'}{\partial x} \tag{128}$$

$$\frac{\partial v'}{\partial t} + \left(\frac{2\Omega}{a} + \frac{\bar{u}}{a^2}\right) yu' = -\frac{\partial \Phi'}{\partial y} \tag{129}$$

$$\frac{\partial u'}{\partial x} + \frac{\partial v'}{\partial y} + \frac{1}{\rho_0}\frac{\partial}{\partial z}\left(\rho_0 w'\right) = 0 \tag{130}$$

$$\frac{\partial^2 \Phi'}{\partial t \partial z} + w' N^2 = 0 \tag{131}$$

With the approximations above, this system looks the same as the "textbook" case of linear equatorial waves in a stratified rotating atmosphere where the beta-effect only comes from the Coriolis terms - check Holton and Hakim (2012) Chapters 11 and 12 for a mathematically almost equivalent treatment. One can search for solutions of the form

$$\begin{pmatrix} u' \\ v' \\ w' \\ \Phi' \end{pmatrix} = e^{z/2H} \begin{pmatrix} \hat{u}(y) \\ \hat{v}(y) \\ \hat{w}(y) \\ \hat{\Phi}(y) \end{pmatrix} \exp[i(kx + mz - \nu t)] \tag{132}$$

Upon substitution to the system above and following algebra similar to Holton and Hakim (2012) 11.4.1, a separate differential equation for the structure function $\hat{v}(y)$ can be derived. Its non-dimensionalised solutions are:

$$\hat{v}(\xi) = V_0 \mathrm{H}_n(\xi) e^{-\xi^2/2} \tag{133}$$

Here, H_n is the n-th Hermite polynomial in the non-dimensional unit $\xi = \sqrt{\frac{\tilde{\beta}m}{N}}y$. By writing $e^{\xi^2/2} = e^{y^2/2\sigma^2}$, we can identify σ in terms of physical variables that can be read from the simulation to assess how well this simplified picture holds for various Ω^*. Written out in full (see 2.2 for the conversion between S_p and N^2):

$$\sigma = \left\{ \frac{1}{\left(\frac{2\Omega}{a} + \frac{\bar{u}}{a^2}\right) m} \left(\frac{g^2 p S_p}{R\bar{T}_s^2}\right)^{\frac{1}{2}} \right\}^{\frac{1}{2}} \tag{134}$$

The null hypothesis is that there is a continuum of behaviours in the space from $\Omega^* = 1$ to 1/64 and that the type of wave that dominates the stratosphere is principally the same, just being quantitatively modified by the changing influence of Ω^*.

Even in the best case, the model outlined here might not hold very well for long, as Ω^* is decreased. At least initially, $\frac{2\Omega}{a} \gg \frac{\bar{u}}{a^2}$ and thus $\sigma \sim \Omega^{-1/2}$, i.e. it eventually becomes larger that the region in which an equatorial beta-plane approximation is valid. Note that the latter is just slightly dependent on Ω^*, only through the fact that $\phi(y)$ becomes non-linear sooner than $f(y)$ as one goes away from the equator. At some point, the decrease in Ω starts being softened by the increase in $\frac{\bar{u}}{a^2}$, but it is a priori unlikely to constrain σ enough. In theory the worst case scenario is that the $n = 0$ mode is not the one present, and there are nodes of wave activity at some latitudes. Judging from figure 28, this should not be the case.

Figure 31 shows the t.m.z.m. wave half-amplitude $|v'|$ at various wavenumber cutoffs $k_{*,min}$ such that $k_* \geq k_{*,min}$, taking values 5 (up), 10 (middle) and 20 (down). This means that the signal of v' was first Fourier-transformed in the zonal direction, then part of the spectrum below $k_{*,min}$ was cut off, then the signal was inverse Fourier transformed back to spatial domain, then the absolute value and the t.m.z.m. were taken. The figure should show almost exclusively the signal from inertia-gravity waves as opposed to Rossby waves, since the wavenumber cutoff values are so large, except $k_{*,min} = 5$ and $\Omega^* = 1$, where the Rossby waves dominate (note the

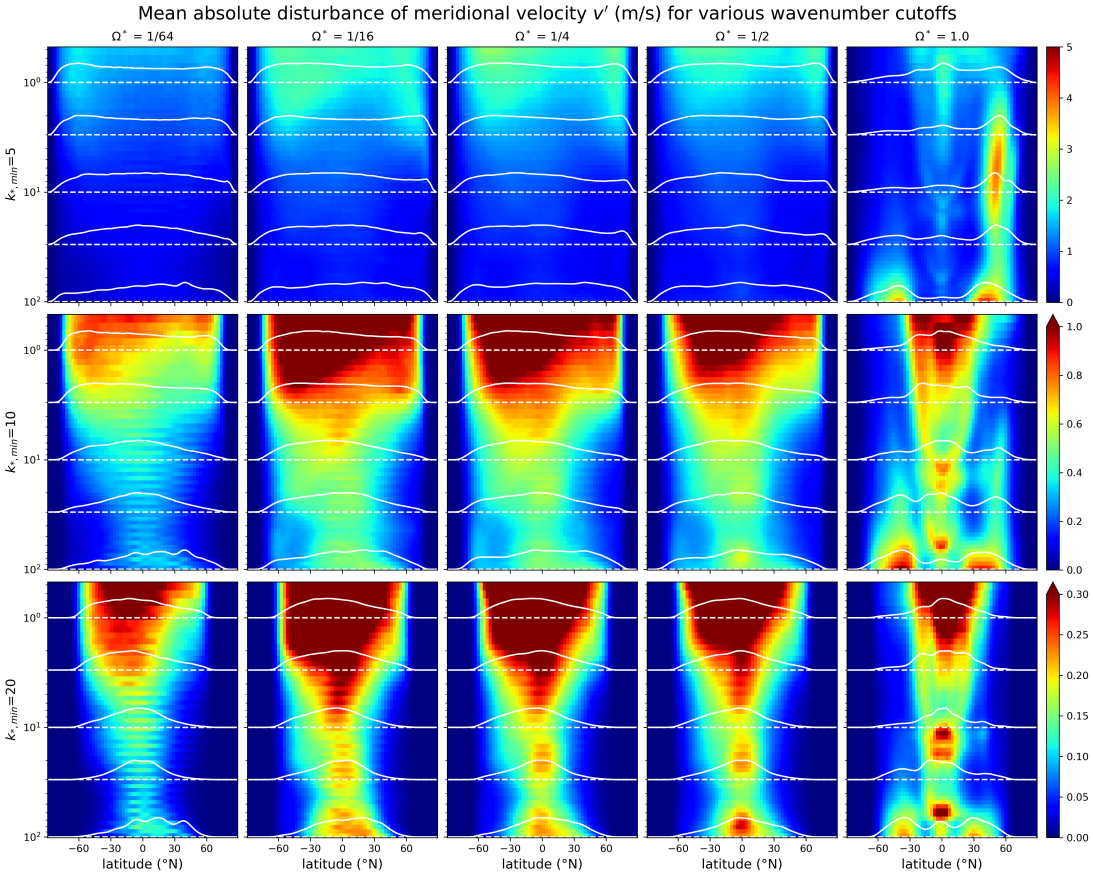

Figure 31: Temporal and zonal mean meridional wave amplitude v' at various wavenumber cutoffs $k_{*,min}$ such that $k_* \geq k_{*,min}$, taking values 5 (up), 10 (middle) and 20 (down). Note that each row has its own colour scheme, and these are always linear.

presence of tropospheric jets all the way down and the WSJ on the center right). Also note the isolated maxima in lower and middle stratosphere at the equator. These are the strongest for $\Omega^* = 1$, where they correspond to isolated spatial zonal wind reversals (see figure 4). By discussion with Dr. Hella Garny, it was made clear that the for $\Omega^* = 1$ the model is known to produce a QBO-like pattern with much longer period (of roughly 10 years). I can only speculate that these contribute to create some sort of localized critical layers for gravity wave propagation.

Figure 31 also allows us to asses how likely is the "equatorial trapping" model based on equation 134. The white dashed lines label the pressure levels at which a meridional cross section of the profile is plotted, so the height of the white solid curve about the white dashed line shows v' at that pressure level, i.e. the same thing that corresponds to the colour variable at that pressure level. The purpose of this is to demonstrate the shape of the v' profile, and if mathematical model of equation 134 holds, the white solid line should look roughly as a Gaussian with standard deviation σ. In table 2, find the σ values from equation 134 for the stratosphere, averaged along pressure levels and latitude, to get an idea of the lengthscale. Note that presence of the cyclostrophic term has an influence of more than 10% only for $\Omega^* \geq \frac{1}{16}$, peaking at 74° instead of 58° if cyclostrophic term was missing for $\Omega^* = \frac{1}{64}$. It is clear that equatorial trapping is not a very good model for explaining the meridional structure of gravity wave amplitude, even though there clearly is an element of truth to it.

Ω^*	σ (° lat)
1/64	58
1/32	46
1/16	34
1/8	25
1/4	17
1/2	12
1	8

Table 2: Mean meridional standard deviation in the (Gaussian-like) decay function $\hat{v}(y)$ expected based on equation 134, averaged over the stratosphere ,where it moderately ($\sim 50\%$) changes from place to place due to variations in $N^2 (\sim pS_p)$ and $\bar{u}$.

However, the most important takeaway from figure 31 is the following: in upper stratosphere (a few hPa) of intermediate and slow rotators, there is a notable growth of gravity wave amplitude with height, consistent with the fact that wave breaking occurs there (refer back to the eddy forcing column in figure 19). This intensification is stronger and starts at lower levels in the summer hemisphere, creating a triangular shape seen mainly in the second row of figure 31. The mechanism of wave breaking in upper summer stratosphere remains an open question.

Research into the wave motions was ongoing at the time of the end of this project, and in particular efforts were made to measure the dispersion relations and phase properties of waves at various places in the meridional plane, especially in the upper summer stratosphere.

9 Summary discussion

This section gets back to crucial points of this study and gives a summarizing verdict on their realism, and proposes where this line of research can be taken in the future

9.1 Validity of model and findings

Previous 4 sections focused on discussing different aspects of atmospheric circulation on slowly rotating planets during permanent solstice-like conditions. The phenomena that were studied the most were the emergence of the so-called stratospheric Hadley cell, and stratospheric superrotation. For both of these phenomena, it is important to ask how likely they are, and under which conditions, to appear on real planets. This has to consider several factors. On which time scale does a phenomenon arise, and under which conditions - and what would be their timescales and preconditions, etc.? Further to that, are the assumptions in the simulation physically justified and reasonable in wider context?

Many of these were addressed at their appropriate points in previous sections, so let us briefly recapitulate them, starting with the underlying model assumptions:

1. Through constants in geophysical equations, the model implicitly assumed a constant, roughly Earth-like planetary radius, bulk atmospheric composition and surface pressure. These were not parameters of interest for this study, so they were not varied.

2. Through the spatial form of the restoration temperature profile, the model implicitly assumed a constant, roughly Earth-like net insolation by its star, net strength of well-mixed greenhouse gases, and similar stratospheric radiative forcing from the ozone layer. These were not parameters of interest for this study, so they were not varied. For the tropospheric effects of most of the parameters in this and preceding point, see Kaspi and Showman (2015).

3. Through a restoration temperature independent of time and longitude, it was assumed that the rotation rate is fast enough so that the dynamics is not dictated by day-night temperature gradients. Radiative timescale in the stratosphere was 40 days, and ideally 1/2 of rotation period should be much smaller than this. This assumption becomes very problematic at $\Omega^* = \frac{1}{64}$ (32 days), and to some extent $\Omega^* = \frac{1}{32}$ (16 days).

4. Through a restoration temperature independent of time, the influence of changing seasons was neglected. The stratospheric restoration profile was inspired by the Earth's (time-dependent!) radiatively determined state, as is customary in many similar and less similar studies, see Wang et al. (2019) and Becker (2012).

5. Because of the coarse resolution, the short and intermediate wavelength gravity waves are missing, producing a manifestly weaker Brewer-Dobson circulation for $\Omega^* = 1$.

With regards to the realism and plausibility of the main results, the following can be said, starting with the stratospheric Hadley cell:

1. For a given planet, the emergence of this phenomenon is dependent on the radiative forcing gradient at the polar front. This is made of two contributions: low latitude winter stratosphere being still receiving substantial energy from ozone, and high latitude winter stratosphere being very strongly radiatively cooled. It is likely that a circulation like that would emerge even if one of the two ingredients was missing, ozone being the more likely candidate to be missing. In this case, the Hadley cell would be expected to be somewhat weaker and more narrowly confined to winter hemisphere.

2. Wave forcing in the simulation is negligible for $\Omega^* = \frac{1}{64}$, but not quite for $\Omega^* = \frac{1}{16}$. On a real planet with orography and potentially continent/ocean contrasts, there would be even more waves that could influence stratospheric dynamics (plus the unresolved gravity waves), so the real circulation in such case would likely be a hybrid of the purely radiatively driven Hadley cell, and a more familiar Brewer-Dobson-like circulation.

3. For the radiatively driven stratospheric Hadley cell, time scale should not be an issue precluding its existence on real planets. It is seen to fully develop roughly on a 3 month timescale under January-like radiative forcing, and should develop in similar way also for a continuously developping forcing on a real planet. A major difference of the autumn-winter transition compared to the spin-up phase of these simulations is that wave motions are already present in the atmosphere to begin with. However, when the eddies eventually built up in the simulation (slightly later than the Hadley cell), they did not modify its essential characteristics.

My conclusion is that a relatively strong radiatively dominated Hadley cell is a plausible result that should be expected as a seasonal effect in slowly rotating stratospheres. It would still be interesting to try to perturb either the ozone layer, or the polar night region, and see how the system responds. Unfortunately, it is not possible to (easily) change the amount of ozone heating, as it is hard-wired deeper down in the model code, and this thought emerged rather late in the project. What is possible to change easily is the lapse rate of the radiatively determined profile in the polar night region. Based (especially) on section 7 it is expected to be more important than ozone.

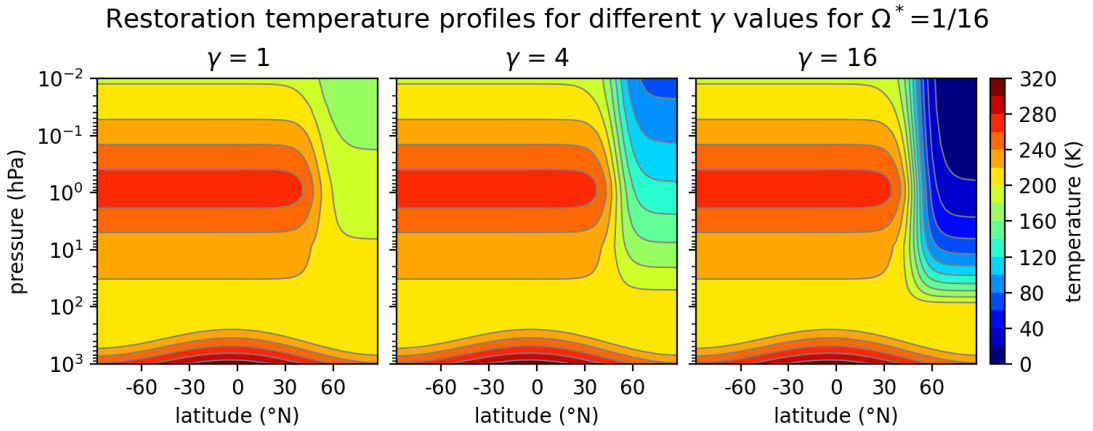

Figure 32: Modified temperature profiles with changed polar night lapse rate γ (in K km^{-1}), 4x smaller on the left, 4x larger on the right, and the original version in the middle.

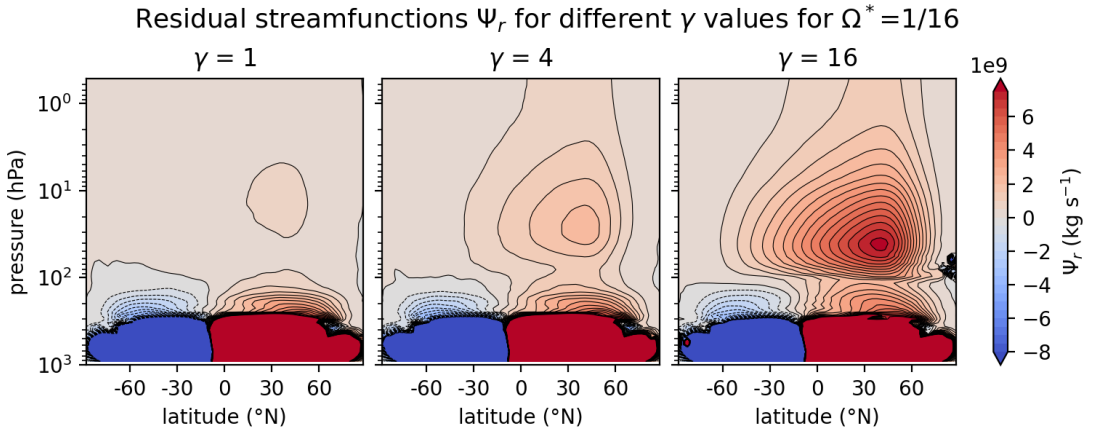

Figure 33: Residual streamfunctions corresponding to the modified temperature profiles with changed polar night lapse rate γ, see the preceeding figure.

Note that this creates a slight problem with consistency, since the lapse rate in the polar

night region is supposed to be consistent with Earth like parameters (e.g. greenhouse gases), and by changing only that parameter and not all the rest, we are creating a somewhat artificial setup. In particular the troposphere is held constant. In another way, this is also an advantage, since we isolate the effects to be purely stratospheric. I do not claim that this scenario is necessarily realistic, but it shows the sensitivity of the found circulation to such changes. Find the new temperature profiles in figure 32, and the associated residual streamfunctions in figure 33. Figure 33 shows that the streamfunction is sensitive to the polar night lapse rate in a roughly linear way. This is also roughly in line with the linear equation 112, although the regime is strongly non-linear for $\gamma = 4$ or 16. The longer the seasons are, and the easier it is to radiatively cool down the stratosphere, the stronger the polar forcing is, and the stronger the stratospheric Hadley cell would be, regardless of ozone layer.

Another important thing to note is the great influence that the absence of surface features like continents and orography had on the results of this study. As a result, the influence of wave driving of the stratospheric mean flow on such a "bare" planet was systematically smaller than on Earth. Figure 34 is an analog of 9, but unlike a smooth planet with $\Omega^* = 1$, this planet had a sinusoidal mountain range with zonal wavenumber 2, which helped create the corresponding planetary waves that drive the Brewer-Dobson circulation. Unlike figure 9, where the meridional wind in the stratosphere is order of magnitude smaller, now it is almost the same as on Earth. Also the eastward WSJ is somewhat weaker than if the surface was smooth, likely because of the westward momentum deposited by the same extra planetary waves that make the meridional circulation stronger. Nothe that the meridional wind shown here is Eulerian, so the figure cannot be used to make inferences about the shape of Brewer-Dobson circulation, just the overall scale of atmospheric winds.

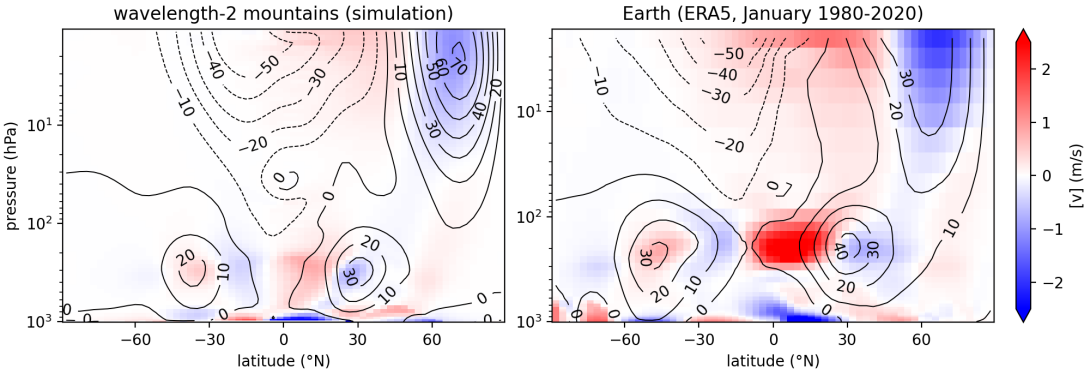

Figure 34: Comparison of climatology of t.m.z.m. meridional wind component $[v]$ (colour, m/s) and t.m.z.m. zonal wind component $[u]$ (black contours, m/s). Unlike figure 9, here the simulation had a sinusoidal height perturbation with amplitude of 3 km and zonal wavenumber 2.

Let us now move to stratospheric superrotation. There, it is not clear to which extent it could arise with these parameters on a real planet with annual cycle not longer than Earth's, because of the long timescale of almost 12 months it needs to develop in the simulation $\Omega^* = \frac{1}{16}$ *given* an already existing suitable eddy forcing. It would only be possible to answer that question with deeper understanding of its wave driving, or eventually a GCM with an explicit radiative scheme (or at least a temporally dependent restoration temperature). Another drawback is that most of the GW spectrum is not resolved, and it is not known to which extent the breaking of short and intermediate GWs would change the wave forcing in the seemingly crucial summer stratosphere. As an additional experiment, to get somewhat closer to the conditions of the autumn-winter transition, I first ran a simulation with the Held-Suarez restoration temperature (see section 3.3), i.e. with hemispherically symmetric tropospheric pattern, and featurless stratosphere. While the ozone layer is missing, it is still a more physically realistic initial condition than the motionless and eddy-free initial state. Then I re-started this simulation with

the usual Polvani-Kushner forcing, typical for northern hemisphere winter. Unfortunately this did not yield very useful results, because the sharp transition in forcing interacted with the already existing wind and eddy pattern, and created a prolonged unstable regime, even less physically realistic than the spin-up state.

9.2 Dimensionless numbers

Since the stated purpose of this work was to begin understanding the parametric dependence in a similar way to troposphere, let me summarize some of the scaling properties, and finally link them with the dimensionless parameters in use. Going back to equations 112 (which said $\nabla^2_*[\omega] = \mu\frac{\partial^2[\tilde{T}]}{\partial y^2}$) and in particular 115, we can identify the following as the rough physical scale of the ratio of the two terms on the left hand side:

$$\mathcal{R} = \frac{S_p p R}{\Omega^2 a^2 \varepsilon^2} \tag{135}$$

where ε now denotes the tilt of planetary axis w.r.t. the orbital plane ($\varepsilon \sim$ latitude extent of the polar night region). Converting S_p to $N^2 = \frac{S_p p g^2}{R\bar{T}^2} \approx \frac{\Delta\Theta_v}{\Theta H}$, we can write this ratio as:

$$\mathcal{R} = \frac{R^2\bar{T}^2\Delta\Theta_v^2}{gH^2\Omega^2\Theta a^2\varepsilon^2} \tag{136}$$

Finally we can recall the definition of Burger number in section 2.9, and find that the crucial ratio in equation 112 is simply:

$$\mathcal{R} = \frac{\mathcal{B}u}{\varepsilon^2} \tag{137}$$

note that some constant dimensionless terms of order 10^0 were neglected. This number determines whether the dominant response to large scale diabatic forcing is downwelling or temperature relaxation. **Slowly rotating planets have stronger radiatively driven statospheric circulation for given amount of forcing**.

Further, let us inquire about the influence of the horizontal temperature gradient $\Delta\Theta_h \sim \gamma H$, where γ is the polar night lapse rate, and H is again a characteristic height scale of the atmosphere. We can immediately link this with the thermal Rossby number $\mathcal{R}o_T = \frac{R\Delta\Theta_h}{\Omega^2 a^2}$. Note that the circulation strength scales with $\mathcal{R}o_T^{3/2}$, which is roughly consistent with figure 33, where Ψ increases at least linearly with $\gamma(\sim \mathcal{R}o_T)$. **Larger polar night lapse rate creates stronger radiatively driven stratospheric circulation for given rotation rate**.

Finally, what was not changed in this study at all was the relaxation timescale, it had stratospheric values of around 40 days. Unlike in tropospheric studies, where frictional damping is given priority in the definition of Taylor number, in the stratosphere it should be the radiative damping. Therefore, the third critical dimensionless number is $\mathcal{T}a_r = (\Omega\tau)^4 = \left(\frac{\Omega}{\mu}\right)^4$. The relevance of this study is mainly for planets that have $\mathcal{T}a_r$ still large-enough ($\gg 1$), so that the modelling assumption of zonally symmetric restoration temperature still holds. In the context of my work, $\Omega^* = \frac{1}{16}$ should satisfy this very well. In the other extreme may lie the tidally locked planets, where the day-night temperature contrasts are dominant in the dynamics.

9.3 Ideas for further reseach

This research had many limitations in terms of realism, mainly stemming from the model setup available for the project. The obvious way how to eliminate most of them is to run a more complex GCM with an explicit radiative scheme, and preferably a higher spatial resolution. For the sake of the argument, let me forget about this option, and suggest a few "cheaper" alternatives, that are potentially realistic with current model setup, and that could improve the realism of results. It is my understanding that introducing a time dependence into the restoration temperature profile would require to modify the original code. This should be a reasonable option, but even without that, it should be fairly easy to make numerous slightly

modified profiles and gradually restart the simulations, while switching from one to another in small steps (e.g. via a shell script). It would still be preferable to be able to make a continuously changing restoration temperature that would mimic yearly cycle. There is to my knowledge no existing template for this (such as the Held-Suarez or Polvani-Kushner setup), but it could be produced relatively easily based on the radiative state of the Earth's atmosphere. To be realistic for the very slowly rotating planets, this should also include the temperature anomalies that develop on the day and night hemispheres over time, i.e. to have a 3-dimensional profile slowly "rotating" around the globe. This would be the peak of what a model with de-coupled radiation and dynamics could do.

A very legitimate question is whether it is even appropriate to decouple the radiation from dynamics. For Earth, this approach can produce a rather realistic wind and temperature field, when coupled to a simple dynamical core (see Becker (2012)). For planets that are very slowly rotating, but their rotation still prevents unlimited accumulation and loss of heat from their day and night sides, the decoupling should in principle still be a valid strategy, provided that it captures the day/night contrasts. The issues come when the planet is *tidally locked*, and temperature differences become severe. The original ambition of this thesis was to study the dynamics on tidally locked exoplanets in collaboration with the DLR Institute for Planetary Research in Berlin, which would provide the restoration temperature, and our group at the DLR Institute for Atmospheric Physics would do the dynamics. However, it turned out that this approach could not work for the planets selected, among other reasons because the one dimensional (column) radiative-convective model produced a $T_{eq}(p, \theta)$ with a large temperature discontinuity at some critical angular distance away from the sub-stellar point. This was not investigated in detail by our group, but it seemed from the discussion with our colleagues from Berlin that it was due to the ocean being evaporated in a runaway greenhouse effect, that was initiated at some critical insolation. This is an extreme example of a case where the decoupling can never work, since the dynamics would not only modify the actual temperature to a point in which the runaway evaporation of the ocean might not occur, but more importantly, in the case of a runaway, they would redistribute the water vapour so that there is not a step of hundreds of Kelvins in the radiative state, just while going from one grid point to another. This is a much more severe inconsistency than e.g. the ozone layer being slightly modified by stratospheric circulation. This was already addressed near the beginning of this document, where it was argued that ozone layer has greatest influence on temperatures in its upper regions, near its maximum mixing ratio, where it is photochemically controlled, as opposed to lower levels that are also dynamically controlled, and prone to advection.

10 Summary conclusion

This work used an idealized GCM with parametrized radiative forcing similar to a permanent January condition on Earth. The main focus were the zonal mean stratospheric dynamics that arise under such conditions on a sequence of slowly rotating planets with the rotation speed relative to Earth, Ω^*, in range 1 down to 1/64. For this, the Eulerian zonal mean equations were inspected term by term, and an appropriate transformed Eulerian (TEM) system $([v]_r, [\omega]_r)$ was found, reflecting the scales present in the simulation output. The proposed causal mechanism in the TEM equations is seen in figure 35:

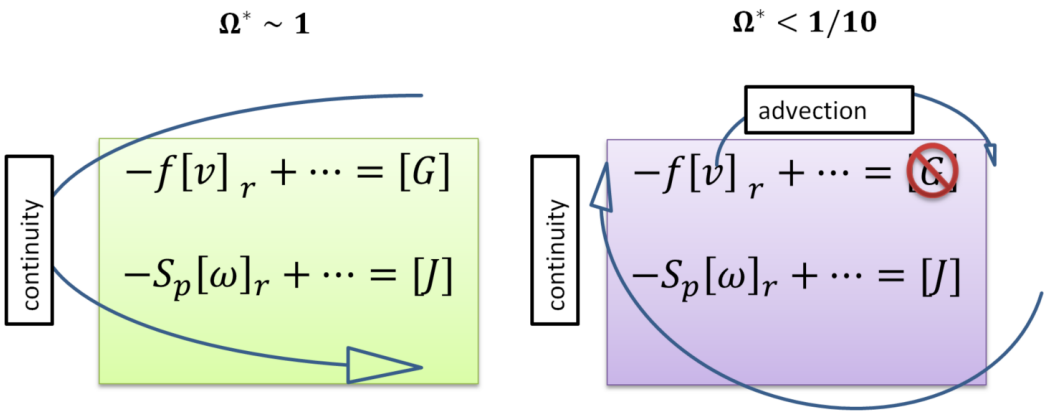

Figure 35: Proposed causality in the TEM view for a terrestrial planet with a normal Earth-like rotation rate (left) and much smaller rotation rate (right). $[G]$ stands for eddy forcing, $[J]$ stands for radiative forcing, S_p is the stability parameter.

On Earth, the mainstream view (Becker (2012)) is that eddies are the dominant drivers of residual meridional wind $[v]_r$, which generates vertical motions that drive the stratosphere away from radiative balance, which is counteracted with diabatic heating to preserve a long-term steady state in temperature. On very slowly rotating planets, the stratospheric dynamics near a solstice gets non-linear. There is a strong and meridionally extensive (almost pole-to-pole) Hadley-like thermally direct overturning, which redistributes momentum, while partially conserving the angular momentum. It is predominantly radiatively driven, with strong downwelling over the winter polar stratosphere. Such stratosphere is much further from the radiative balance than that of Earth.

Another important phenomenon in the stratosphere is the superrotation, present and significant for $\Omega^* \leq \frac{1}{16}$. It is thought that it originates from the eastward momentum deposited by gravity wave breaking in the middle and upper summer stratosphere. The angular momentum is advected from there across the equator to the winter hemisphere, and homogenized over a wide area spanning from southern to northern subpolar regions by the stratospheric Hadley cell. This is somewhat supported by how well the northern (winter hemisphere) edge of the Hadley cell overlaps with the rather sharp edge of anomalous angular momentum. There remain gaps in the understanding of both the initial driving and the spatial transport of this angular momentum.

It is recommended that future research looks at the influence of Burger number, radiative Taylor number and thermal Rossby number for a more methodic overview of parametric dependence of stratospheric dynamics, comparable to that for tropospheric dynamics, which is usually done in the plane of thermal Rossby number and frictional Taylor number. As a bottom line, it is recommended that a serious research into this topic has an explicit radiative scheme in the model.

References

D. Andrews and M. E. Mcintyre. Planetary waves in horizontal and vertical shear: The generalized eliassen-palm relation and the mean zonal acceleration. *Journal of Atmospheric Sciences*, 33(11):2031–2048, 1976.

D. Andrews, J. Mahlman, and R. Sinclair. Eliassen-palm diagnostics of wave-mean flow interaction in the gfdl" skyhi" general circulation model. *Journal of the atmospheric sciences*, 40 (12):2768–2784, 1983.

U. S. Atmosphere. *US standard atmosphere*. National Oceanic and Atmospheric Administration, 1976.

E. Becker. Dynamical control of the middle atmosphere. *Space Science Reviews*, 168:283–314, 2012.

N. Butchart. The brewer-dobson circulation. *Reviews of geophysics*, 52(2):157–184, 2014.

R. Caballero, R. T. Pierrehumbert, and J. L. Mitchell. Axisymmetric, nearly inviscid circulations in non-condensing radiative-convective atmospheres. *Quarterly Journal of the Royal Meteorological Society: A journal of the atmospheric sciences, applied meteorology and physical oceanography*, 134(634):1269–1285, 2008.

J. G. Charney and P. G. Drazin. Propagation of planetary-scale disturbances from the lower into the upper atmosphere. *Journal of Geophysical Research*, 66(1):83–109, 1961.

N. Y. Cohen, E. P. Gerber, and O. Bühler. What drives the brewer–dobson circulation? *Journal of the Atmospheric Sciences*, 71(10):3837–3855, 2014.

A. D. Del Genio and R. J. Suozzo. A comparative study of rapidly and slowly rotating dynamical regimes in a terrestrial general circulation model. *Journal of Atmospheric Sciences*, 44(6):973–986, 1987.

T. Dunkerton. On the mean meridional mass motions of the stratosphere and mesosphere. *Journal of Atmospheric Sciences*, 35(12):2325–2333, 1978.

W. Ferrel. The influence of the earth's rotation upon the relative motion of bodies near its surface. *Astronomical Journal, vol. 5, iss. 109, p. 97-100 (1858).*, 5:97–100, 1858.

H. Garny, R. Walz, M. Nützel, and T. Birner. Extending the modular earth submodel system (messy v2. 54) model hierarchy: the echam/messy idealized (emil) model setup. *Geoscientific Model Development*, 13(11):5229–5257, 2020.

J. E. Geisler, E. J. Pitcher, and R. C. Malone. Rotating-fluid experiments with an atmospheric general circulation model. *Journal of Geophysical Research: Oceans*, 88(C14):9706–9716, 1983.

A. Goetz. Quantitative classification of atmospheric circulation regimes of terrestrial planets, 2023a.

A. Goetz. Quantitative classification of atmospheric circulation regimes of terrestrial planets. In *IUGG*, Berlin, July 2023b.

G. Hadley. Vi. concerning the cause of the general trade-winds. *Philosophical Transactions of the Royal Society of London*, 39(437):58–62, 1735.

I. M. Held and A. Y. Hou. Nonlinear axially symmetric circulations in a nearly inviscid atmosphere. *Journal of the Atmospheric Sciences*, 37(3):515–533, 1980.

I. M. Held and M. J. Suarez. A proposal for the intercomparison of the dynamical cores of atmospheric general circulation models. *Bulletin of the American Meteorological society*, 75 (10):1825–1830, 1994.

I. Hirota and T. Hirooka. Normal mode rossby waves observed in the upper stratosphere. part i: First symmetric modes of zonal wavenumbers 1 and 2. *Journal of Atmospheric Sciences*, 41(8):1253–1267, 1984.

J. Holton and G. Hakim. *An Introduction to Dynamic Meteorology 5th edition*. 2012.

A. Y. Hou. Axisymmetric circulations forced by heat and momentum sources: A simple model applicable to the venus atmosphere. *Journal of Atmospheric Sciences*, 41(24):3437–3455, 1984.

P. Jöckel, R. Sander, A. Kerkweg, H. Tost, and J. Lelieveld. the modular earth submodel system (messy)-a new approach towards earth system modeling. *Atmospheric Chemistry and Physics*, 5(2):433–444, 2005.

Y. Kaspi and A. P. Showman. Atmospheric dynamics of terrestrial exoplanets over a wide range of orbital and atmospheric parameters. *The Astrophysical Journal*, 804(1):60, 2015.

P. J. Kushner and L. M. Polvani. Stratosphere–troposphere coupling in a relatively simple agcm: The role of eddies. *Journal of climate*, 17(3):629–639, 2004.

E. Lorenz. The nature and theory of the general circulation of the atmosphere. *World meteorological organization*, 161, 1967.

T. Matsuno. Lagrangian motion of air parcels in the stratosphere in the presence of planetary waves. *pure and applied geophysics*, 118:189–216, 1980.

M. Mayor and D. Queloz. A jupiter-mass companion to a solar-type star. *nature*, 378(6555): 355–359, 1995.

A. S. Medvedev and E. Yiğit. Gravity waves in planetary atmospheres: Their effects and parameterization in global circulation models. *Atmosphere*, 10(9):531, 2019.

J. L. Mitchell and G. K. Vallis. The transition to superrotation in terrestrial atmospheres. *Journal of Geophysical Research: Planets*, 115(E12), 2010.

J. Pedlosky. *Geophysical fluid dynamics*. Springer Science & Business Media, 2013.

J. R. D. Pinto and J. L. Mitchell. Atmospheric superrotation in an idealized gcm: Parameter dependence of the eddy response. *Icarus*, 238:93–109, 2014.

P. L. Read and S. Lebonnois. Superrotation on venus, on titan, and elsewhere. *Annual Review of Earth and Planetary Sciences*, 46:175–202, 2018.

P. L. Read, S. R. Lewis, and G. K. Vallis. Atmospheric dynamics of terrestrial planets. *Handbook of Exoplanets*, 144:2537–2557, 2018.

E. Roeckner, G. Bäuml, L. Bonaventura, R. Brokopf, M. Esch, M. Giorgetta, S. Hagemann, I. Kirchner, L. Kornblueh, E. Manzini, et al. The atmospheric general circulation model echam 5. part i: Model description. 2003.

E. Roeckner, R. Brokopf, M. Esch, M. Giorgetta, S. Hagemann, L. Kornblueh, E. Manzini, U. Schlese, and U. Schulzweida. Sensitivity of simulated climate to horizontal and vertical resolution in the echam5 atmosphere model. *Journal of Climate*, 19(16):3771–3791, 2006.

G. K. Vallis. Dynamics of terrestrial atmospheres: From earth to titan, in parameter space with some discussion of superrotation. Presented at GFDL Princeton University, 2012.

G. K. Vallis. *Atmospheric and oceanic fluid dynamics*. Cambridge University Press, 2017.

D. Vincent. Mean meridional circulations in the northern hemisphere lower stratosphere during 1964 and 1965. *Quarterly Journal of the Royal Meteorological Society*, 94(401):333–349, 1968.

C. C. Walker and T. Schneider. Eddy influences on hadley circulations: Simulations with an idealized gcm. *Journal of the atmospheric sciences*, 63(12):3333–3350, 2006.

Y. Wang, P. Read, F. Tabataba-Vakili, and R. Young. Comparative terrestrial atmospheric circulation regimes in simplified global circulation models: I. from cyclostrophic super-rotation to geostrophic turbulence. *arXiv preprint arXiv:1906.07561*, 2019.

G. P. Williams. The dynamical range of global circulations—i. *Climate Dynamics*, 2(4):205–260, 1988a.

G. P. Williams. The dynamical range of global circulations—ii. *Climate Dynamics*, 3:45–84, 1988b.

G. P. Williams and J. L. Holloway. The range and unity of planetary circulations. *Nature*, 297: 295–299, 1982.